

IMPROVEMENT AND STABILITY OF ZEOLITE-BASED CATALYSTS
FOR TRANSESTERIFICATION OF PALM OIL AND GLYCEROL
CONVERSION TO GLYCEROL CARBONATE



SIRIPORN KOSAWATTHANAKUN

A Thesis Submitted in Partial Fulfillment of the Requirements for the
Degree of Doctor of Philosophy in Chemistry
Suranaree University of Technology
Academic Year 2021

การปรับปรุงและเสถียรภาพของตัวเร่งปฏิกิริยาที่มีซีโอไลต์เป็นหลักสำหรับ
ทรานส์เอสเทอร์ฟิเคชันของน้ำมันปาล์มและการเปลี่ยน
กลีเซอรอลเป็นกลีเซอรอลคาร์บอนเนต

นางสาวศิริพร โกษาวัฒนกุล

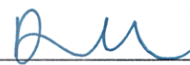


วิทยานิพนธ์นี้เป็นส่วนหนึ่งของการศึกษาตามหลักสูตรปริญญาวิทยาศาสตรดุษฎีบัณฑิต
สาขาวิชาเคมี
มหาวิทยาลัยเทคโนโลยีสุรนารี
ปีการศึกษา 2564

IMPROVEMENT AND STABILITY OF ZEOLITE-BASED CATALYSTS FOR
TRANSESTERIFICATION OF PALM OIL AND GLYCEROL
CONVERSION TO GLYCEROL CARBONATE

Suranaree University of Technology has approved this thesis submitted in partial fulfillment of the requirements for the Degree of Doctor of Philosophy.

Thesis Examining Committee



(Asst. Prof. Dr. Anyanee Kamkaew)

Chairperson



(Prof. Dr. Jatuporn Wittayakun)

Member (Thesis advisor)



(Prof. Dr. Frank Rößner)

Member



(Dr. Svetlana Mintova)

Member



(Assoc. Prof. Dr. Sanchai Prayoonpokarach)

Member



(Assoc. Prof. Dr. Chatchai Jothityangkoon)

Vice Rector for Academic Affairs

and Quality Assurance

(Prof. Dr. Santi Maensiri)

Dean of Institute of Science

ศิริพร โกษาวัฒนกุล : การปรับปรุงและเสถียรภาพของตัวเร่งปฏิกิริยาที่มีซีโอไลต์เป็นหลัก สำหรับทรานส์เอสเทอร์ริฟิเคชันของน้ำมันปาล์มและการเปลี่ยนกลีเซอรอลเป็นกลีเซอรอลคาร์บอเนต (IMPROVEMENT AND STABILITY OF ZEOLITE-BASED CATALYSTS FOR TRANSESTERIFICATION OF PALM OIL AND GLYCEROL CONVERSION TO GLYCEROL CARBONATE) อาจารย์ที่ปรึกษา : ศาสตราจารย์ ดร.จตุพร วิทยาคุณ, 89 หน้า

คำสำคัญ: เสถียรภาพ/ ซีโอไลต์/ ตัวเร่งปฏิกิริยา/ พูจาไซต์/ ทรานส์เอสเทอร์ริฟิเคชัน/ น้ำมันปาล์ม/ กลีเซอรอล/ กลีเซอรอลคาร์บอเนต/ ซีโอไลต์ BPH / ซีโอไลต์ขนาดนาโน/ นาโนซีต

ในช่วงหลายปีที่ผ่านมา อุตสาหกรรมน้ำมันปาล์มดิบในประเทศไทยยังคงเผชิญกับภาวะอุปทานส่วนเกินอย่างต่อเนื่อง ทำให้อุตสาหกรรมที่เกี่ยวข้อง เช่น การผลิตน้ำมันไบโอดีเซล และอุตสาหกรรมโอเลโอเคมีคอล เป็นต้น ต้องช่วยกันจัดการกับปัญหาข้างต้น โดยวิทยานิพนธ์นี้ได้สาธิตการใช้ประโยชน์ปฏิกิริยาทรานส์เอสเทอร์ริฟิเคชันของน้ำมันปาล์มและการเพิ่มมูลค่าแก่สารกลีเซอรอลให้กลายเป็นสารเคมีที่มีมูลค่าสูง ซึ่งเน้นการปรับปรุงและการศึกษาเสถียรภาพของตัวเร่งปฏิกิริยาวิวิธพันธุ์ที่มีซีโอไลต์เป็นหลัก

ในการศึกษาส่วนแรกนี้เริ่มต้นด้วยการเปรียบเทียบสมบัติเคมีกายภาพและประสิทธิภาพในการผลิตน้ำมันไบโอดีเซลของตัวเร่งปฏิกิริยาโพแทสเซียม (K) ที่รองรับบนซีโอไลต์ NaX และ NaY (K/NaX และ K/NaY ตามลำดับ) ซึ่งที่ผ่านมายังไม่มีมีการนำตัวเร่งปฏิกิริยาเหล่านี้ไปทดสอบในปฏิกิริยาทรานส์เอสเทอร์ริฟิเคชันภายใต้สภาวะที่กำหนดและใช้น้ำมันพืชชนิดเดียวกัน ในงานนี้ใช้วิธีการเอ็บซุ่มด้วยสารตั้งต้นจากบัพเฟอร์โพแทสเซียมอะซิเตตร่วมกับวิธีอัลตราซาวด์ในการเตรียมตัวเร่งปฏิกิริยา จากผลการศึกษาพบว่า โครงสร้างของซีโอไลต์ NaX มีเสถียรภาพมากกว่าโครงสร้างของซีโอไลต์ NaY ภายหลังจากการเอ็บซุ่มและการเผา นอกจากนี้ยังพบว่า K/NaX มีความเป็นเบสสูงกว่า K/NaY จากนั้นทั้ง K/NaX และ K/NaY ได้นำไปทดสอบการเร่งปฏิกิริยาทรานส์เอสเทอร์ริฟิเคชันของน้ำมันปาล์มและเมทานอล เพื่อให้ได้ไบโอดีเซลที่เป็นผลิตภัณฑ์หลัก และกลีเซอรอลที่เป็นผลิตภัณฑ์ร่วมตามลำดับ โดยตัวเร่งปฏิกิริยาเหล่านี้ให้ผลผลิตไบโอดีเซลสูง เมื่อทำการทดสอบทรานส์เอสเทอร์ริฟิเคชันในครั้งแรก ขณะที่ตัวเร่งปฏิกิริยา K/NaX ให้ผลผลิตที่สูงกว่า K/NaY ในการทดสอบรอบที่สอง จากผลการศึกษา ตัวเร่งปฏิกิริยา K/NaX มีความเหมาะสมกับปฏิกิริยานี้

การศึกษาส่วนที่สองนี้ได้สาธิตกระบวนการทางเลือกและความยั่งยืนเพื่อที่จะเปลี่ยนสารกลีเซอรอลที่เป็นผลิตภัณฑ์ร่วมจากปฏิกิริยาทรานส์เอสเทอร์ริฟิเคชันที่กล่าวไว้ข้างต้นให้กลายเป็นสารเคมีที่มีมูลค่าสูง งานในส่วนนี้ได้อธิบายผลเชิงสัมพันธวิทยาของนาโนซีตซีโอไลต์ BPH ที่มีผลต่อการแปรสภาพของกลีเซอรอลให้เป็นกลีเซอรอลคาร์บอเนต ในการสังเคราะห์ซีโอไลต์ BPH ที่มีขนาด

และสัดส่วน Si/Al ที่แตกต่างกัน ด้วยวิธีไฮโดรเทอร์มัล หลังจากนั้นจึงแลกเปลี่ยนไอออนของซีโอไลต์ ทั้งสองชนิดที่สังเคราะห์ขึ้น (nano CsBPH_AP และ micro KBPH_AP) กับสารตั้งต้นโพแทสเซียม (K) หรือซีเซียม (Cs) จากผลการศึกษาพบว่า nano CsBPH_AP ที่ผ่านการแลกเปลี่ยนกับไอออน โพแทสเซียม (nano K-CsBPH_IE) และ micro KBPH_AP ที่ผ่านแลกเปลี่ยนกับไอออนซีเซียม (micro Cs-KBPH_IE) มีลักษณะโครงสร้าง สัณฐานวิทยา และหมู่ฟังก์ชัน คล้ายกับซีโอไลต์ตั้งต้น ในขณะที่ nano CsBPH_AP มีขนาดอนุภาคเล็กและมีช่องทางการแพร่เชิงโมเลกุลสั้น จึงทำให้ตัวเร่ง ปฏิกริยานี้มีประสิทธิภาพในการเร่งปฏิกิริยาที่เหมาะสม จากการศึกษาสภาวะเหมาะสมในการเร่ง ปฏิกริยาได้แก่อุณหภูมิ 120 °C เวลา 3 ชั่วโมง กับตัวเร่งปฏิกิริยาร้อยละ 6 โดยน้ำหนัก และใช้ สัดส่วนโดยโมลของกลีเซอรอลต่อไดเมทิลคาร์บอเนตเป็น 1 ต่อ 5 โดยตัวเร่งปฏิกิริยานี้ให้ ประสิทธิภาพในการเร่งปฏิกิริยาที่ดีถึงการทดสอบรอบที่สี่



สาขาวิชาเคมี

ปีการศึกษา 2564

ลายมือชื่อนักศึกษา ศิริพร โทษามงคล
ลายมือชื่ออาจารย์ที่ปรึกษา อุทพร ทอดกุล

SIRIPORN KOSAWATTHANAKUN : IMPROVEMENT AND STABILITY OF ZEOLITE-BASED CATALYSTS FOR TRANSESTERIFICATION OF PALM OIL AND GLYCEROL CONVERSION TO GLYCEROL CARBONATE. THESIS ADVISOR : PROF. JATUPORN WITTAYAKUN, Ph.D. 89 PP.

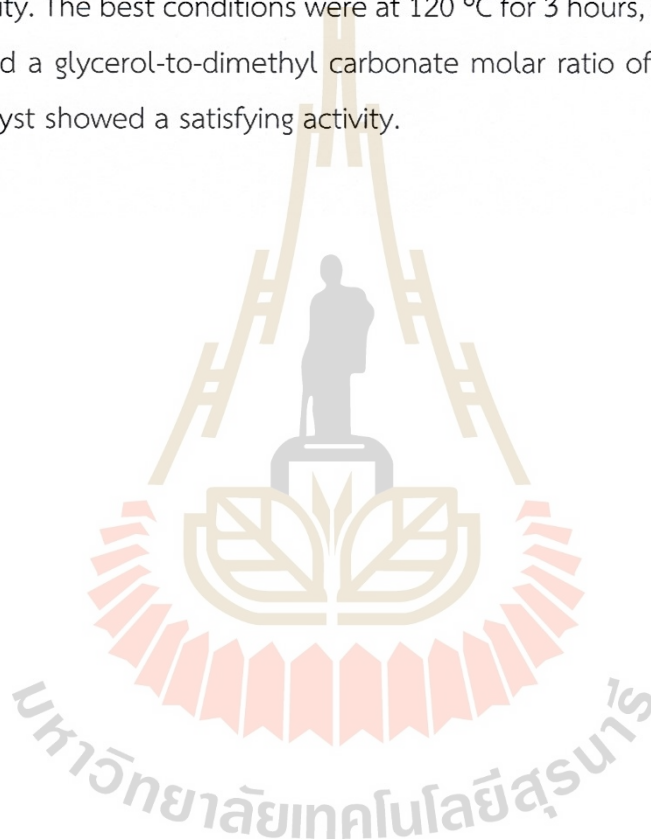
Keyword: Stability/ Zeolite/ Catalyst/ Faujasite/ Transesterification/ Palm oil/ Glycerol/ Glycerol carbonate/ BPH Zeolite/ Nanosized zeolite/ Nanosheet

From many years ago, Thailand's crude palm oil industry has experienced an oversupply. Accordingly, several relevant industries such as biodiesel production and oleochemicals industry have to overcome the situation. Hence, this thesis demonstrates the utilization of transesterification of palm oil and the valorization of glycerol towards high-valued chemicals. This involves the improvement and stability studies of heterogeneous zeolite-based catalysts.

The first part of this study started by comparing physicochemical properties and catalytic performance for biodiesel production by potassium (K) catalysts supported on zeolite NaX and NaY (K/NaX and K/NaY, respectively). Although the K/NaX and K/NaY catalysts are active for the transesterification of Jatropha seed and palm oils, they were prepared by different methods and have not been tested with the same oil. In this work, the catalysts were prepared by ultrasound-assisted impregnation using a potassium acetate buffer. The structure of NaX was more stable than that of the NaY after the impregnation and then calcination. Furthermore, K/NaX had higher basicity than K/NaY. Then, both K/NaX and K/NaY were catalytically evaluated in the transesterification of palm oil and methanol to achieve biodiesel and glycerol as major and co-products, respectively. These catalysts produced high biodiesel yields in the first run of the transesterification. K/NaX produced a higher yield than K/NaY in the second run. As a result, the K/NaX catalyst is appropriate for this reaction.

The second part demonstrates an alternative and sustainable process to converse glycerol as a co-product from the transesterification above to high-valued chemicals. This part elucidates the morphological effect of BPH zeolite nanosheets on

the conversion of glycerol towards glycerol carbonate. A hydrothermal approach was used to synthesize as-prepared BPH zeolites with different sizes and Si/Al ratios. Both as-prepared ones (nano CsBPH_AP and micro KBPH_AP) were ion-exchanged with either K or Cs precursors. The structures, morphologies, and functional groups of ion-exchanged nano CsBPH_AP and ion-exchanged micro BPH_AP (nano K-CsBPH_IE and micro Cs-KBPH_IE, respectively) were identical to their parents. Because of its tiny particle size and short molecular diffusional path, nano CsBPH_AP provided optimum reaction activity. The best conditions were at 120 °C for 3 hours, with a catalyst loading of 6 wt % and a glycerol-to-dimethyl carbonate molar ratio of 1:5. Up to the fourth run, the catalyst showed a satisfying activity.



School of Chemistry
Academic Year 2021

Student's Signature ศิวพร ไชยกุล
Advisor's Signature ดร.พร อุดม

ACKNOWLEDGEMENTS

I would like to express my gratitude to all people who help me to complete my Ph.D. journey.

First, I would like to thank my advisor, Prof. Dr. Jatuporn Wittayakun, for giving me the great opportunity to study my Ph.D. under his wing and financial support through the Royal Golden Jubilee Ph.D. program of the Thailand Research Fund. His guidance, support, help me to learn new things, and allow me to make mistakes which contributed to make me a better scientist. Moreover, I would like to acknowledge the thesis committee.

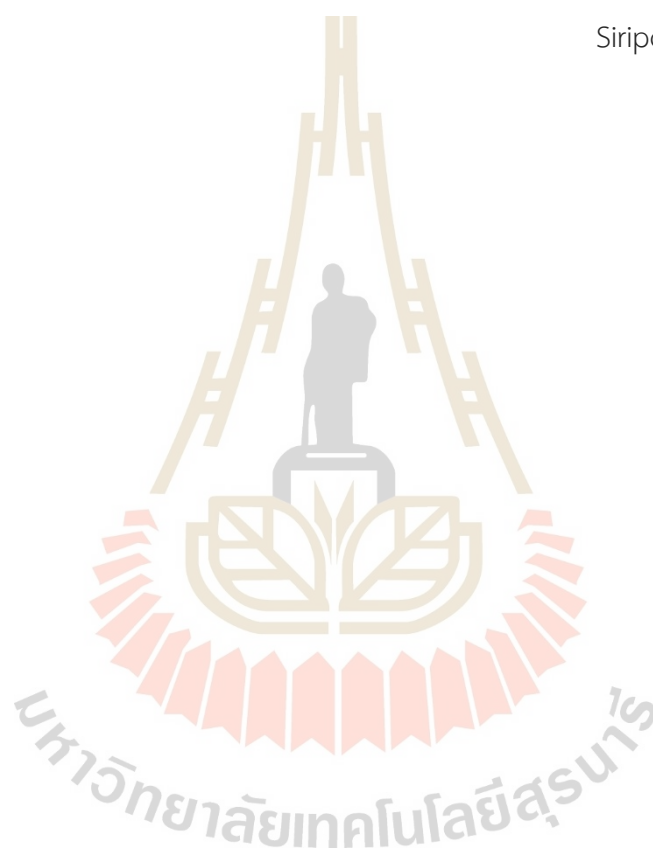
Dr. Svetlana Mintova is acknowledged as wonderful advisor during my research study at the Catalysis & Spectrochemistry Laboratory (LCS), ENSICAEN, University of Caen Normandie, France. Her encouragement, scientific guidance, and support are appreciated. She is always listening carefully to what I say, to work from what I am creating and furthering me with experience and knowledge. Moreover, I would also like to extend my gratitude to the French Embassy in Thailand with contribution to the RGJ-Ph.D. program for co-financial support during my one year in France. I am grateful to colleagues in the LCS lab: Dr. Edwin B. Clatworthy, Dr. Sajjad Ghojavand, Dr. Justyna Wawa, etc. Their friendly, dedicated, support, and skilled supervision made my work become smoother and enjoyable experience.

Furthermore, I extend my appreciation to Prof. Dr. Frank Rößner for his great support and assistance during my research study at Industrial Chemistry 2, Carl von Ossietzky Universität Oldenburg, Germany. I would like to thank co-financial support from Thai-German S&T Cooperation 3rd Researcher Mobility Scheme financed by the International Bureau of the German Federal Ministry of Education and Research (BMBF) Germany, the National Science and Technology Development Agency (NSTDA), Thailand and Suranaree University of Technology (SUT) to give me the opportunity to research study in Germany.

I would like to thank all my colleagues in the Catalysis research group for support my research activities. I also thank all people from School of Chemistry, the Center for Scientific and Technological Equipment (CSTE), and the Synchrotron Light Research Institute (SLRI, Public Organization).

Finally, I would like to express my deepest gratitude to my family for their support, motivation, and confidence in me.

Siriporn Kosawatthanakun



CONTENTS

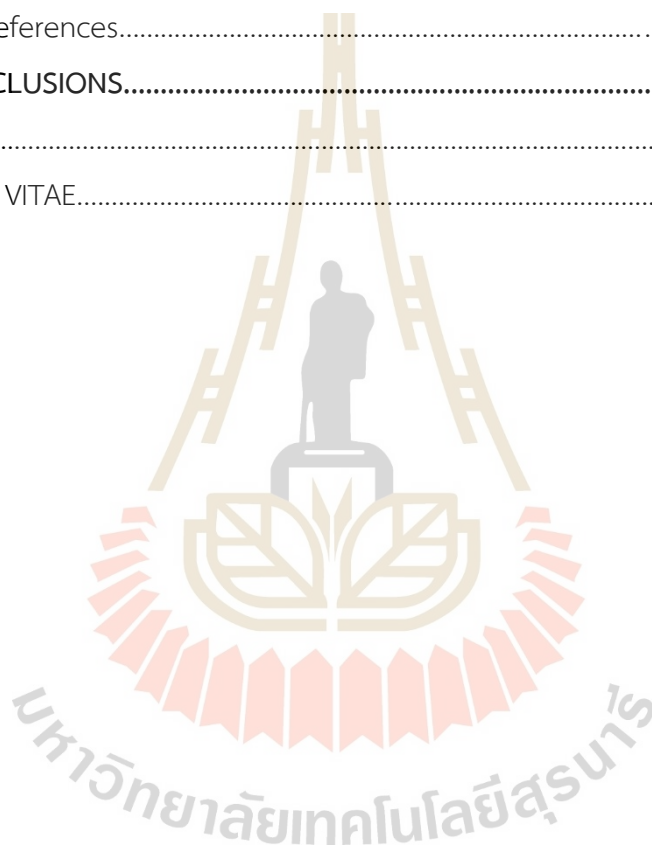
	Page
ABSTRACT IN THAI.....	I
ABSTRACT IN ENGLISH.....	III
ACKNOWLEDGEMENTS.....	V
CONTENTS.....	VII
LIST OF TABLES.....	X
LIST OF FIGURES.....	XI
CHAPTER	
I INTRODUCTION.....	1
1.1 Introduction.....	1
1.2 Scope and limitation of the study.....	3
1.3 Organization of the thesis.....	3
1.4 References.....	4
II LITERATURE REVIEW.....	7
2.1 Transesterification for biodiesel production.....	7
2.1.1 Potassium catalyst on faujasite (FAU) zeolite for biodiesel production.....	9
2.1.2 Ultrasound-assisted impregnation for catalyst preparation.....	12
2.2 Glycerol upgrading to glycerol carbonate by transesterification.....	13
2.2.1 Transesterification of glycerol and dimethyl carbonate.....	13
2.2.2 BPH zeolite catalysts for glycerol carbonate production.....	16
2.2.3 Improvement of BPH zeolite basicity by ion-exchange method....	18
2.3 Possible pathway of catalyst deactivation.....	19
2.4 References.....	23
III COMPARATIVE PROPERTIES OF K/NAX AND K/NAY FROM ULTRASOUND-ASSISTED IMPREGNATION AND PERFORMANCE IN TRANSESTERIFICATION OF PALM OIL.....	30

CONTENTS (Continued)

	Page
3.1 Abstract.....	30
3.2 Introduction.....	31
3.3 Experimental.....	33
3.3.1 Synthesis of zeolite NaX.....	33
3.3.2 Synthesis of zeolite NaY.....	34
3.3.3 Catalyst preparation.....	35
3.3.4 Catalyst characterization.....	35
3.3.5 Transesterification of palm oil.....	37
3.4 Results and discussion.....	39
3.4.1 Characterization of potassium catalysts impregnated on FAU zeolite.....	39
3.4.2 Catalytic activity on transesterification of palm oil.....	48
3.4.3 Stability of catalysts.....	50
3.5 Conclusions.....	53
3.6 References.....	54
IV MORPHOLOGICAL EFFECT OF BPH ZEOLITE NANOSHEETS ON CONVERSION OF GLYCEROL TOWARDS GLYCEROL CARBONATE.....	59
4.1 Abstract.....	59
4.2 Introduction.....	60
4.3 Experimental.....	62
4.3.1 Synthesis of BPH zeolite nanosheet.....	62
4.3.2 Synthesis of micron-sized BPH (Linde Q).....	62
4.3.3 Catalysts preparation.....	63
4.3.4 Catalyst characterization.....	63
4.3.5 Transesterification between glycerol and dimethyl carbonate.....	64
4.4 Results and discussion.....	65
4.4.1 Characterization of the catalysts.....	65
4.4.2 Catalytic activity on transesterification of glycerol and DMC.....	71

CONTENTS (Continued)

	Page
4.4.2.1 Catalyst screening.....	71
4.4.2.2 Effect of different reaction parameters.....	72
4.4.2.3 Reusability of the catalyst.....	76
4.5 Conclusions.....	79
4.6 References.....	80
VI CONCLUSIONS.....	84
APPENDIX.....	85
CURRICULUM VITAE.....	89



LIST OF TABLES

Table	Page
2.1 Geometrical parameters of reagent molecules. Reproduced from Pan et al. (2012) with permission.....	17
2.2 Synthesis of GC from glycerol and DMC over various zeolite catalysts. Reproduced from Pan et al. (2012) with permission.....	17
2.3 Causes of K-based catalysts deactivation on transesterification.....	19
2.4 Leaching of K from various support into various medium. Reproduced from Čapek et al. (2014) with permission.....	21
3.1 BET surface area and micropore volume of K/NaX and K/NaY compared to parent zeolites from N ₂ sorption analysis and K content from ICP analysis.....	43
3.2 Conversion and selectivity of products from the decomposition of MBOH and basicity by CO ₂ -TPD of K/NaX and K/NaY compared to the parent zeolites.....	47
3.3 Comparison of the catalyst performance in transesterification between K/NaX and K/NaY with 12 wt.% K loading from conventional and ultrasound-assisted impregnation from this work and previous literature.....	50
4.1 Elemental composition of BPH-type zeolite nanosheets by ICP-MS.....	67
4.2 Comparison of BPH nanosheets with various particle sizes from hydrothermal and ion-exchange method for transesterification of glycerol and DMC.....	72

LIST OF FIGURES

Figure	Page
2.1	Transesterification of triglyceride and methanol.....8
2.2	Possible reaction pathway of transesterification by KOH supported on zeolite. Reproduced from Farobie, and Matsumura (2017) with permission.....9
2.3	Faujasite zeolite structure and positions of their potential charge compensating cations. Reproduced from Yang et al. (2014) with permission.....10
2.4	Ultrasound-assisted impregnation of K precursor on zeolite support.....13
2.5	Different catalytic transformations of glycerol into value-added compounds are presented after the transesterification for biodiesel and glycerol production. Adapted from Houache et al. (2019) with permission.....14
2.6	Direct and indirect applications of glycerol carbonate. Reproduced from Sonnati et al. (2013) with permission.....14
2.7	Possible mechanism of base catalyst catalyzed transesterification of glycerol with DMC. Reproduced from Ochoa-Gómez et al. (2009).....16
2.8	Fouling and agglomeration of catalyst. Adapted from Moulijn et al. (2008) with permission.....20
2.9	Leaching of active species into the reaction medium. Adapted from Moulijn et al. (2008) with permission.....21
2.10	Application of hot filtration to the Mg-Fe layered double oxide catalyst for the transesterification. Reproduced from Xu et al. (2015).....22
3.1	XRD patterns of as-prepared and calcined (a) K/NaX and (b) K/NaY compared with their parent zeolites; symbol (*) = potassium acetate phase.....40
3.2	SEM images of (a) NaX, (b) calcined K/NaX, (c) NaY, and (d) calcined K/NaY catalysts with 10k and 30k magnification.....41

LIST OF FIGURES (Continued)

Figure	Page
3.3 N ₂ sorption isotherms of (a) calcined K/NaX and (b) calcined K/NaY compared to their parent zeolites; filled symbols = adsorption and hollow symbols = desorption.....	42
3.4 FTIR of as-prepared and calcined K/NaX and K/NaY catalysts compared with their parent zeolites.....	44
3.5 Raman spectra of calcined K/NaX and K/NaY catalysts compared with Their parent zeolites.....	45
3.6 XPS spectra of the chemical state of carbon (C 1s) and potassium (K 2p) peaks of calcined K/NaX and K/NaY catalysts.....	46
3.7 (a) MBOH conversion at various times and (b) CO ₂ -TPD profiles from calcined K/NaX and K/NaY compared to the bare zeolite supports.....	47
3.8 GC chromatograms from the conversion of palm oil obtained from (a) K/NaX (1 st run), (b) K/NaX (2 nd run), (c) K/NaY (1 st run), (d) K/NaY (2 nd run), and (e) biodiesel yield from first and second run on K/NaX and K/NaY at 60 °C for 3 h.....	49
3.9 XRD patterns of (a) spent K/NaX and (b) spent K/NaY compared with fresh catalysts.....	51
3.10 SEM images of (a) spent K/NaX and (b) spent K/NaY catalysts with 10k and 30k magnification.....	52
3.11 Comparison between fresh and spent catalysts by FTIR (ATR mode) spectra of (a) K/NaX and (b) K/NaY and Raman spectra of (c) K/NaX and (d) K/NaY.....	53
4.1 SEM images of (a) nano CsBPH_AP and (b) micro KBPH_AP.....	66
4.2 XRD pattern of as-prepared BPH zeolite and ion-exchanged BPH zeolite compared with their parent zeolites.....	68
4.3 FTIR spectra of as-prepared BPH zeolite and ion-exchanged BPH zeolite compared with their parent zeolites.....	69

LIST OF FIGURES (Continued)

Figure	Page
4.4 TG profiles of (a) nano CsBPH _{AP} and nano K-CsBPH _{IE} and (b) micro KBPH _{AP} and micro Cs-KBPH _{IE}	70
4.5 CO ₂ -TPD profiles of (a) nano CsBPH _{AP} and nano K-CsBPH _{IE} and (b) micro KBPH _{AP} and micro Cs-KBPH _{IE}	71
4.6 Effects of temperature on transesterification of glycerol with DMC using nano CsBPH _{AP} catalyst. Condition: Gly-to-DMC molar ratio of 1:3, 8 wt.% catalyst, 3 h.....	73
4.7 Effects of time on transesterification of glycerol with DMC using nano CsBPH _{AP} catalyst. Condition: Gly-to-DMC molar ratio of 1:3, 8 wt.% Catalyst, 120 °C.....	74
4.8 Effects of catalyst loading on transesterification of glycerol with DMC using nano CsBPH _{AP} catalyst. Condition: Gly-to-DMC molar ratio of 1:3, 120 °C, 3 h.....	75
4.9 Effects of Gly-to-DMC molar ratio on transesterification of glycerol with DMC using nano CsBPH _{AP} catalyst. Condition: 6 wt.% catalyst, 120 °C, 3 h.....	76
4.10 (a) Reusability test and (b) leaching test of nano CsBPH _{AP} under reaction conditions: temperature of 120 °C; time of 3h; molar ratio of Gly-to-DMC of 1:5; catalyst loading of 6 wt.%.....	77
4.11 Comparison structural stability between reused and fresh catalysts by (a) XRD patterns and (b) ²⁷ Al MAS NMR spectra.....	77
4.12 TG profiles of reused catalysts washed by different solvent compared with fresh catalyst.....	78
4.13 CO ₂ -TPD profiles of reused catalysts compared with fresh catalyst.....	79

CHAPTER I

INTRODUCTION

1.1 Introduction

Thailand's palm oil industry continues to face an oversupply during 2017-2022, driving down prices. To overcome this situation, the biodiesel industry, oleochemicals industry, and refined palm oil drive industrial demand for palm oil (Sowcharoensuk, 2020; Tunpaiboon, 2021). Therefore, palm oil is used as a feedstock for biodiesel production in this work.

Transesterification is a reaction between triglyceride and methanol to produce biodiesel under a homogeneous or heterogeneous catalytic process. Although homogeneous catalysis is faster and requires less catalyst amount than the heterogeneous one, the spent catalyst in the liquid phase is difficult to separate and reuse. Moreover, the process produces a large amount of wastewater for neutralization. These problems could be avoided by using heterogeneous catalysts (carbonates, alkali, metal oxides, and zeolites). One of the promising catalysts consists of potassium (K) species on various supports (Hindryawati et al., 2014; Rakmae et al., 2016; Supamathanon et al., 2011). They have higher basicity and better resistivity to free fatty acids contaminating triglyceride sources than those with lithium and sodium (Hindryawati et al., 2014). Moreover, the dispersion of active species on porous materials could improve the catalyst activity.

Zeolites faujasite (FAU) including NaX and NaY are interested in this work because of their well-defined frameworks with a three-dimensional pore system, large surface areas, and thermal stability (Verboekend et al., 2016). There are several works on catalysts with potassium impregnated on NaX and NaY for transesterification (Manadee et al., 2017; Noiroj et al., 2009; Peña et al., 2013; Xie et al., 2007). The catalysts are prepared by impregnation with potassium hydroxide (KOH), potassium

nitrate (KNO_3), and potassium acetate buffer solution ($\text{CH}_3\text{COOK}/\text{CH}_3\text{COOH}$) (Manadee et al., 2017; Noiroj et al., 2009; Peña et al., 2013). Some of those catalysts have problems from the collapse of zeolite structure or the agglomeration of potassium species. Hence, ultrasound-assisted impregnation is proposed to improve the dispersion due to increasing the mass transfer of precursor, dispersion of active species, and reducing synthesis time.

Although the previous literature shows that the K/NaX and K/NaY are active in the transesterification of various oils, those catalysts were prepared either by different methods or tested on different oils. Besides, there are no reports about the preparation of K/NaX catalysts by ultrasound-assisted impregnation. Consequently, the first part aims to compare the physicochemical properties of K/NaX and K/NaY catalysts prepared similarly by ultrasound-assisted impregnation from a potassium acetate buffer solution and their catalytic performance in the transesterification of palm oil under the same condition. Moreover, the properties of the spent catalysts are compared.

Although biodiesel production has been continually developed by transesterification, a large amount of glycerol (Gly) was produced as a co-product. Hence, the industrial challenge is how to utilize glycerol for high value-added chemicals namely, acrolein by dehydration (Qureshi et al., 2019), glycerol carbonate (GC) by transesterification (She et al., 2021), and 1,3-propanediol by dehydroxylation (Tan et al., 2013).

Among the glycerol-based products, glycerol carbonate via transesterification with dimethyl carbonate has been attractive in heterogeneous catalysis by zeolites (Khanday et al., 2017), micro-mesoporous silicas (Qureshi et al., 2019; She et al., 2021), silicates (Wang et al., 2017), titanosilicate (Xiang, and Wu, 2018), and hydrotalcites (Liu et al., 2014). Although these catalysts provide high performance in reaction testing, they suffer from molecular hindrance by the diffusion limitation of reactants and forming products and accessibility of basic sites (She et al., 2021).

Accordingly, the development of catalyst morphology (e.g. pore diameters, particle sizes, and shapes) becomes one of the promising solutions to such problems. Intrinsic basic nanosized zeolites with specific morphology are interesting. Among these

nanosized zeolites, BPH-type zeolite (Linde Q) with a pore window of 0.63x0.63 nm which is larger than the optimum pore against the literature mentioned earlier (Moliner et al., 2015). Recently, BPH zeolite nanosheets with different morphologies (shapes, thickness, and particle sizes) were developed by Clatworthy et al. (2020). The nanosheet with three alkali cations (Na^+ , K^+ , and Cs^+) as intrinsic basic species was synthesized at a hydrothermal temperature of 60 °C without an organic structure-directing agent (OSDA). The BPH zeolite nanosheet could be one of the promising green catalyst candidates for the transesterification of Gly with DMC.

The second part focuses on the correlation of BPH zeolite nanosheets' morphologies and catalytic activities for transesterification between glycerol and dimethyl carbonate. The reaction factors affecting the catalytic abilities including BPH morphologies, reactant mole ratios, catalyst dosage, reaction temperature and time, and reusability are discussed as well.

1.2 Scope and limitation of the study

Regarding the first section of research, Zeolite NaX ($\text{Si}/\text{Al} = 1.2$) and Zeolite NaY ($\text{Si}/\text{Al} = 2.4$) was synthesized according to the previous verified approach (Ginter, 2016; Lechert, and Staelin, 2016). The catalysts with potassium loading of 12 wt.% were prepared by ultrasound-assisted impregnation (Rakmae et al., 2016). Transesterification of palm oil was performed according to the literature (Rakmae et al., 2016).

In the second section, BPH zeolite nanosheets with micro and nano sizes were synthesized according to the literature (Clatworthy et al., 2020). Both BPH zeolites were ion-exchanged with either potassium or cesium solution. The transesterification of glycerol and dimethyl carbonate (DMC) to yield glycerol carbonate (GC) was carried out in a heavy wall pressure vessel at atmospheric pressure.

1.3 Organization of the thesis

The thesis is divided into five chapters. This chapter is the first chapter "introduction," and it is followed by chapter II "literature reviews", which concludes the basic knowledge of transesterification of palm oil to produce biodiesel and glycerol upgrading to glycerol carbonate by transesterification. Both chapters indicate the

understanding of the purposed of this thesis. Chapter III give details of comparative properties of potassium supported on faujasite zeolite (K/NaX and K/NaY) from ultrasound-assisted impregnation and performance in transesterification of palm oil. Chapter IV presents the morphological effect of BPH zeolite nanosheets on the conversion of glycerol towards glycerol carbonate. Finally, chapter V summarizes the research finding from this thesis.

1.4 References

- Clatworthy, E. B., Debost, M., Barrier, N., Gascoin, S., Boullay, P., Vicente, A., Gilson, J.-P., Dath, J.-P., Nesterenko, N., and Mintova, S. (2020). Room-temperature synthesis of BPH zeolite nanosheets free of organic template with enhanced stability for gas separations. *ACS Applied Nano Materials*. 4 (1), 24-28.
- Ginter, D. (2016). Linde Type Y. In S. Mintova (Ed.), *Verified syntheses of zeolitic materials* (third ed., pp. 221-223): The Synthesis Commission of the International Zeolite Association.
- Hindryawati, N., Maniam, G. P., Karim, M. R., and Chong, K. F. (2014). Transesterification of used cooking oil over alkali metal (Li, Na, K) supported rice husk silica as potential solid base catalyst. *Engineering Science and Technology, an International Journal*. 17(2), 95-103.
- Khanday, W. A., Okoye, P. U., and Hameed, B. H. (2017). Biodiesel byproduct glycerol upgrading to glycerol carbonate over lithium–oil palm ash zeolite. *Energy Conversion and Management*. 151, 472-480.
- Lechert, H., and Staelin, P. (2016). Linde Type X. In S. Mintova (Ed.), *Verified syntheses of zeolitic materials* (third ed., pp. 215-217): The Synthesis Commission of the International Zeolite Association.
- Liu, P., Derchi, M., and Hensen, E. J. M. (2014). Promotional effect of transition metal doping on the basicity and activity of calcined hydrotalcite catalysts for glycerol carbonate synthesis. *Applied Catalysis B: Environmental*. 144, 135-143.
- Manadee, S., Sophiphun, O., Osakoo, N., Supamathanon, N., Kidkhunthod, P., Chanlek, N., Wittayakun, J., and Prayoonpokarach, S. (2017). Identification of potassium

- phase in catalysts supported on zeolite NaX and performance in transesterification of Jatropha seed oil. *Fuel Processing Technology*. 156, 62-67.
- Moliner, M., Martínez, C., and Corma, A. (2015). Multipore Zeolites: Synthesis and Catalytic Applications. *Angewandte Chemie International Edition*. 54(12), 3560-3579.
- Noiroj, K., Intarapong, P., Luengnaruemitchai, A., and Jai-In, S. (2009). A comparative study of KOH/Al₂O₃ and KOH/NaY catalysts for biodiesel production via transesterification from palm oil. *Renewable Energy*. 34(4), 1145-1150.
- Peña, R., Romero, R., Martínez, S. L., Natividad, R., and Ramírez, A. (2013). Characterization of KNO₃/NaX catalyst for sunflower oil transesterification. *Fuel*. 110, 63-69.
- Qureshi, B. A., Lan, X., Arslan, M. T., and Wang, T. (2019). Highly active and selective nano H-ZSM-5 catalyst with short channels along b-axis for glycerol dehydration to acrolein. *Industrial & Engineering Chemistry Research*. 58(28), 12611-12622.
- Rakmae, S., Keawkumay, C., Osakoo, N., Montalbo, K. D., de Leon, R. L., Kidkhunthod, P., Chanlek, N., Roessner, F., Prayoonpokarach, S., and Wittayakun, J. (2016). Realization of active species in potassium catalysts on zeolite NaY prepared by ultrasound-assisted impregnation with acetate buffer and improved performance in transesterification of palm oil. *Fuel*. 184, 512-517.
- She, Q. M., Huang, W. J., Talebian-Kiakalaieh, A., Yang, H., and Zhou, C. H. (2021). Layered double hydroxide uniformly coated on mesoporous silica with tunable morphologies for catalytic transesterification of glycerol with dimethyl carbonate. *Applied Clay Science*. 210.
- Sowcharoensuk, C. (2020). *Thailand industry outlook 2020-2022: Palm oil industry*. Retrieved from [https://www.krungsri.com/en/research/industry/industry-outlook/agriculture/sugar-\(1\)/IO/io-oil-palm-20-th](https://www.krungsri.com/en/research/industry/industry-outlook/agriculture/sugar-(1)/IO/io-oil-palm-20-th)
- Supamathanon, N., Wittayakun, J., and Prayoonpokarach, S. (2011). Properties of Jatropha seed oil from Northeastern Thailand and its transesterification catalyzed by potassium supported on NaY zeolite. *Journal of Industrial and Engineering Chemistry*. 17(2), 182-185.

- Tan, H. W., Abdul Aziz, A. R., and Aroua, M. K. (2013). Glycerol production and its applications as a raw material: A review. *Renewable and Sustainable Energy Reviews*. 27, 118-127.
- Tunpaiboon, N. (2021). *Industry Outlook 2021-2023: Biodiesel*. Retrieved from <https://www.krungsri.com/en/research/industry/industry-outlook/Energy-Utilities/Biodiesel/IO/io-biodiesel-21>
- Verboekend, D., Nuttens, N., Locus, R., Van Aelst, J., Verolme, P., Groen, J. C., Perez-Ramirez, J., and Sels, B. F. (2016). Synthesis, characterisation, and catalytic evaluation of hierarchical faujasite zeolites: milestones, challenges, and future directions. *Chemical Society Reviews*. 45(12), 3331-3352.
- Wang, S., Hao, P., Li, S., Zhang, A., Guan, Y., and Zhang, L. (2017). Synthesis of glycerol carbonate from glycerol and dimethyl carbonate catalyzed by calcined silicates. *Applied Catalysis A: General*. 542, 174-181.
- Xiang, M., and Wu, D. (2018). Transition metal-promoted hierarchical ETS-10 solid base for glycerol transesterification. *RSC Advances*. 8(58), 33473-33486.
- Xie, W., Huang, X., and Li, H. (2007). Soybean oil methyl esters preparation using NaX zeolites loaded with KOH as a heterogeneous catalyst. *Bioresource Technology*. 98(4), 936-939.

CHAPTER II

LITERATURE REVIEW

Literature review is divided into two parts including the improvement of K supported on FAU zeolite catalysts for transesterification of palm oil and the second part is BPH zeolite nanosheets as a catalyst on conversion of glycerol towards glycerol carbonate.

2.1 Transesterification for biodiesel production

Biodiesel (Fatty Acid Methyl Ester, FAME) is a biodegradable and renewable diesel fuel that can be made from vegetable oils or animal fats. The oils and fats consist of triglycerides that is the mainly reactant for transesterification. This is reaction between triglyceride and alcohol (methanol or ethanol) over acid or base catalysts to form FAME or biodiesel and glycerol as a co-product shown in **Figure 2.1**.

The catalysts for transesterification can be divided into three subclass such as homogeneous, heterogeneous, and enzymatic catalyst (Mohiddin et al., 2021). Although the homogeneous catalysis is faster and requires a less catalyst amount than the heterogeneous catalysts, the spent catalyst in liquid phase is difficult to separate and reuse. Moreover, the process produces a large amount of wastewater for neutralization (Rakmae et al., 2016). These problems could be avoided by using heterogeneous catalysts. Many heterogeneous base catalysts such as carbonates, alkali, metal oxides and zeolites (Perego et al., 2017; Refaat, 2011; Romero et al., 2005) are widely used in the biodiesel production. It is easy to separate the liquid product from the catalyst and they require a smaller alcohol volume than the heterogeneous acid catalysts (Muciño et al., 2016).

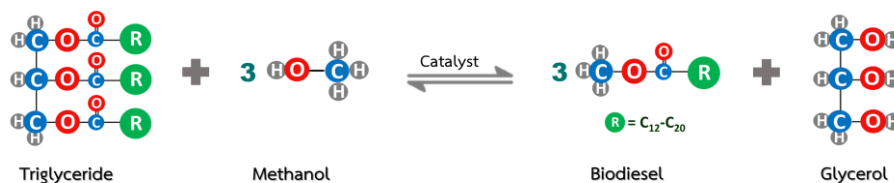


Figure 2.1 Transesterification of triglyceride and methanol.

The possible mechanism of transesterification using KOH supported on zeolite as a heterogeneous catalyst is shown in **Figure 2.2**. This reaction consists of four steps. The step (1) is the generation of methoxide ion (CH_3O^-) by proton abstraction from methanol by K_2O as a basic site of the base catalyst. In the step (2), the methoxide ion attacks the carbonyl group of triglycerides to generate a tetrahedral intermediate ion. The step (3) is rearrangement of tetrahedral intermediate to form one fatty acid methyl ester (biodiesel) and one diglyceride ion. In the next step (4a and 4b), the diglyceride ion reacts with the protonated base catalyst to create a diglyceride molecule. Then, the diglyceride reacts with another methanol to generate methoxide ion by starting the next cycle. Finally, the similar step is repeated to monoglyceride to form fatty acid methyl ester (FAME or biodiesel) and glycerol as a final product (Farobie, and Matsumura, 2017).

Currently, the research about biodiesel production from transesterification has become an interesting study. In addition, there are several researchers have focused to solve the disadvantage of homogeneous catalytic by using heterogeneous catalysts for biodiesel production.

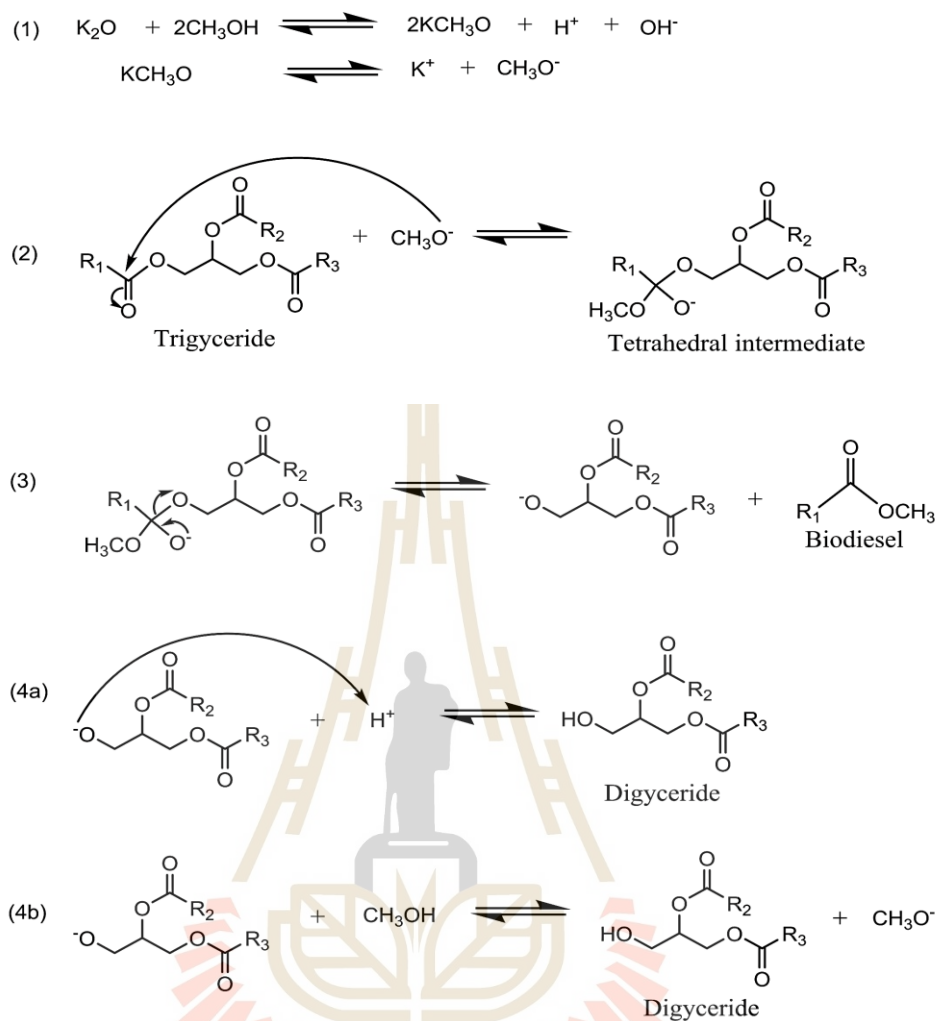


Figure 2.2 Possible reaction pathway of transesterification by KOH supported on zeolite modified from Farobie, and Matsumura (2017).

2.1.1 Potassium catalyst on faujasite (FAU) zeolite for biodiesel production

Following several reports, the potassium (K) species has been considered as one of the promising catalyst candidates for transesterification (Hindryawati et al., 2014; Rakmae et al., 2016; Supamathanon et al., 2011). The K-supported catalyst has higher basicity and better resistivity to contaminated free fatty acids in triglyceride sources than those of Li-based and Na-based catalysts (Hindryawati et al., 2014). In addition, it could be reused with fewer activity losses in the biodiesel production than that of other mentioned alkalis. Moreover, the dispersion of active

species on porous materials could improve the catalyst activity. Faujasite zeolites are among those promising materials (Verboekend et al., 2016).

Faujasite zeolites (FAU) are crystalline aluminosilicates containing sodalite cages and supercages with pore diameter of 0.74 nm as shown in **Figure 2.3**. The faujasite can be classified into two types including zeolite X and Y base on the chemical compositions (Barthomeuf, 1996). Si/Al ratios of zeolite X and Y are 1-1.5 and 2-5, respectively. The presence of aluminum in the zeolite structure requires an equal amount of extraframework cations for charge balancing. Moreover, the basic properties of zeolite NaX is higher than zeolite NaY. The different Si/Al ratio leads to different basicity and reactivity (Ma et al., 2021). In many applications such as the transesterification for biodiesel production, zeolite X and Y are used owing to an easy synthesis, high surface area and large pore volume, stability, and their well-defined framework (Polisi et al., 2019; Zito et al., 2015).

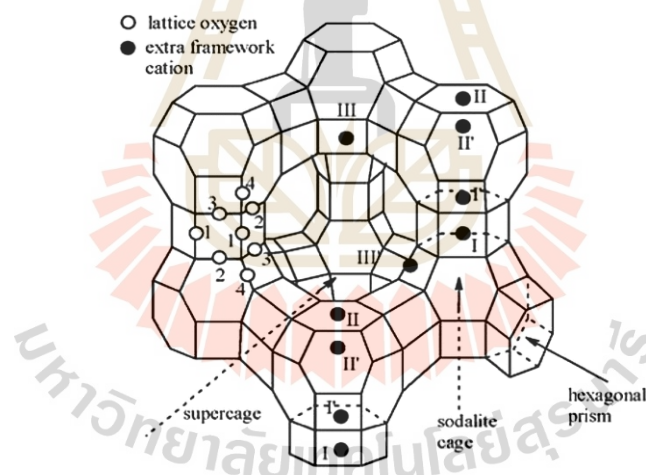


Figure 2.3 Faujasite (FAU) zeolite structure and positions of their potential charge compensating cations (Yang et al., 2014).

From the literature review, there are several works on catalysts with potassium supported on NaX and NaY for transesterification of various oils such as palm, soybean, sunflower, and Jatropha. Intarapong et al. (2011) prepared KOH supported on zeolite NaY. The KOH/NaY catalysts were prepared by an impregnation method with various KOH concentrations (5-20 wt.%). The catalysts were studied in

the transesterification of palm oil. The catalyst with 15 wt.% KOH loading provided the highest biodiesel yield of 92.2% at 60 °C in 7 h. However, the structure of zeolite NaY collapsed with an increase of the K content. To prevent the structure collapse, Supamathanon et al. (2011) prepared K catalysts supported on zeolite NaY by impregnation using CH₃COOK buffer solution as a precursor. This acetate buffer solution was employed in order to prevent the collapse of the zeolite framework. The prepared catalysts were applied in the transesterification of Jatropha seed oil. The optimum catalyst with K loading of 12 wt.% provided high biodiesel yield of 73.4% under the reaction temperature of 65 °C in 3 h. To further increase the catalytic performance, Manadee et al. (2017) changed faujasite-type zeolite from NaY to NaX as a support for potassium loading (K/NaX) by impregnation with various K content (4-16 wt.%) of CH₃COOK buffer solution for transesterification of Jatropha seed oil. Interestingly, the obtained catalyst with 12 wt.% K loading gave biodiesel yield of 83% in 3 h. From our previous results of transesterification of Jatropha seed oil catalyzed by the same K loading, zeolite NaX exhibits better catalytic activity than zeolite NaY probably due to higher basicity of zeolite NaX compared to another.

According to the previous work, both zeolite NaY and NaX were used as catalyst supports for various K species. However, stability against leaching has not been clearly studied. Moreover, the surface interaction between K species and support is still unclear. In similar case, Castro et al. (2013) studied the influence of supports on basicity and stability of Li-based catalyst for the transesterification of methyl acetate and ethanol. The basicity of prepared catalyst was ranged in the following order: Li/MgAl oxide > Li/Al₂O₃ > Li/MgO. In addition, the stability in term of Li leaching was ranged in the following order: Li/MgO > Li/MgAl oxide > Li/Al₂O₃. From the reaction testing, Li/MgAl oxide was the best catalyst. This literature suggested that Al species played an important role to enhance the basicity and minimize leaching of active species.

There are not many reports about the effect of Si/Al molar ratio on catalyst stability and active species leaching. Thus, the work is aimed to compare the effect of zeolite supports for the preparation of K/NaX and K/NaY by ultrasound-

assisted impregnation using an acetate buffer as potassium precursor. Their catalytic activity for transesterification of palm oil is also evaluated.

2.1.2 Ultrasound-assisted impregnation for catalyst preparation

Although the microporous material and zeolite provide excellent textural properties such as high surface area and large micropore volumes, they also limit the diffusion of chemical precursor for conventional wet impregnation inside the pore zeolite. Thus, the sonication is used to solve this problem.

Ultrasound vibration has been recognized as green techniques for catalysts preparation and modification of materials. It could be improved the mass transfer of precursor, dispersion of active species, and reducing synthesis time (Dehghani, and Haghghi, 2017; Louyot et al., 2018; Sosa et al., 2020). Ultrasound irradiation causes acoustic cavitation providing the bubble formation, growth, and collapse of hot gas bubbles in a liquid system as shown in **Figure 2.4**. Then, the collapsed bubbles increase temperature and pressure, which assist the diffusion of the precursor into support pores and improve surface interaction. Louyot et al. (2018) synthesized Co/Al₂O₃ and Fe-Co/Al₂O₃ catalyst for Fischer-Tropsch reaction and compared the total time for catalyst preparation by impregnation. The catalyst prepared with sonication, reducing the impregnation time from 12 h to 4 h and the particle size smaller than without sonication. In addition, Rakmae et al. (2016) compared the preparation of K catalysts supported on zeolite NaY with and without sonication during the impregnation using CH₃COOK buffer solution with 12 wt.% of K loading. The results indicated that the catalyst produced with sonication showed better dispersion of active species than that without sonication. For the transesterification of palm oil, the catalyst prepared by sonication provided a higher biodiesel yield and shorter reaction time than that produced without sonication. Hence, it is proposed in this work to shorten the K/FAU catalyst preparation time using ultrasound-assisted impregnation.

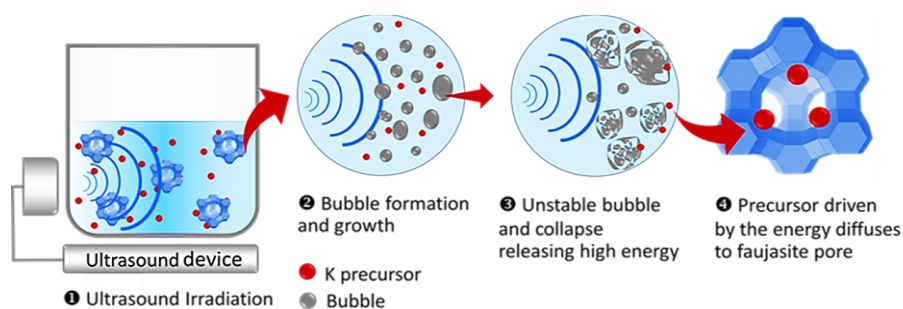


Figure 2.4 Ultrasound-assisted impregnation of K precursor on zeolite support.

2.2 Glycerol upgrading to glycerol carbonate by transesterification

2.2.1 Transesterification of glycerol and dimethyl carbonate

Nowadays, many worldwide industries have been looking forward to alternative and renewable energy resources instead of limited fossil fuels. Accordingly, this leads to the remarkable expansion of biomass-based fuel and chemical production, especially biodiesel from vegetable oils and animal fats. This process generates larger glycerol amount than the global demand (Li et al., 2018). There are several attempts to convert glycerol as an initial reactant to value-added chemicals such as glycerol ethers, solketal, acrolein, propanediol, and glycerol carbonate through different chemical reactions as shown in **Figure 2.5** (Bagheri et al., 2015; Houache et al., 2019; Marakatti et al., 2014).

Among these glycerol-derived fine chemicals mentioned above, glycerol carbonate (4-hydroxymethyl-1,3-dioxolan-2-one) has been considered in much industrial utilization such as cosmetic ingredients, electrolyte for lithium-ion batteries and detergent components as shown in **Figure 2.6**. Moreover, it can be used as a platform chemical to produce other reaction intermediates, surfactants, and plasticizers because of its active two functional groups including hydroxyl and 2-oxo-1,3-dioxolane. Hence, several research groups have optimized different types of reaction to achieve a satisfactory quantity of this interesting chemical.

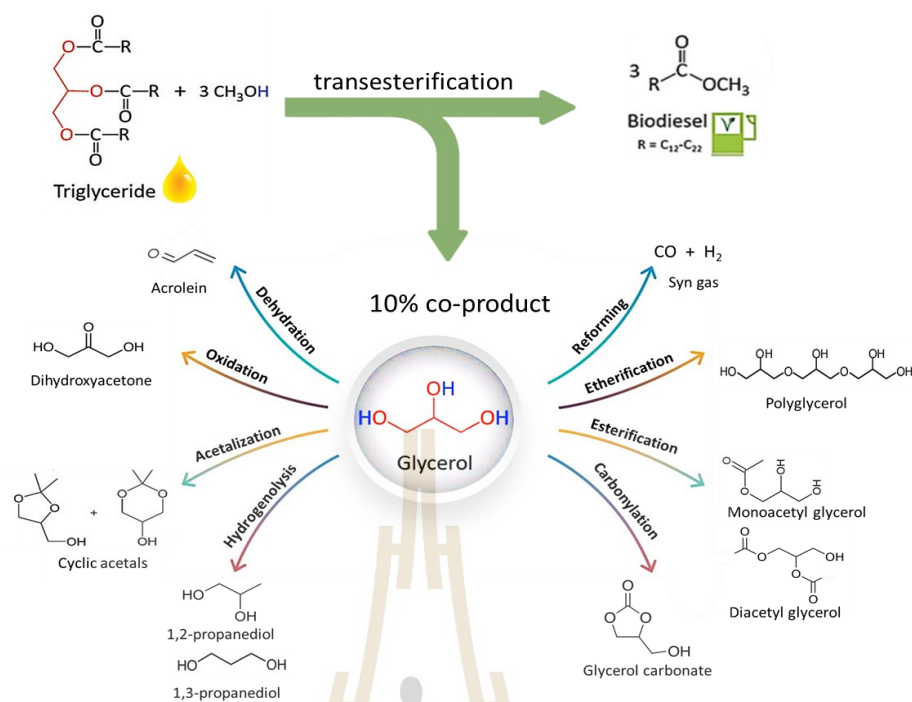


Figure 2.5 Different catalytic transformations of glycerol into value-added compounds are presented after the transesterification reaction for biodiesel and glycerol production (Houache et al., 2019; Sudarsanam et al., 2019).

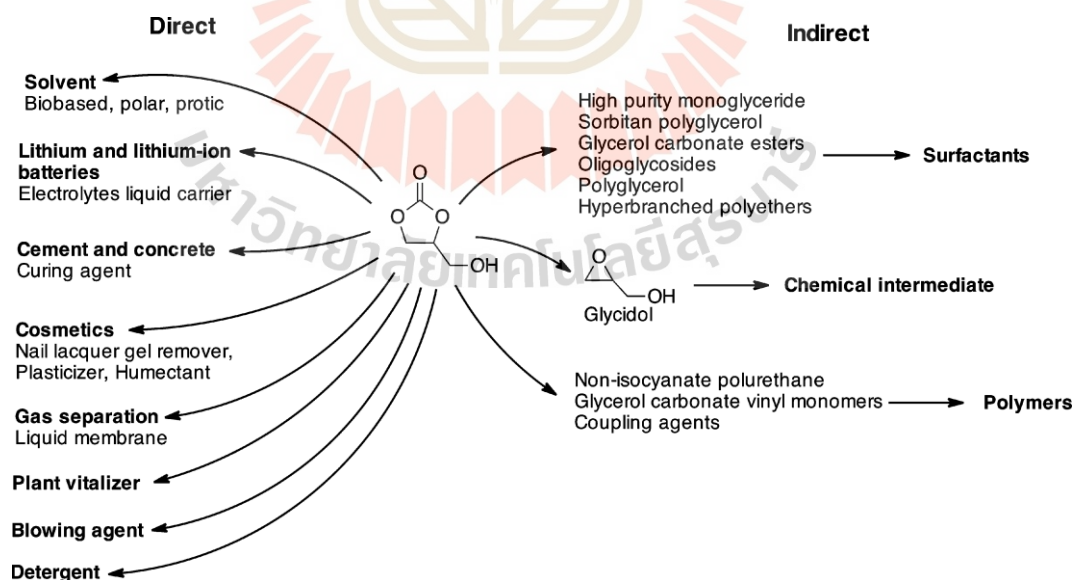


Figure 2.6 Direct and indirect applications of glycerol carbonate (Sonnati et al., 2013).

Many chemical routes to produce glycerol carbonate have been considered, namely, transesterification with alkyl carbonate, carbonylation with phosgene, urea, carbon dioxide. Among these processes, the reaction of glycerol with dimethyl carbonate is applicable to prepare glycerol carbonate due to non-toxic raw materials, required mild operating conditions, high yield, and simple purification of glycerol carbonate (Das, and Mohanty, 2019; Liu et al., 2015). The possible mechanism of base catalyst catalyzed transesterification of glycerol with dimethyl carbonate (DMC) is shown in **Figure 2.7**. In the first step, the basic site on the surface of catalyst attacks with a proton from the primary hydroxyl group of glycerol to produce glyceroxide anion. In the second step, the carbonyl group of DMC is attacked with nucleophilic of glyceroxide anion to generate intermediate and methoxide as a co-product. Then, methoxide reacts with the proton on the basic site to get the methanol. Finally, the intermediate reacts with basic site to form anion leading to a cyclization reaction through a nucleophilic reacted with oxygen from the secondary hydroxyl group to carbonyl group productive glycerol carbonate and methanol. In term of reaction operation, various heterogeneous catalysts are proposed to facilitate the transesterification of according to their excellent catalytic activities to provide high yield and satisfactory selectivity to glycerol carbonate, for example; Li/Mg₄AlO_{5,5} (Liu et al., 2015), Na₂SiO₃ (Wang et al., 2017), CaO (Roschat et al., 2018), K-zeolite (Algoufi, and Hameed, 2014), zeolite beta, and zeolite FAU (Pan et al., 2012).

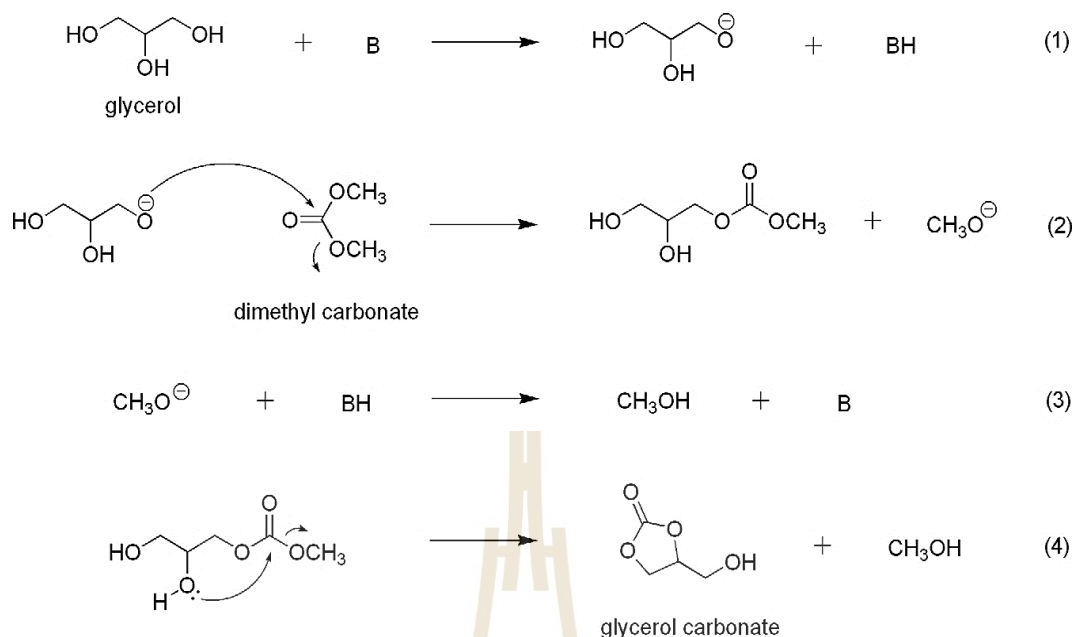


Figure 2.7 Possible mechanism of base catalyst catalyzed transesterification of glycerol with DMC (Ochoa-Gómez et al., 2009).

2.2.2 Zeolite catalysts for glycerol carbonate production

From this literature survey, there are many heterogeneous catalysts such as CaO, Li/Mg₄AlO_{5.5}, Na₂SiO₃, Li/OPAZ, red mud, beta zeolite and NaY zeolite (Das, and Mohanty, 2019; Khanday et al., 2017; Liu et al., 2015; Ochoa-Gómez et al., 2009; Pan et al., 2012; Wang et al., 2017). These catalysts show the high conversion and selectivity in the first cycle. However, the activity decreased after reusability. Although the zeolite catalysts shown lower conversion. But its resists the leaching of active sites into the liquid product and intrinsic base property. Therefore, zeolite is proposed by many works to improve this drawback.

The zeolites composed of crystalline aluminosilicate, consisting of (SiO₄)⁴⁻ and (AlO₄)³⁻ tetrahedral units, sharing oxygen atom between every two consecutive units. Zeolite consists of different basic and acid site with different synthesis method. The strength of basic site of zeolite increase with increasing Al content (Al-Ani et al., 2019). In addition, zeolite have large surface area, well pore size, and shape selectivity. Moreover, pore diameter of zeolites in the transesterification of glycerol and DMC should be larger than the molecular dimension of reagents to

improve mass transfer. Geometrical parameters of reagent molecules from the reaction are calculated using ChemOffice as shown in **Table 2.1**.

Table 2.1 Geometrical parameters of reagent molecules (Pan et al., 2012).

Reagents	Geometrical parameter (nm)	
	Diameter	Length
Dimethyl carbonate (DMC)	0.37	0.45
Glycerol (Gly)	0.47	0.52
Glycerol carbonate (GC)	0.33	0.65

From previous studies in the glycerol upgrading, zeolite-based and mesoporous catalysts with different pore sizes are reported. Pan et al. (2012) studied the activity of different base zeolites for the transesterification between glycerol and DMC as shown in **Table 2.2**. The zeolites with a small pore diameter show poor activity due to pore hindrance and space limitation of the reagent diffusion. The result suggested that NaY was more active than beta zeolite due to larger pore diameter and higher number of basic sites.

Table 2.2. Synthesis of GC from glycerol and DMC over various zeolite catalysts (Pan et al., 2012).

Catalyst	Basicity (mmol/g)	Ring	Pore channel (nm)	Gly conversion (%)	GC selectivity (%)
3A	1.02	8	0.31x0.35	0	0
4A	1.02	8	0.41x0.41	0	0
NaZSM-5	0.63	10	0.51x0.55, 0.53x0.56	0	0
Na β	0.64	12	0.66x0.67, 0.56x0.56	37	100
NaY	4.20	12	0.74x0.74	80	100

Reaction conditions: glycerol 54.3 mmol, DMC 162.9 mmol, CH₃OH 10 mL, catalyst 0.5 g, 343 K, 4 h.

For the conversion of the glycerol towards glycerol carbonate, the proper pore size of porous catalysts is not only preferable, but their shapes and particle sizes are also necessary. Mesoporous silicas containing layered double hydroxides (LDH) were proposed as nanosized composites for transesterification between Gly and DMC in three distinct forms such as rice shape, short and long rods (She et al., 2021). The rice-shaped catalyst with shorter meso-channels improved the internal diffusion pathlengths of both reactants and reaction products. Moreover, the nanosized composite with the highest surface area has a high density of surface basic sites, indicating that it might be used for catalysis. Hence, the transesterification could be a morphology-dependent reaction. BPH-type zeolite (Linde Q) with the pore window of 0.63×0.63 nm which is larger than the optimum pore against the literature mentioned earlier (Moliner et al., 2015). Recently, Clatworthy et al. (2020) prepared BPH zeolite nanosheets with various morphologies (shapes, thicknesses, and particle sizes). The zeolite nanosheet containing three alkali cations (Na^+ , K^+ , and Cs^+) as intrinsic basic species was synthesized without the presence of an organic structure-directing agent (OSDA) at a hydrothermal temperature less than 60 °C. The BPH zeolite nanosheet could be one of the promising green catalyst candidates for the transesterification of Gly with DMC.

2.2.3 Improvement of zeolite basicity by ion-exchange method

Ion exchange is a chemical reaction that exchanges free mobile ions of a solid, the ion exchanger, for other ions of comparable charge in solution. Usually, the presence of cations on its channels and cages resulted in the ion exchange property of zeolites. There are numerous cation sites in zeolite structures that differ in framework location and bond energy. When the zeolite contacts with an electrolytic solution, its cations leave and are replaced by cations from the solution. Moreover, the exchange is performed with specific concentration of metal ions and zeolite solid suspension in nitrate, chloride, sulfate, and hydroxide solution. It can be employed to different types of zeolites. Ion-exchange has been extensively used in zeolite for several applications (Kumar, and Jain, 2013). In the transesterification, there are several reports using zeolite as base catalysts and support (Al-Ani et al., 2018; Al-Ani et al., 2019; Algoufi, and Hameed, 2014). The zeolite is synthesized by base conditions using

alkali ions such as Na^+ , K^+ form. To improve the intrinsic basicity, the zeolites can be exchanged with other alkali ions (Li^+ , Cs^+) by either ion-exchange method (Al-Ani et al., 2019; Danuthai et al., 2011) or direct synthesis prepared zeolite NaX and NaY exchanged with K^+ , Cs^+ , gismondine with maximum aluminium P (KMAP) in a K form (Al-Ani et al., 2019). These zeolite catalysts were employed for the transesterification of rapeseed oil and methanol. They suggested that the zeolite basicity was improved by increasing Al content with a high electropositivity of alkali cations ($\text{Cs} > \text{K} > \text{Na}$). This also enhanced the reaction activity (Joshi et al., 2003).

2.3 Passible pathway of catalyst deactivation

In transesterification, the efficiency of catalyst is evaluated in terms of activity and lifetime. Thus, catalyst stability and deactivation in the reaction have been studied. In case of K-based catalysts, the main cause of catalyst deactivation can be classified as shown in **Figure 2.8**, **Figure 2.9**, and **Table 2.3** (Čapek et al., 2014; Kosawatthanakun et al., 2022; Muciño et al., 2016; Oueda et al., 2017).

Table 2.3 Causes of K-based catalysts deactivation on transesterification.

Nature	Type	Mechanism	Description
Physical	Fouling	Lack of accessibility	Physical deposition of chemical species onto catalyst surface or pore.
Physical	Agglomeration	Lack of accessibility	Increase of particle size
Chemical	Leaching	Loss of active species	Dissolution of active species into the reaction medium.

Fouling is defined as the physical deposition of organic compound from the reaction onto the catalyst surface, resulting in activity loss owing to active site and pore blockage. Muciño et al. (2016) studied the deactivation of alkali metal precursor impregnated on NaX zeolite ($\text{K}_2\text{O}/\text{NaX}$ and $\text{Na}_2\text{O}/\text{NaX}$) catalysts in safflower oil transesterification at 60 °C. They found that the methyl ester yield of the unwashed catalyst in a second cycles dramatically decreased from 94% to 24% due to organic

moiety deposition on the catalyst surface. It confirmed by using the FTIR technique, indicating the band at 3347 (O-H), 2923, 2853, 1744 (C=O), and 1377 cm^{-1} are assigned to the glycerol and methyl ester. Moreover, the organic residue from liquid product affected to particles agglomeration, corresponding to increasing of particles size by SEM analysis. In this context, there are several works have been conducted to solve the problem by using some solvent (methanol, acetone, hexane, etc.) for washing the catalyst between testing cycles.

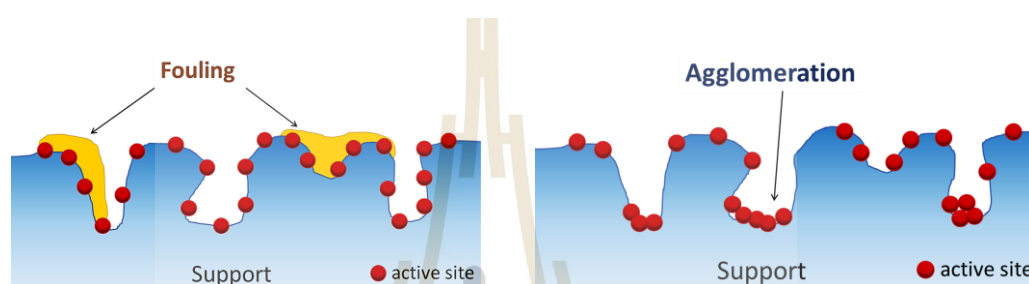


Figure 2.8 Fouling and agglomeration of catalyst modified from Moulijn et al. (2008).

Leaching is the dissolution of active species into a reaction medium as illustrated in **Figure 2.9**. In general, a leaching effect can be classified to three possible scenarios (Arends, and Sheldon, 2001; Sheldon et al., 1998) as follows:

- 1) The active species leaches but is an inactive homogeneous catalyst.
- 2) The active species leaches and behaves an active homogeneous one.
- 3) The active species does not leach and exhibits a catalytic manner.

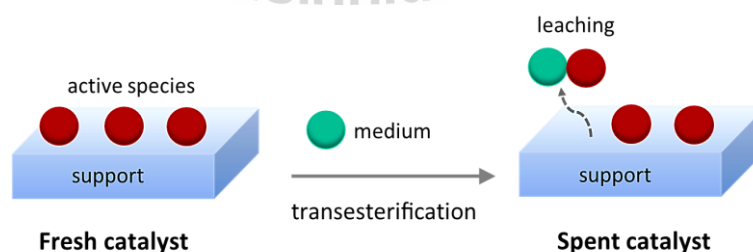


Figure 2.9 Leaching of active species into the reaction medium modified from Moulijn et al. (2008).

The unclear question of zeolite FAU supported potassium species is whether they are actually heterogeneous in nature. Despite being reused numerous times, supported catalysts maintained significant activity. These catalysts may serve as a reservoir of active species that are progressively released into the liquid phase. Several publications have reported potassium species leaching from K-based catalysts in the case of non-zeolite NaY as a support, such as Al_2O_3 , MgO , or cinder. Alonso et al. (2007) reported that KAlO_2 -like species on $\gamma\text{-Al}_2\text{O}_3$ support could react with methanol to form a dissolved component during reaction operation. The leaching species as homogeneous catalyst was responsible to the reaction. Liu et al. (2011) reported glycerol was a main possibility for releasing some potassium amount from surface of K_2CO_3 impregnated on cinder ($\text{K}_2\text{CO}_3/\text{cinder}$) after reaction time of 9 h. Čapek et al. (2014) also suggested the proposed mechanism of potassium leaching caused by the reaction with glycerol to form potassium glyceroxide which further reacted with either water or methanol. In addition, they described listed in **Table 2.4** the active species could be released with different alcohols in the following order: glycerol > 1,3-propanediol > 1,2-propanediol > ethylene glycol > methanol > methyl ester > oil > water. Thus, glycerol plays an important role in K leaching during transesterification. The loss of K active species affects poor catalytic activity and stability for further cycles. This leads to a motivation for this work to further explore the minimization of leaching of active species. To solve the leaching problem for transesterification reaction, several factors should be verified including solvents and interaction between a support and active species. This leads to further study to improve catalyst stability for industrial benefits. Among approaches for leaching study in heterogeneous catalysis, hot filtration is one of effective strategies.

Table 2.4 Leaching of K from various support into various medium (Čapek et al., 2014).

Medium	K leaching (wt.%)		
	K-Al ₂ O ₃	K-CaO	K-MgO
Water	1.22	1.30	1.05
Oil	1.09	0.56	0.90
Methyl ester	2.44	1.45	2.97
Methanol	3.54	2.82	4.47
Ethylene glycol	29.99	28.36	31.65
1,2-Propanediol	35.55	34.77	34.76
1,3-Propanediol	46.74	51.22	49.45
Glycerol	48.70	56.08	53.06

The hot filtration test, also known as the split test, is used to determine the presence of soluble active species. The solid catalysts are filtered out of the reaction mixture and the hot filtrate is monitored for continuing activity under the same reaction condition. Both of filtrate and solid catalyst are adopted to quantify content of leached active species by means of atomic absorption spectrometry (AAS) (Arzamendi et al., 2007; Rakmae et al., 2016), inductively coupled plasma-atomic emission spectrometry (ICP-AES) (Alonso et al., 2007; Shan et al., 2016), and X-ray fluorescence spectrometry (XRF) (Noiroj et al., 2009). For example case of hot filtration test, Xu et al. (2015) applied hot filtration to study Fe leaching from Mg-Fe layered double oxide (Mg-Fe LDO) which was a catalyst for the transesterification of microalgae oil. The hot filtration was performed after the regular reaction procedure for 30 min with ester conversion of 41.7%. The reaction was interrupted immediately by filtration and transferred to another reactor at the same temperature for another 1 h. As shown in **Figure 2.10**, the experimental result from ICP-AES analysis indicated there was the leaching of active Fe ions. Moreover, the catalyst after filtration was still active for the reaction producing the conversion of 64.5%.

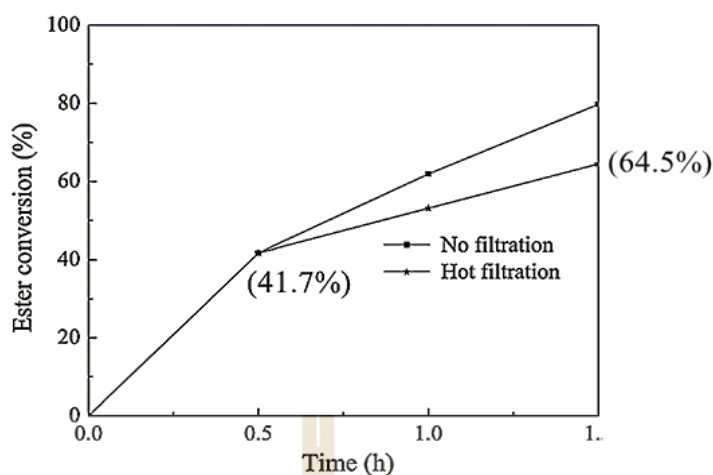


Figure 2.10 Application of hot filtration to the Mg–Fe layered double oxide catalyst for the transesterification (Xu et al., 2015).

According to the previous works, there are crucial parameters to further clarify including catalyst reusability and leaching. Consequently, it will be focused on this work to study the leaching of K species from K/NaY and K/NaX to understand the effect of media (such as oil, methanol, biodiesel, and glycerol) and interaction between K species and the supports.

2.4 References

- Al-Ani, A., Darton, R. J., Sneddon, S., and Zholobenko, V. (2018). Nanostructured zeolites: the introduction of intracrystalline mesoporosity in basic faujasite-type catalysts. *ACS Applied Nano Materials*. 1(1), 310-318.
- Al-Ani, A., Mordvinova, N. E., Lebedev, O. I., Khodakov, A. Y., and Zholobenko, V. (2019). Ion-exchanged zeolite P as a nanostructured catalyst for biodiesel production. *Energy Reports*. 5, 357-363.
- Algoufi, Y. T., and Hameed, B. H. (2014). Synthesis of glycerol carbonate by transesterification of glycerol with dimethyl carbonate over K-zeolite derived from coal fly ash. *Fuel Processing Technology*. 126, 5-11.

- Alonso, D. M., Mariscal, R., Moreno-Tost, R., Poves, M. D. Z., and Granados, M. L. (2007). Potassium leaching during triglyceride transesterification using $K/\gamma\text{-Al}_2\text{O}_3$ catalysts. *Catalysis Communications*. 8(12), 2074-2080.
- Arends, I. W. C. E., and Sheldon, R. A. (2001). Activities and stabilities of heterogeneous catalysts in selective liquid phase oxidations: recent developments. *Applied Catalysis A: General*. 212(1-2), 175-187.
- Arzamendi, G., Campo, I., Arguñarena, E., Sánchez, M., Montes, M., and Gandía, L. M. (2007). Synthesis of biodiesel with heterogeneous NaOH/alumina catalysts: Comparison with homogeneous NaOH. *Chemical Engineering Journal*. 134(1), 123-130.
- Bagheri, S., Julkapli, N. M., and Yehye, W. A. (2015). Catalytic conversion of biodiesel derived raw glycerol to value added products. *Renewable and Sustainable Energy Reviews*. 41, 113-127.
- Barthomeuf, D. (1996). Basic zeolites: characterization and uses in adsorption and catalysis. *Catalysis Reviews*. 38(4), 521-612.
- Čapek, L., Hájek, M., Kutálek, P., and Smoláková, L. (2014). Aspects of potassium leaching in the heterogeneously catalyzed transesterification of rapeseed oil. *Fuel*. 115, 443-451.
- Castro, C. S., Ferreti, C., Di Cosimo, J. I., and Assaf, J. M. (2013). Support influence on the basicity promotion of lithium-based mixed oxides for transesterification reaction. *Fuel*. 103, 632-638.
- Clatworthy, E. B., Debost, M., Barrier, N., Gascoïn, S., Boullay, P., Vicente, A., Gilson, J.-P., Dath, J.-P., Nesterenko, N., and Mintova, S. (2020). Room-temperature synthesis of BPH zeolite nanosheets free of organic template with enhanced stability for gas separations. *ACS Applied Nano Materials*. 4 (1), 24-28.
- Danuthai, T., Sooknoi, T., Jongpatiwut, S., Rirksomboon, T., Osuwan, S., and Resasco, D. E. (2011). Effect of extra-framework cesium on the deoxygenation of methylester over CsNaX zeolites. *Applied Catalysis A General*. 409-410, 74-81.
- Das, B., and Mohanty, K. (2019). A green and facile production of catalysts from waste red mud for the one-pot synthesis of glycerol carbonate from glycerol. *Journal of Environmental Chemical Engineering*. 7(1), 102888.

- Dehghani, S., and Haghghi, M. (2017). Sono-sulfated zirconia nanocatalyst supported on MCM-41 for biodiesel production from sunflower oil: Influence of ultrasound irradiation power on catalytic properties and performance. *Ultrasonics Sonochemistry*. 35, 142-151.
- Farobie, O., and Matsumura, Y. (2017). State of the art of biodiesel production under supercritical conditions. *Progress in Energy and Combustion Science*. 63, 173-203.
- Hindryawati, N., Maniam, G. P., Karim, M. R., and Chong, K. F. (2014). Transesterification of used cooking oil over alkali metal (Li, Na, K) supported rice husk silica as potential solid base catalyst. *Engineering Science and Technology, an International Journal*. 17(2), 95-103.
- Houache, M. S. E., Hughes, K., and Baranova, E. A. (2019). Study on catalyst selection for electrochemical valorization of glycerol. *Sustainable Energy & Fuels*. 3(8), 1892-1915.
- Intarapong, P., Luengnaruemitchai, A., and Jai-In, S. (2011). Transesterification of palm oil over KOH-NaY zeolite in a packed-bed reactor. *International Journal Of Renewable Energy Research*. 1, 271-280.
- Joshi, U. D., Joshi, P. N., Tamhankar, S. S., Joshi, V. V., Rode, C. V., and Shiralkar, V. P. (2003). Effect of nonframework cations and crystallinity on the basicity of NaX zeolites. *Applied Catalysis A: General*. 239(1), 209-220.
- Khanday, W. A., Okoye, P. U., and Hameed, B. H. (2017). Biodiesel byproduct glycerol upgrading to glycerol carbonate over lithium-oil palm ash zeolite. *Energy Conversion and Management*. 151, 472-480.
- Kosawatthanakun, S., Pansakdanon, C., Sosa, N., Chanlek, N., Roessner, F., Prayoonpokarach, S., and Wittayakun, J. (2022). Comparative properties of K/NaX and K/NaY from ultrasound-assisted impregnation and performance in transesterification of palm oil. *ACS Omega*. 7(11), 9130-9141.
- Kumar, S., and Jain, S. (2013). History, Introduction, and Kinetics of Ion Exchange Materials. *Journal of Chemistry*. 2013, 957647.

- Li, Z., Yan, J., Sun, J., Xu, P., Ma, C., and Gao, C. (2018). Production of value-added chemicals from glycerol using in vitro enzymatic cascades. *Communications Chemistry*. 1(1), 71.
- Liu, H., Su, L., Liu, F., Li, C., and Solomon, U. U. (2011). Cinder supported K_2CO_3 as catalyst for biodiesel production. *Applied Catalysis B: Environmental*. 106(3), 550-558.
- Liu, Z., Wang, J., Kang, M., Yin, N., Wang, X., Tan, Y., and Zhu, Y. (2015). Structure-activity correlations of $LiNO_3/Mg_4AlO_{5.5}$ catalysts for glycerol carbonate synthesis from glycerol and dimethyl carbonate. *Journal of Industrial and Engineering Chemistry*. 21, 394-399.
- Louyot, P., Neagoe, C., Galli, F., Pirola, C., Patience, G. S., and Boffito, D. C. (2018). Ultrasound-assisted impregnation for high temperature Fischer-Tropsch catalysts. *Ultrasonics Sonochemistry*. 48, 523-531.
- Ma, Y.-K., Rigolet, S., Michelin, L., Paillaud, J.-L., Mintova, S., Khoerunnisa, F., Daou, T. J., and Ng, E.-P. (2021). Facile and fast determination of Si/Al ratio of zeolites using FTIR spectroscopy technique. *Microporous and Mesoporous Materials*. 311.
- Manadee, S., Sophiphun, O., Osakoo, N., Supamathanon, N., Kidkhunthod, P., Chanlek, N., Wittayakun, J., and Prayoonpokarach, S. (2017). Identification of potassium phase in catalysts supported on zeolite NaX and performance in transesterification of Jatropha seed oil. *Fuel Processing Technology*. 156, 62-67.
- Marakatti, V. S., Halgeri, A. B., and Shanbhag, G. V. (2014). Metal ion-exchanged zeolites as solid acid catalysts for the green synthesis of nopol from Prins reaction. *Catalysis Science & Technology*. 4(11), 4065-4074.
- Mohiddin, M. N. B., Tan, Y. H., Seow, Y. X., Kasedo, J., Mubarak, N. M., Abdullah, M. O., Chan, Y. S., and Khalid, M. (2021). Evaluation on feedstock, technologies, catalyst and reactor for sustainable biodiesel production: A review. *Journal of Industrial and Engineering Chemistry*. 98, 60-81.
- Moliner, M., Martínez, C., and Corma, A. (2015). Multipore Zeolites: Synthesis and Catalytic Applications. *Angewandte Chemie International Edition*. 54(12), 3560-3579.

- Moulijn, J. A., van Diepen, A. E., and Kapteijn, F. (2008). Deactivation and Regeneration. In Gerhard Ertl, Helmut Knözinger, Ferdi Schüth, and J. Weitkamp (Eds.), *Handbook of Heterogeneous Catalysis* (second ed., Vol. 1, pp. 1829-1845). Germany: Wiley-VCH Verlag.
- Muciño, G. E. G., Romero, R., García-Orozco, I., Serrano, A. R., Jiménez, R. B., and Natividad, R. (2016). Deactivation study of K_2O/NaX and Na_2O/NaX catalysts for biodiesel production. *Catalysis Today*. 271, 220-226.
- Noiroj, K., Intarapong, P., Luengnaruemitchai, A., and Jai-In, S. (2009). A comparative study of KOH/Al_2O_3 and KOH/NaY catalysts for biodiesel production via transesterification from palm oil. *Renewable Energy*. 34(4), 1145-1150.
- Ochoa-Gómez, J. R., Gómez-Jiménez-Aberasturi, O., Maestro-Madurga, B., Pesquera-Rodríguez, A., Ramírez-López, C., Lorenzo-Ibarreta, L., Torrecilla-Soria, J., and Villarán-Velasco, M. C. (2009). Synthesis of glycerol carbonate from glycerol and dimethyl carbonate by transesterification: Catalyst screening and reaction optimization. *Applied Catalysis A: General*. 366(2), 315-324.
- Oueda, N., Bonzi-Coulibaly, Y. L., and Ouédraogo, I. W. (2017). Deactivation processes, regeneration conditions and reusability performance of CaO or MgO based catalysts used for biodiesel production—a review. *Materials Sciences and Applications*. 8(01), 94.
- Pan, S., Zheng, L., Nie, R., Xia, S., Chen, P., and Hou, Z. (2012). Transesterification of glycerol with dimethyl carbonate to glycerol carbonate over Na-based zeolites. *Chinese Journal of Catalysis*. 33(11), 1772-1777.
- Perego, C., Bosetti, A., Ricci, M., and Millini, R. (2017). Zeolite materials for biomass conversion to biofuel. *Energy and Fuels*. 31(8), 7721-7733.
- Polisi, M., Grand, J., Arletti, R., Barrier, N., Komaty, S., Zaarour, M., Mintova, S., and Vezzalini, G. (2019). CO_2 adsorption/desorption in FAU zeolite nanocrystals: in situ synchrotron X-ray powder diffraction and in situ Fourier transform infrared spectroscopic study. *The Journal of Physical Chemistry C*. 123(4), 2361-2369.
- Rakmae, S., Keawkumay, C., Osakoo, N., Montalbo, K. D., de Leon, R. L., Kidkhunthod, P., Chanlek, N., Roessner, F., Prayoonpokarach, S., and Wittayakun, J. (2016). Realization of active species in potassium catalysts on zeolite NaY prepared by

- ultrasound-assisted impregnation with acetate buffer and improved performance in transesterification of palm oil. *Fuel*. 184, 512-517.
- Refaat, A. A. (2011). Biodiesel production using solid metal oxide catalysts. *International Journal of Environmental Science & Technology*. 8(1), 203-221.
- Romero, M. D., Ovejero, G., Rodríguez, A., and Gómez, J. M. (2005). Enhancement of the basic properties in FAU zeolites by impregnation with cesium hydroxide. *Microporous and Mesoporous Materials*. 81(1-3), 313-320.
- Roschat, W., Phewphong, S., Kaewpuang, T., and Promarak, V. (2018). Synthesis of glycerol carbonate from transesterification of glycerol with dimethyl carbonate catalyzed by CaO from natural sources as green and economical catalyst. *Materials Today: Proceedings*. 5(6), 13909-13915.
- Shan, R., Shi, J., Yan, B., Chen, G., Yao, J., and Liu, C. (2016). Transesterification of palm oil to fatty acids methyl ester using K_2CO_3 /palygorskite catalyst. *Energy Conversion and Management*. 116, 142-149.
- She, Q. M., Huang, W. J., Talebian-Kiakalaieh, A., Yang, H., and Zhou, C. H. (2021). Layered double hydroxide uniformly coated on mesoporous silica with tunable morphologies for catalytic transesterification of glycerol with dimethyl carbonate. *Applied Clay Science*. 210.
- Sheldon, R. A., Wallau, M., Arends, I. W. C. E., and Schuchardt, U. (1998). Heterogeneous catalysts for liquid-phase oxidations: Philosophers' stones or Trojan horses? *Accounts of Chemical Research*. 31(8), 485-493.
- Sonnati, M. O., Amigoni, S., Taffin de Givenchy, E. P., Darmanin, T., Choulet, O., and Guittard, F. (2013). Glycerol carbonate as a versatile building block for tomorrow: synthesis, reactivity, properties and applications. *Green Chemistry*. 15(2), 283-306.
- Sosa, N., Chanlek, N., and Wittayakun, J. (2020). Facile ultrasound-assisted grafting of silica gel by aminopropyltriethoxysilane for aldol condensation of furfural and acetone. *Ultrasonics Sonochemistry*. 62, 104857.
- Sudarsanam, P., Peeters, E., Makshina, E. V., Parvulescu, V. I., and Sels, B. F. (2019). Advances in porous and nanoscale catalysts for viable biomass conversion. *Chemical Society Reviews*. 48(8), 2366-2421.

- Supamathanon, N., Wittayakun, J., and Prayoonpokarach, S. (2011). Properties of Jatropha seed oil from Northeastern Thailand and its transesterification catalyzed by potassium supported on NaY zeolite. *Journal of Industrial and Engineering Chemistry*. 17(2), 182-185.
- Verboekend, D., Nuttens, N., Locus, R., Van Aelst, J., Verolme, P., Groen, J. C., Perez-Ramirez, J., and Sels, B. F. (2016). Synthesis, characterisation, and catalytic evaluation of hierarchical faujasite zeolites: milestones, challenges, and future directions. *Chemical Society Reviews*. 45(12), 3331-3352.
- Wang, S., Hao, P., Li, S., Zhang, A., Guan, Y., and Zhang, L. (2017). Synthesis of glycerol carbonate from glycerol and dimethyl carbonate catalyzed by calcined silicates. *Applied Catalysis A: General*. 542, 174-181.
- Xu, S., Zeng, H.-Y., Cheng, C.-R., Duan, H.-Z., Han, J., Ding, P.-X., and Xiao, G.-F. (2015). Mg-Fe mixed oxides as solid base catalysts for the transesterification of microalgae oil. *RSC Advances*. 5(87), 71278-71286.
- Yang, Y., Burke, N., Zhang, J., Huang, S., Lim, S., and Zhu, Y. (2014). Influence of charge compensating cations on propane adsorption in X zeolites: experimental measurement and mathematical modeling. *RSC Advances*. 4(14), 7279-7287.
- Zito, P. F., Caravella, A., Brunetti, A., Drioli, E., and Barbieri, G. (2015). Estimation of Langmuir and Sips models adsorption parameters for NaX and NaY FAU zeolites. *Journal of Chemical & Engineering Data*. 60(10), 2858-2868.

CHAPTER III

COMPARATIVE PROPERTIES OF K/NaX AND K/NaY FROM ULTRASOUND-ASSISTED IMPREGNATION AND PERFORMANCE IN TRANSESTERIFICATION OF PALM OIL

3.1 Abstract

This work aims to compare physicochemical properties and catalytic performance of potassium supported on zeolite NaX and NaY (K/NaX and K/NaY, respectively) prepared by ultrasound-assisted impregnation from potassium acetate buffer precursor. Calcination converts the potassium precursor to carbonate which occupies the zeolite cavities and disperses on the external surface. Both calcined samples show a decrease in zeolite phases, BET surface areas and pore volumes. With the smaller changes, K/NaX is more stable than K/NaY. Moreover, K/NaX has higher basicity than K/NaY and is more active in decomposition of 2-methylbut-3-yn-2-ol (MBOH), producing dominant products from basic sites. Both K/NaX and K/NaY are active in transesterification of palm oil, producing more than 94% of the biodiesel yields in the first run. However, the yields drop in the second run due to the leaching of potassium species into glycerol and biodiesel products. The spent K/NaX has similar phase to the fresh one whereas the spent K/NaY shows more structure collapse. With better structural stability, less potassium leaching and less decline in biodiesel yields in the second run, K/NaX is a better catalyst than K/NaY.

3.2 Introduction

Biodiesel is an alternative fuel produced from various renewable feedstocks. The process involves transesterification, a reaction between triglyceride and alcohol (such as methanol) in the presence of a catalyst. One of the most used catalysts is homogeneous alkaline solutions which provide a high product yield. However, a large amount of wastewater is generated from the product purification step. Consequently, there is an increased interest in developing heterogeneous catalysts which are easy to separate from the products and reusable. Examples of heterogeneous base catalysts for transesterification are carbonates, alkali, metal oxides, and zeolites (Perego et al., 2017; Refaat, 2011; Romero et al., 2005). Those catalysts require a smaller alcohol volume than acid catalysts (Muciño et al., 2016). Currently, there are several review articles on various aspects of the development of heterogeneous catalysis for biodiesel production including current status and challenges (Mathew et al., 2021; Mukhtar et al., 2022); evaluation of feedstocks, technologies, catalysts and reactors (Ganesan et al., 2021; Mohiddin et al., 2021); advances in reactors (Okolie et al., 2022) and processing technologies (Bashir et al., 2022).

Potassium (K) species on various supports are among the promising catalysts due to their higher basicity and better resistivity to free fatty acids contaminating triglyceride sources than those with lithium and sodium (Hindryawati et al., 2014; Rakmae et al., 2016; Supamathanon et al., 2011). They could be reused with fewer activity losses than the other catalysts. Furthermore, active species dispersion on porous materials could enhance catalytic activity. This work is particularly interested in zeolites faujasite (FAU), including NaX and NaY. They have well-defined frameworks with a three-dimensional pore system, large surface areas, high ion-exchange abilities, and thermal stability (Verboekend et al., 2016). Moreover, they are commercially available on a large scale. Both NaX and NaY zeolite have the same FAU structure but different Si/Al ratios, namely, 1-1.5 in NaX and >1.5 in NaY. The presence of aluminum in the zeolite structure generates a framework negative charge which requires extraframework cations for charge balancing (Polisi et al., 2019; Zito et al., 2015).

Several studies have been conducted on catalysts with potassium supported on NaX and NaY for transesterification of various plant oils such as palm, soybean,

sunflower, and Jatropha (Manadee et al., 2017; Noiroj et al., 2009; Peña et al., 2013; Xie et al., 2007). Impregnation with potassium hydroxide (KOH), potassium nitrate (KNO_3), and potassium acetate buffer solution ($\text{CH}_3\text{COOK}/\text{CH}_3\text{COOH}$) is a typical method for catalyst preparation (Manadee et al., 2017; Noiroj et al., 2009; Peña et al., 2013). The basicity increases with potassium loading, resulting in better biodiesel yields. Some of these catalysts suffer from zeolite structural collapse or aggregation of potassium species. Moreover, there is not much comparison of catalysts in the same condition or the same oil. The understanding of catalyst properties is crucial to pursuing the challenges in catalyst design and development.

The early works focused on the preparation of catalysts that produced high biodiesel yields. Noiroj et al. (2009) prepared K/NaY with 10 wt.% KOH as an effective catalyst for the transesterification of palm oil. Intarapong et al. (2011) that the increase of KOH loading on NaY increased the basicity but destroyed the zeolite structure. Xie et al. (2007) reported that K/NaX from 10% KOH was the best catalyst in the transesterification of soybean oil. The increase of KOH loading increased basicity but led to the collapse of the zeolite framework and agglomeration of potassium species. Peña et al. (2013) demonstrated that K/NaX from KNO_3 gave a high biodiesel yield from the transesterification of sunflower oil.

There are some works that concern the stability of zeolite supports. Supamathanon et al. prepared K/NaY and K/NaX by impregnating the zeolites with potassium acetate buffer solution to produce active catalysts for the transesterification of Jatropha seed oil. This potassium precursor could minimize the zeolite structure collapse. Both studies showed that the catalysts have smaller surface areas than the parent zeolites after loading with K precursor, probably due to the agglomeration of potassium species. Hence, ultrasound-assisted impregnation was proposed to improve the dispersion.

Ultrasound has been applied to assist material modification and synthesis. The ultrasound causes acoustic cavitation providing the formation, growth, and collapse of hot gas bubbles in a liquid system. Then, the collapsed bubbles increase temperature and pressure, which assist the diffusion of the precursor into support pores and improve surface interaction (Sosa et al., 2020). There are a few reports on ultrasound-

assisted impregnation of metal precursors on FAU zeolite. Rakmae et al. (2016) used ultrasound-assisted impregnation to prepare 12 wt.% potassium on NaY from potassium acetate buffer. The catalyst provided a better biodiesel yield than that from conventional impregnation. Recently, Ketzer et al. (2020) used ultrasound-assisted impregnation to prepare 20% WO_3 on ultra-stable zeolite Y (USY) for the production of methyl oleate from oleic acid esterification. The catalyst exhibited a high dispersion of active species with strong interaction over the support and provided a good performance.

Although the previous reports demonstrate that the K/NaX and K/NaY are active for the transesterification of various oils, these catalysts were done either by different methods or tested on different oils. Besides, there are no reports about the preparation of K/NaX catalysts by ultrasound-assisted impregnation. This work aims to compare the physicochemical properties of K/NaX and K/NaY catalysts prepared by ultrasound-assisted impregnation from a potassium acetate buffer solution. Then, catalytic performance is evaluated in the transesterification of palm oil under the same condition. Moreover, the catalyst stability is also studied. The in-depth comparison provides an understanding that would be helpful in catalyst design and development.

3.3 Experimental

3.3.1 Synthesis of zeolite NaX

Zeolite NaX ($\text{Si}/\text{Al} = 1.2$) was synthesized according to the previous verified approach (Lechert, and Staelin, 2016). A precursor gel with the molar ratio of NaAlO_2 : 4 SiO_2 : 16 NaOH : 325 H_2O was produced as the following procedure. Firstly, the sodium aluminate solution was prepared by adding alumina trihydrate powder (45.6% Al_2O_3 , 29.65% Na_2O) of 23.21 g into the sodium hydroxide solution prepared by mixing sodium hydroxide (NaOH , 98%, Carlo-Erba) of 23.81 g and distilled water (DI) of 23.81 g. The mixture was further magnetically stirred in a steam bath until clear dissolved (colorless) and cooled to an ambient temperature. Then, the clear solution was added to DI water of 48.21 g. After that, the mixture solution of 23.81 g was added to another NaOH solution containing NaOH of 14.08 g in DI water of 145.71 g and stirred until dissolved. This resulted solution is called **solution A**. Secondly, the sodium

silicate solution was prepared by adding fumed silica (SiO_2 , Sigma-Aldrich) of 27.35 g into the NaOH solution containing NaOH of 10.71 g and DI water of 61.94 g. The mixture was mixed on a steam bath until dissolved (colorless). Then, the supernatant solution of 52.31 g was added to another NaOH solution containing NaOH of 14.08 g in DI water of 145.71 g and blended until homogenization. This obtained solution is called **solution B**. Finally, the **solution A** and **B** were quickly combined and stirred with 750 rpm for 30 min. The resultant was transferred into a 250-mL Teflon-lined autoclave and crystallized at 90 °C for 14 h without agitation. Afterward the resulted zeolite was washed with DI water and separated by centrifugation several times until the pH of the washing solution is around 7. The obtained zeolite was dried in hot air oven at 100 °C overnight.

3.3.2 Synthesis of zeolite NaY

Zeolite NaY ($\text{Si}/\text{Al} = 2.4$) was synthesized according to the previous verified approach (Ginter, 2016). A precursor gel with the molar ratio of 4.62 Na_2O : Al_2O_3 : 10 SiO_2 : 180 H_2O was produced by two-type gels including seed and feed gel as the following procedure. Firstly, a **seed gel** with the molar ratio of 10.67 Na_2O : Al_2O_3 : 10 SiO_2 : 180 H_2O was prepared by mixing both sodium aluminate and sodium silicate solution. The sodium aluminate solution was prepared by adding NaOH of 1.16 g, DI water of 5.70 g and sodium aluminate (NaAlO_2 containing Al_2O_3 ~55–56%, Riedel-de Haën) of 0.60 g into a 50-mL polyethylene bottle under stirring with a speed of 300 rpm for 15 min until clear solution. Sodium silicate solution was prepared by adding fumed silica of 28.70 g into the NaOH solution containing NaOH of 11.52 g and DI water of 59.78 g and stirred on a steam bath until clearly dissolved. After both solutions are mixed, the container was sealed and aged at ambient temperature for 24 h to produce to seed gel. Secondly, a **feed gel** with the molar ratio of 4.30 Na_2O : Al_2O_3 : 10 SiO_2 : 180 H_2O was prepared by mixing both sodium aluminate and sodium silicate solution. The sodium aluminate solution was prepared by adding NaOH of 0.040 g, DI water of 37.42 g and NaAlO_2 of 3.74 g in a 250-mL polyethylene bottle under stirring with a speed of 300 rpm for 15 min at an ambient temperature until clearly dissolved. Then, the sodium silicate solution of 40.70 g was added dropwise into the sodium aluminate solution under vigorous stirring (750 rpm) until the gel is apparently homogeneous.

Finally, the seed gel was slowly added to the feed gel under a vigorous stirring for 30 min and then transferred to a 250-mL Teflon-lined autoclave. Afterwards the mixture was aged at an ambient temperature for 24 h and crystallized at 100 °C for 24 h. When the hydrothermal step is done, the autoclave was cool down to room temperature. The resulted zeolite was centrifuged and washed with DI water until pH of the washed solution is around 7. The product zeolite was dried at 110 °C overnight.

3.3.3 Catalyst preparation.

The catalysts with potassium loading of 12 wt.% were prepared by ultrasound-assisted impregnation modified from Rakmae et al. (2016). The zeolite supports were dried in a vacuum oven at 100 °C overnight. An acetate buffer was prepared by dissolving 5.70 g potassium acetate (CH_3COOK , 99.0%, Carlo Erba) in 1.00 M acetic acid (CH_3COOH , 99.7%, RCI Labscan) and adjusted to 25.00 mL. The buffer of 1.20 mL was added to the dried zeolite of 1.00 g and sonicated with frequency 37 kHz, power 80 W (Elmasonic E 30H model, Elma) for 10 min. The mixture was dried in a vacuum oven at 100 °C overnight and calcined at 480 °C under a static air atmosphere for 3 h with heating rate 1 °C·min⁻¹). The obtained catalysts were notated K/NaY and K/NaX.

3.3.4 Catalyst characterization

Phase characteristics of the catalysts were studied by X-ray diffraction (XRD) on a Bruker XRD-D8 Advance with Cu K α radiation ($\lambda = 0.154$ nm) operated with a voltage of 40 kV and a current of 40 mA. All patterns were collected by a 2θ scan range from 5 to 50° with a step size of 0.02° at a scan speed of 0.5 s·step⁻¹.

Isotherms of all samples were measured by N₂ adsorption-desorption using a BELSORP-mini II. These samples were degassed at 200 °C for 24 h. Surface areas were calculated by Brunauer-Emmett-Teller (BET) method and micropore volumes were estimated by *t*-plot method from the desorption branch.

Functional groups of samples were confirmed by Fourier transform infrared spectroscopy (FTIR) on a Bruker, Tensor27-Hyperion, spectrometer equipped with a microscope using the KBr pellet technique. The spectrum was recorded from 4000-400 cm⁻¹ with a resolution of 4 cm⁻¹ and 64 scans.

Raman spectra were collected with FT-Raman spectrometer on a Bruker, Vertex 70v-RAM II equipped with Nd: YAG laser with an excitation wavelength of 1064 nm operated at a power of 300 mW. A signal was detected by a liquid nitrogen-cooled Ge diode. Each spectrum was recorded from 1500-50 cm^{-1} with 500 scans and a resolution of 4 cm^{-1} .

The Si/Al ratio of NaX and NaY and potassium content of the catalysts were determined by an inductive coupled plasma optical emission spectrometer (ICP-OES) using an Optima 8000 (Perkin Elmer) instrument. Prior to measurement, the catalyst powder was digested using a microwave digestion method (Multiwave 3000 model, Anton Parr).

Both chemical surface species and surface interaction were identified by X-ray photoelectron spectroscopy (XPS) using a ULVAC-PHI PHI5000 VersaProbe II with Al K_{α} radiation. All binding energy (BE) peaks were calibrated corresponding to the standard C 1s peak at 284.6 eV. A Shirley background subtraction was applied to correct the XPS spectra stemming from inelastic electron scattering. XPS peaks were fitted with a combination of Gaussian (G) and Lorentzian (L) functions with the G to L ratio of 20 to 80. The full width half maximum (FWHM) of fitted peaks are in the range of 1.1-1.8 eV and 1.1-1.7 eV for C 1s and K 1s, respectively.

The basicity of the samples compared to the parent zeolites was studied by the decomposition of 2-methylbut-3-yn-2-ol (MBOH) in a fixed-bed reactor described in previous research (Novikova et al., 2014). A sample of 200 mg was loaded into a tubular stainless reactor and pretreated at 350 $^{\circ}\text{C}$ under N_2 atmosphere. Then, the reactor was cooled down to 120 $^{\circ}\text{C}$ and flushed with a vaporized mixture of MBOH and toluene (95:5) using N_2 carrier gas with a flow rate of 10 $\text{mL}\cdot\text{min}^{-1}$. The conversion of MBOH and product selectivity were estimated according to equations reported in the literature (Supamathanon et al., 2012). The MBOH conversion and selectivity of decomposed products were calculated based on the sum peak areas as following the equation (1) and (2), respectively.

$$\text{MBOH conversion (mol\%)} = 1 - \frac{A_{\text{MBOH}} \times r_{\text{RF}_{\text{MBOH}}} / M_{\text{MBOH}}}{\sum (A_i \times r_{\text{RF}_i} / M_i)} \times 100 \quad (1)$$

$$\text{Product selectivity (mol\%)} = \frac{A_p \times rRF_p / M_p}{\sum(A_x \times rRF_x / M_x)} \times 100 \quad (2)$$

where peak area ratio (A), relative response factor (rRF), and molecular weight (M) are mathematical variables for all component (i) including MBOH and all products. The term of the desired product and each obtained product are subscripted by (p) and (x), respectively. The calculation method is based on the relative response factor defined by the effective carbon number concept (ECN) in Appendix A.1.

The basicity of the catalysts was investigated by temperature-programmed desorption of carbon dioxide (CO₂-TPD) using a BELCAT-B chemisorption analyzer. A sample of 50 mg was packed into a tubular glass reactor and pretreated at 300 °C under helium (He) gas flow with a rate of 50 mL·min⁻¹ for 60 min to eliminate physisorbed species. Then, it was cooled down to 70 °C, and a gas mixture of 10% CO₂/He with a flow rate of 50 mL·min⁻¹ was introduced into the sample cell for 30 min. After that, it was purged with He for 30 min and heated to 100 °C with a rate of 10 °C·min⁻¹ and held for 60 min to remove non-adsorbed CO₂. The TPD process was performed in a temperature range of 100 to 800 °C with a temperature ramp of 10 °C·min⁻¹. The basic site density was obtained by integration of peak area.

3.3.5 Transesterification of palm oil.

Transesterification of palm oil was performed according to the previous work. (Rakmae et al., 2016) The catalyst of 0.20 g, methanol (CH₃OH, 99.9%, Carlo Erba) of 2.90 g, and refined palm oil (food grade, Morakot Industries PCL., Thailand) of 5.00 g were stirred in a round bottom flask equipped with a condenser at 60 °C for 3 h. The product mixture was separated by hot filtration following the literature (Sheldon et al., 1998). The liquid phase was transferred to a separatory funnel and allowed to separate overnight. The produced biodiesel in the top layer was collected and evaporated to remove methanol using a rotary evaporator.

The quantitative content of methyl esters ($x_{\text{methyl esters}}$) was determined according to biodiesel test method EN 14103 by gas chromatography (Agilent 7890 GC) equipped with a flame ionization detector (FID) using a capillary column (Agilent J&W CP-Sil 88, CP7489) with a length of 100 m with a film thickness of 0.20 μm and an

internal diameter of 0.25 mm. Helium was used as a carrier gas with a flow rate of 3 mL·min⁻¹. The injection was performed in split mode with a split ratio of 50:1. The injector and detector temperatures were 240 and 300 °C, respectively. In the first step, the oven temperature was started at 70 °C for 4 min and heated to 175 °C with a ramp rate of 13 °C·min⁻¹ and held for 27 min. In the second step, the oven was heated to 215 °C with a ramp rate of 4 °C·min⁻¹ and kept for 15 min. In the final step, the oven temperature was increased to 240 °C with a ramp rate of 4 °C·min⁻¹ and kept for 12 min. Methyl nonadecanoate, so-called C₁₉(CH₃(CH₂)₁₇COOCH₃, 98%, Sigma Aldrich) was used as the internal standard. The content of methyl esters from the received biodiesel was obtained from equation (3) while the content of triglycerides ($x_{\text{triglycerides}}$) was from the literature (Roschat et al., 2016). The yield of produced biodiesel was calculated according to equation (4) below from the literature (Okwundu et al., 2019).

$$x_{\text{methyl esters}} = \left(\frac{(\sum A_{C_{14}-C_{24:1}})}{(A_{C_{19}} \times rRF_x / M_x)} \right) \times \left(\frac{C_{19} \times V_{C_{19}}}{m_{\text{sample}}} \right) \times 100 \quad (3)$$

Where $\sum A_{C_{14}-C_{24:1}}$ is the total peak area from methyl ester in C₁₄ to that in C_{24:1} obtained from GC-FID, and m_{sample} is the mass of the analyzed biodiesel sample. The GC peak area, concentration, and volume of methyl nonadecanoate solution are represented by $A_{C_{19}}$, C_{19} , and $V_{C_{19}}$, respectively.

$$\text{Biodiesel yield (mol \%)} = \left(\frac{m_{\text{biodiesel}}}{m_{\text{palm oil}}} \right) \times \left(\frac{x_{\text{methyl esters}}}{x_{\text{triglycerides}}} \right) \times \left(\frac{M_{\text{triglycerides}}}{3 \times M_{\text{methyl esters}}} \right) \times 100 \quad (4)$$

where $m_{\text{biodiesel}}$ and $m_{\text{palm oil}}$ are the mass of biodiesel and palm oil. $M_{\text{methyl esters}}$ and $M_{\text{triglycerides}}$ are average molecular weight of methyl ester or triglyceride (as indicated with a subscript) while number 3 is the stoichiometric coefficient from the balanced chemical equation of transesterification of triglycerides with methanol.

The catalyst stability was investigated by reusing the spent catalysts and characterization by XRD, SEM, FTIR with Attenuated total reflection (ATR), and Raman spectroscopy. The spent catalysts were washed with methanol (10 mL) and hexane (5 mL) and dried at 90 °C overnight. The potassium leaching was determined by ICP-OES.

The K content from separated liquid products including biodiesel and glycerol was determined. Each liquid product was digested by a microwave digestion method (Multiwave 3000 model, Anton Parr). The percentage of K leaching was calculated according to Čapek et al. (2014).

3.4 Results and discussion

3.4.1 Characterization of K impregnated on FAU zeolite.

XRD patterns of parent NaX and NaY zeolites, as-prepared and calcined K/NaX and K/NaY catalysts are shown in **Figure 3.1**. NaX and NaY have similar peak positions (JCPDS No. 38-0237 and 39-1380, respectively) but different intensities due to the different Si/Al ratios. The as-prepared K/NaX and K/NaY show the zeolite characteristic peaks with lower intensities than the bare zeolites. Both samples show additional peaks at 8.88°, 14.26°, and 27.18°, corresponding to the potassium acetate precursor. The peak at 8.88° of the as-prepared K/NaX sample is stronger than the peak of the zeolite 220 plane. However, the as-prepared K/NaY shows the opposite intensities. The results imply that the potassium acetate precursor covers the external surface of NaX with more extent than that of NaY. After calcination, the peaks of potassium acetate precursor are not observed from both samples, suggesting the complete decomposition. However, the zeolite characteristic peaks from both calcined samples have lower intensities than those of the as-prepared samples. The decreased intensities could be from the partial collapse of the zeolite frameworks by hydrolysis of Si-O-Al bonds (Peña et al., 2013). Although K/NaX and K/NaY have the same potassium loading, the calcined K/NaX shows stronger zeolite peaks suggesting less collapse of the zeolite structure. The XRD results suggest that K/NaX is more stable than K/NaY against the same calcination condition.

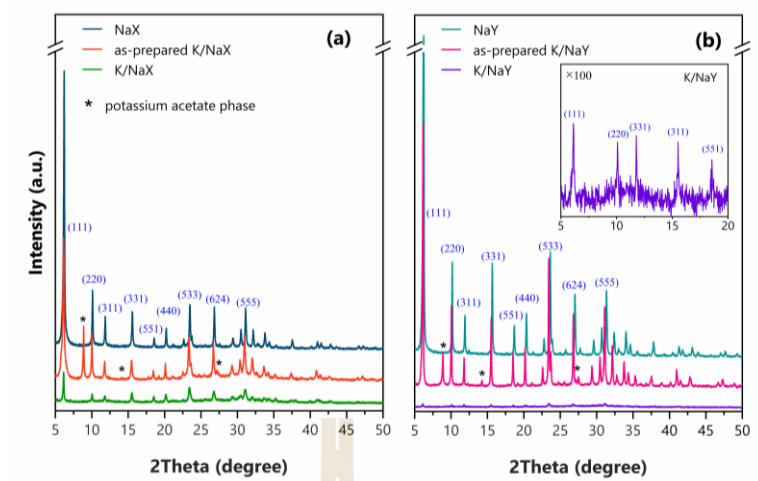


Figure 3.1 XRD patterns of as-prepared and calcined (a) K/NaX and (b) K/NaY compared with their parent zeolites; symbol (*) = potassium acetate phase.

The SEM images of calcined K/NaX and K/NaY are compared with the parents NaX and NaY, respectively, in **Figure 3.2**. Both NaX and NaY are polycrystals with different morphologies. NaX has round-shaped particles with a diameter of about 1.5 μm . Each particle is a cluster of small crystals with various sizes and thicknesses connecting together. The morphology of K/NaX is similar to the parent zeolite but with the poorer sharpness of crystal edges. Some erosion on the surface is visible in the SEM images. NaY consists of single crystals, either perfect octahedra with a diameter of about 500 nm or imperfect polyhedra with various sizes. There are also clusters of crystals with random patterns. The morphology of the calcined K/NaY is similar to that of the parent NaY. The surface of some crystals also shows signs of erosion.

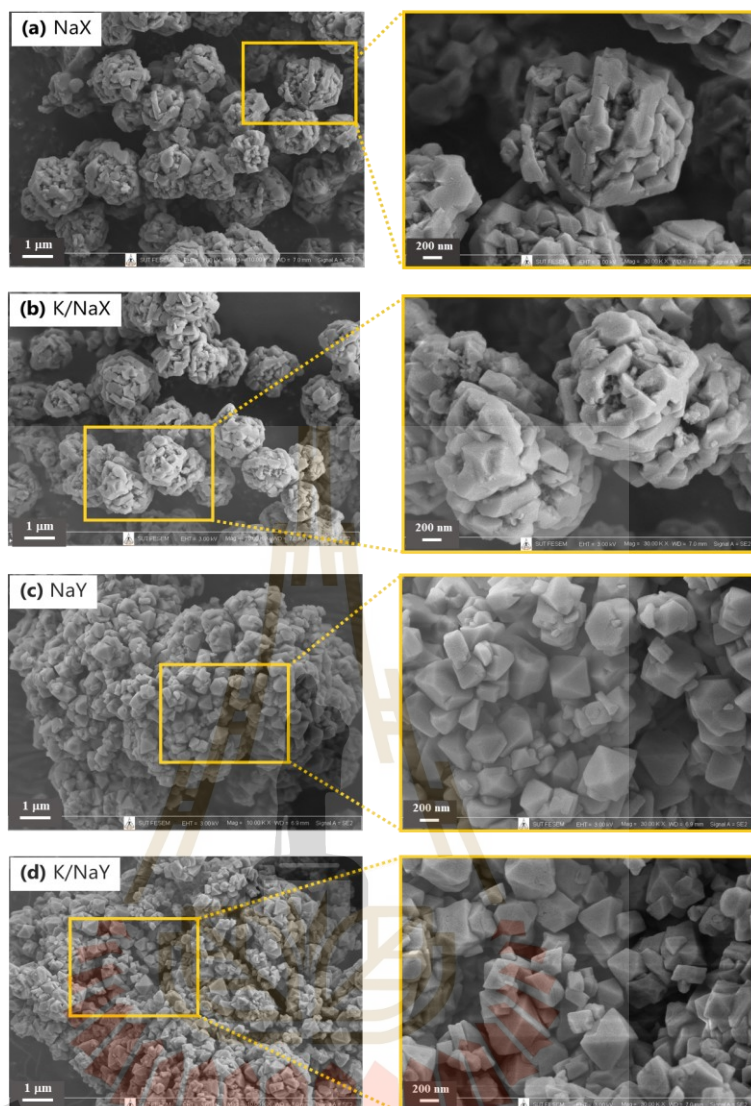


Figure 3.2 SEM images of (a) NaX, (b) calcined K/NaX, (c) NaY, and (d) calcined K/NaY catalysts with 10k and 30k magnification.

The N_2 sorption isotherms of the calcined K/NaX and K/NaY are compared with the parent zeolites in **Figure 3.3**. All samples have type I isotherms, a characteristic of microporous materials (Thommes et al., 2015). The adsorbed volumes of K/NaX and K/NaY, surface areas and pore volumes are smaller than the bare zeolites (see **Table 3.1**). The decrease could be from the occupation of the impregnated species in the zeolite cavities, blockage of the zeolite pores, and the collapse of the zeolite structure (Rakmae et al., 2016). K/NaX shows a smaller decrease of the

adsorbed volume than K/NaY. The results imply that K/NaX has less potassium species in the zeolite cavities or less pore blocking. However, the XRD results indicate that the collapse of zeolite structure in K/NaX is less than that in K/NaY. Since the hydrolysis of the Si-O-Al bond of zeolites under thermal treatment could be assisted by alkali metal species, (Montalbo et al., 2013) the less amount of potassium species in the cavities of NaX could be the reason for the less collapse. Moreover, the hysteresis loops on NaX and K/NaY are type H4 and H2(b) that could be from crystal aggregation and thermal hydrolysis, respectively (Thommes et al., 2015).

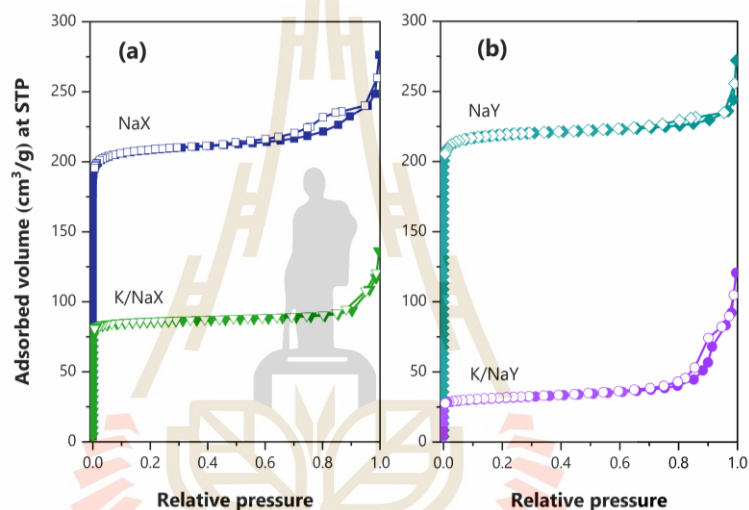


Figure 3.3 N₂ sorption isotherms of (a) calcined K/NaX and (b) calcined K/NaY compared to their parent zeolites; filled symbols = adsorption and hollow symbols = desorption.

Table 3.1 BET surface area and micropore volume of K/NaX and K/NaY compared to parent zeolites from N₂ sorption analysis and K content from ICP analysis.

Sample	BET surface area (m ² ·g ⁻¹)	Micropore volume (cm ³ ·g ⁻¹)	K content (wt.%)
NaX	853	0.254	-
NaY	899	0.331	-
K/NaX	352	0.128	11.03 ± 0.07
K/NaY	121	0.037	11.40 ± 0.17

FTIR spectra and assignment of as-prepared and calcined K/NaX and K/NaY are presented in **Figure 3.4** and **Table A.2** in Appendix A. The as-prepared K/NaX and K/NaY show the new peaks at 1414, 1514, and 2977 cm⁻¹ related to the symmetric stretching of COO⁻ (ν_s), asymmetric stretching of COO⁻ (ν_{as}), and C-H stretching of -CH₃, respectively. These peaks correspond to the potassium acetate precursor species. After calcination, the peaks of potassium acetate precursor are not observed, suggesting the complete decomposition. The peaks at 1388 and 1448 cm⁻¹ from K/NaX and 1388 and 1456 cm⁻¹ from K/NaY correspond to asymmetric stretching (ν_{as}) of carbonate ion (CO₃²⁻) (Lavalley, 1996; Manadee et al., 2017). More intense peaks of carbonate are observed on K/NaY, consistent with the stronger potassium acetate peaks in the XRD patterns. Both samples also show a small peak at around 880 cm⁻¹, corresponding to out-of-plane bending (δ) of CO₃²⁻ (Binet et al., 1999; Lavalley, 1996). The bands of stretching and bending of Si-O-T, where T is the Si or Al atom of the zeolites, decrease due to thermal hydrolysis during the decomposition of the acetate precursor. The formation of K₂CO₃ on the support surface may relate to the collapse of the zeolite framework. The finding agrees with the FTIR results in the literature (Manadee et al., 2017; Rakmae et al., 2016).

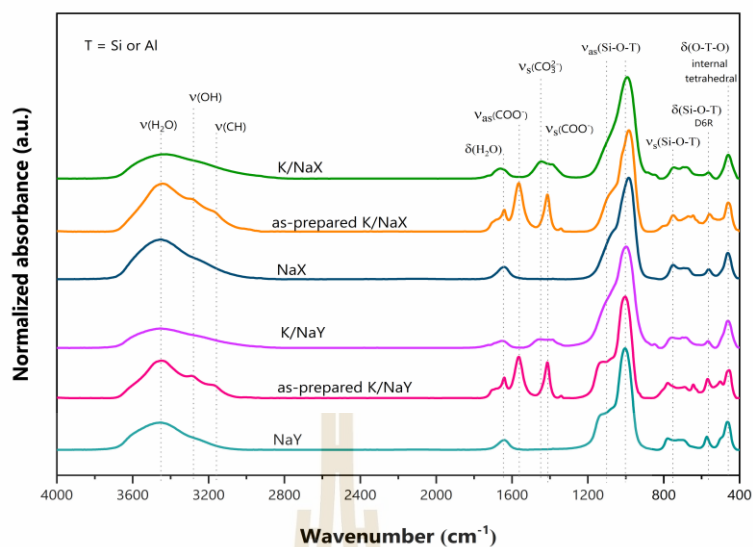


Figure 3.4 FTIR spectra of as-prepared and calcined K/NaX and K/NaY catalysts compared with their parent zeolites.

Raman spectra and peak assignments of both calcined K/NaX and K/NaY are compared with those of the parent zeolites in **Figure 3.5** and **Table A.2** in Appendix A. Both samples show peaks at 1080, 1060, and 700 cm^{-1} corresponding to the stretching and bending modes of K_2CO_3 (Edwards et al., 2005; Frantz, 1998). Although both samples were prepared with the same potassium loading, the signal of K_2CO_3 on K/NaX is stronger than that on K/NaY, implying that more amount of carbonate species is on the external surface (Ishimaru et al., 2018). This could also be from the stronger intrinsic basicity of the NaX zeolite. The vibration of 4- and 6-membered rings of FAU frameworks decreased due to hydrolysis during the thermal treatment of the potassium precursor (Rakmae et al., 2016). The relative peak intensity of the 4-membered ring in the NaX framework is higher than that in the NaY. This result confirms that structure of NaX is more stable, consistent with the XRD results.

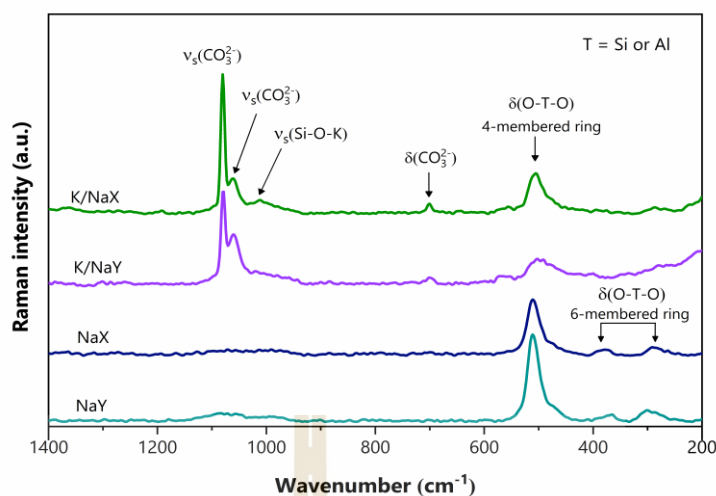


Figure 3.5 Raman spectra of calcined K/NaX and K/NaY catalysts compared with their parent zeolites.

Moreover, the forms of potassium species in calcined K/NaX and K/NaY were determined by X-ray photoelectron spectroscopy (XPS). The spectra of K/NaX and K/NaY are shown in **Figure 3.6**. The peaks of K $2p_{1/2}$ and K $2p_{3/2}$ from K/NaX are observed at 295.7 and 293.0 eV, respectively, corresponding to K_2CO_3 (Swathy et al., 2016). Both K $2p$ peaks from K/NaY shift to lower binding energy, probably due to connection to elements with lower electronegativity (Sun et al., 2010). The binding energy difference between K/NaX and K/NaY could be attributed to the interfacial interaction between K species and the zeolite surface. The higher binding energy in K/NaX implies a stronger interaction. The peak at 288.5 eV from both samples corresponds to carbonate species on the zeolite surface. The peaks at 284.6 and 285.9 eV are assigned to adventitious carbonaceous compounds (Rakmae et al., 2016). These XPS results confirm the presence of K_2CO_3 on both zeolites, which are not observed by XRD.

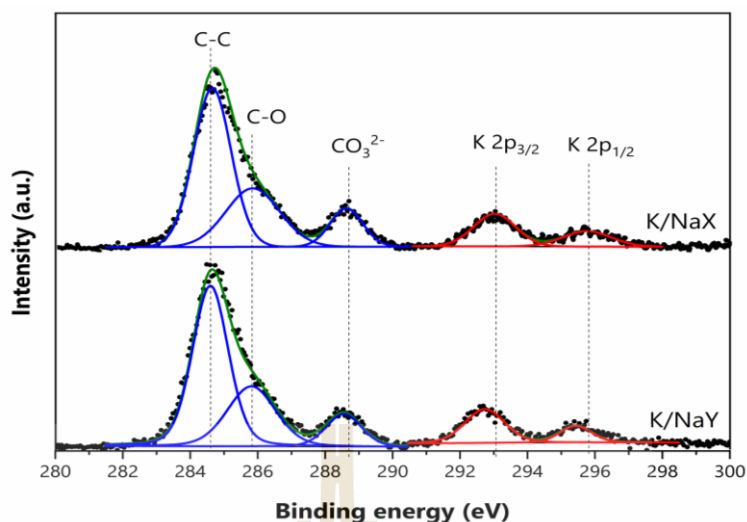


Figure 3.6 XPS spectra of the chemical state of carbon (C 1s) and potassium (K 2p) peaks of calcined K/NaX and K/NaY catalysts.

The acid-base properties of the catalysts are distinguished by the decomposition of MBOH (Lauron-Pernot et al., 1991). The conversions of MBOH over the calcined K/NaX and K/NaY and the parent zeolites are compared in **Figure 3.7a** and **Table 3.2**. The conversions from bare zeolites are very low and much lower than K/NaX and K/NaY. These results ensure that the addition of potassium generates more active sites. The conversions from K/NaX are significantly higher than those from K/NaY, indicating the more active sites. These results are consistent with the higher structural stability and larger surface area, which reflects the better dispersion and accessibility of base species in the zeolite cavities. The selectivities of all products are listed in **Table 3.2**. NaX provides mainly the base-catalyzed products, whereas NaY produces more compounds formed on coordinatively unsaturated sites. These results indicate that NaX has more basic sites than NaY. After loading with potassium, K/NaX and K/NaY only give the base-catalyzed products. The results confirm that the presence of K_2CO_3 on the zeolite significantly improves the basicity.

CO_2 -TPD profiles of calcined K/NaX and K/NaY are shown in **Figure 3.7b**, and the calculated values of basicity are listed in **Table 3.2**. NaY and NaX show a peak at 300 and 330 °C, respectively. The higher temperature from NaX reflects the stronger intrinsic basicity consistent with a lower Si/Al ratio. After loading with potassium, K/NaX

gives a strong peak centered at 680 °C. K/NaY shows peaks in the same temperature range but smaller peak area. This result confirms that K/NaX is more basic than K/NaY. This could be from the better dispersion of base species (Montalbo et al., 2013). The lower basicity in K/NaY is consistent with the result from the MBOH decomposition.

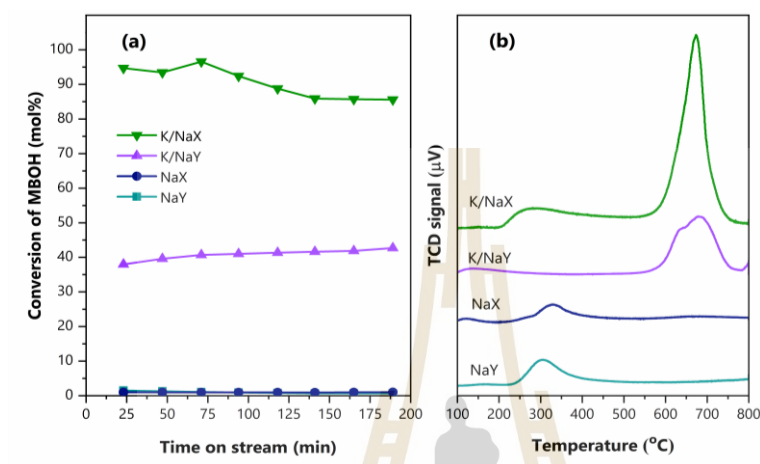


Figure 3.7 (a) MBOH conversion at various times and (b) CO₂-TPD profiles from calcined K/NaX and K/NaY compared to the bare zeolite supports.

Table 3.2 Conversion and selectivity of products from the decomposition of MBOH and basicity by CO₂-TPD of K/NaX and K/NaY compared to the parent zeolites.

Sample	MBOH conversion ^a (mol %)	Product selectivity (mol %)				Basicity by CO ₂ -TPD (mmol CO ₂ ·g ⁻¹)
		Base-catalyzed site		coordinate unsaturated site		
		Acetylene	Acetone	MBYE	Prenal	
NaX	0.93	45.35	48.65	6.00	0.00	0.375
NaY	0.69	14.28	17.70	68.00	0.00	0.222
K/NaX	85.90	48.90	51.32	0.00	0.00	0.867
K/NaY	41.61	48.67	51.33	0.00	0.00	0.532

^a Product selectivity from MBOH decomposition was collected at the time on stream at 140 min after reaching the constant conversion.

3.4.2 Catalytic activity on transesterification of palm oil

Figure 3.8 displays the GC chromatograms of biodiesel products from the transesterification of palm oil obtained from the first and second runs on K/NaX and K/NaY. The biodiesel yields from first runs were 97.9% and 94.4%, respectively. **Table 3.3** compares the yields from this work with those the previous works. The biodiesel yield of K/NaY from this work is higher than the work from Rakmae et al. (2016). The difference might be from the methods used for product separation; namely, hot filtration in this work versus room-temperature filtration in Rakmae et al. (2016). The K/NaX and K/NaY, prepared by the same method, give similar biodiesel yields in the first run despite the more collapse in the zeolite structure in K/NaY. However, the differences are obvious in the second run. From the chromatograms from the second run (**Figure 3.8**), the biodiesel yields from K/NaX and K/NaY decreased to 61.3% and 2.7%, respectively. The decrease was mainly due to the leaching of potassium species which is discussed in Section 3.4.2. This result implies that the amount of K_2CO_3 as a basic site is the key to catalytic activity. Compared to the literature, the performance of K/NaX is better than that of K/NaY, when prepared either from conventional or ultrasound-assisted impregnation.

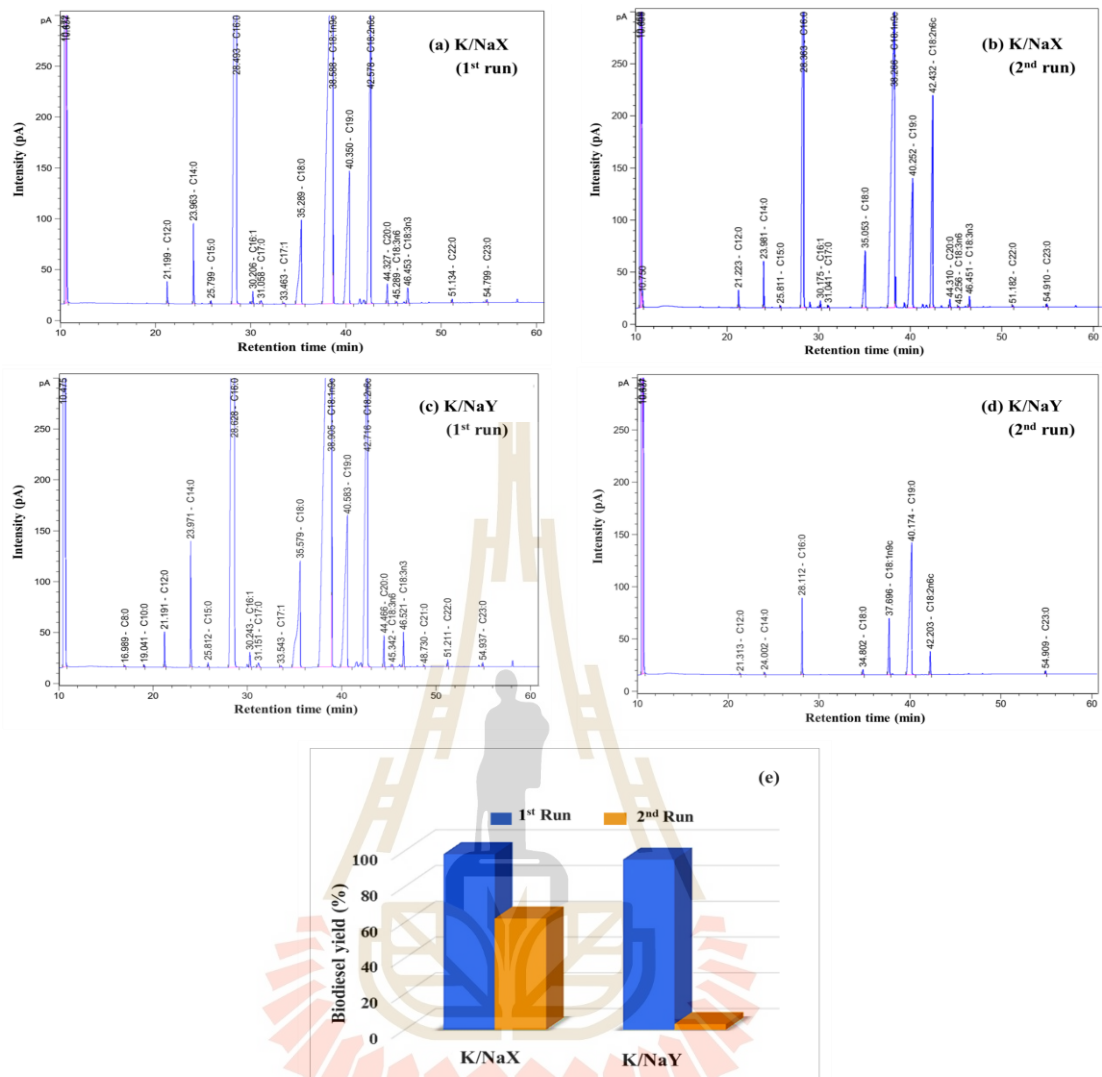


Figure 3.8 GC chromatograms from the conversion of palm oil obtained from (a) K/NaX (1st run), (b) K/NaX (2nd run), (c) K/NaY (1st run), (d) K/NaY (2nd run), and (e) biodiesel yield from first and second run on K/NaX and K/NaY at 60 °C for 3 h.

Table 3.3 Comparison of the catalyst performance in transesterification between K/NaX and K/NaY with 12 wt.% K loading from conventional and ultrasound-assisted impregnation from this work and previous literature.

Catalyst	Preparation method	Oil type	Condition	Biodiesel yield (mol %)	Reference
K/NaX	Impregnation	Jatropha seed oil	65 °C, 3 h	83.0	(Manadee et al., 2017)
K/NaY	Impregnation	Jatropha seed oil	65 °C, 3 h	73.4	(Supamathanon et al., 2011)
K/NaY	impregnation	Palm oil	60 °C, 3 h	68.6	(Rakmae et al., 2016)
K/NaY	Ultrasound-assisted impregnation	Palm oil	60 °C, 3 h	72.4	(Rakmae et al., 2016)
K/NaY	Ultrasound-assisted impregnation	Palm oil	60 °C, 3 h	94.4 ± 0.93	This work
K/NaX	Ultrasound-assisted impregnation	Palm oil	60 °C, 3 h	97.9 ± 0.52	This work

3.4.3 Stability of catalysts

Although K/NaX and K/NaY give high biodiesel yields in the first run, the yields decrease significantly in the second run. The yield from K/NaX is much higher than that from K/NaY. Thus, further investigation on the catalyst stability was conducted. The amount of potassium leaching into glycerol and biodiesel products was determined by ICP-OES. The spent catalysts were characterized by XRD, SEM, FTIR, and Raman spectroscopy.

The total amount of potassium leaching in the glycerol and biodiesel product from K/NaX and K/NaY are 15.6% and 45.2%, respectively. The results indicate that the catalyst deactivation strongly relates to potassium leaching. Namely, the catalyst with more potassium leaching gives the smaller biodiesel yield in the second run. This finding agrees with the reports by Čapek et al. (2014) and Muciño et al. (2016). The potassium surface species reacts with glycerol to form a soluble species. The less leaching from K/NaX is consistent with the XPS results. Potassium species in K/NaX has a stronger interaction with the zeolite support.

The XRD patterns of spent K/NaX and K/NaY are compared with the fresh catalysts in **Figure 3.9**. The patterns of spent and fresh K/NaX are similar, indicating the zeolite stability against the reaction condition. In contrast, the XRD pattern of spent K/NaY shows characteristic peaks of zeolite NaY on a broad baseline indicating an amorphous nature. This data confirms the more collapse of zeolite NaY than that of NaX, consistent with the more decrease in surface area of K/NaY from the bare zeolite.

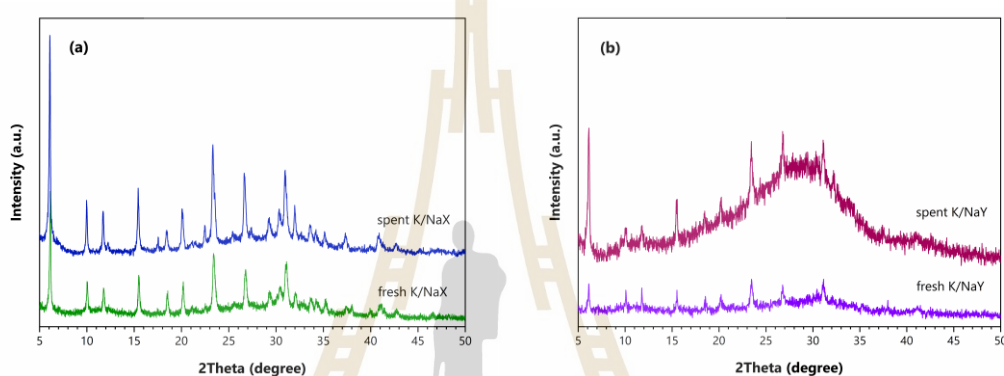


Figure 3.9 XRD patterns of (a) spent K/NaX and (b) spent K/NaY compared with fresh catalysts.

The SEM images of the spent K/NaX and K/NaY with 10k and 30k magnification are shown in **Figure 3.10**. The images of both spent catalysts are similar to their fresh catalysts. However, the changes in zeolite crystallinity are evident in XRD patterns.

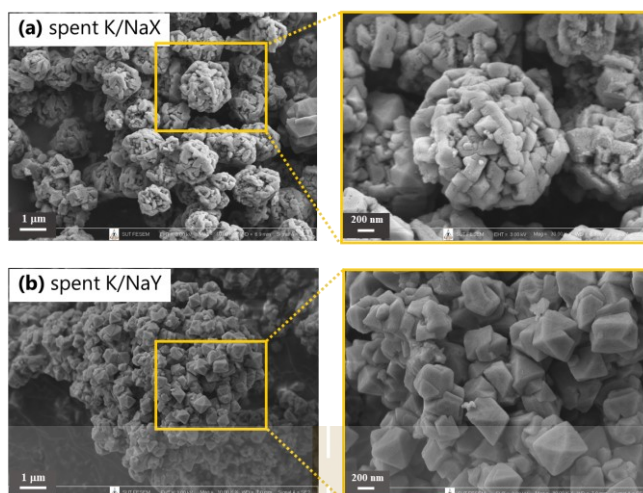


Figure 3.10 SEM images of (a) spent K/NaX and (b) spent K/NaY catalysts with 10k and 30k magnification.

The FTIR-ATR and Raman spectra of spent K/NaX and K/NaY are compared with their fresh catalysts in **Figure 3.11**. The IR spectra of both spent catalysts are different from their fresh samples. The carbonate peaks have either lower intensities or different shapes indicating changes after the catalytic test. The changes of the spent catalysts from Raman spectra are more evident than from IR spectra. The decreases of the peaks at 1080 and 1060 cm^{-1} (symmetric stretching) and 700 cm^{-1} (symmetric deformation) agree with the leaching of potassium species. The different shapes of carbonate peaks of spent K/NaX and K/NaY indicate the different interaction.

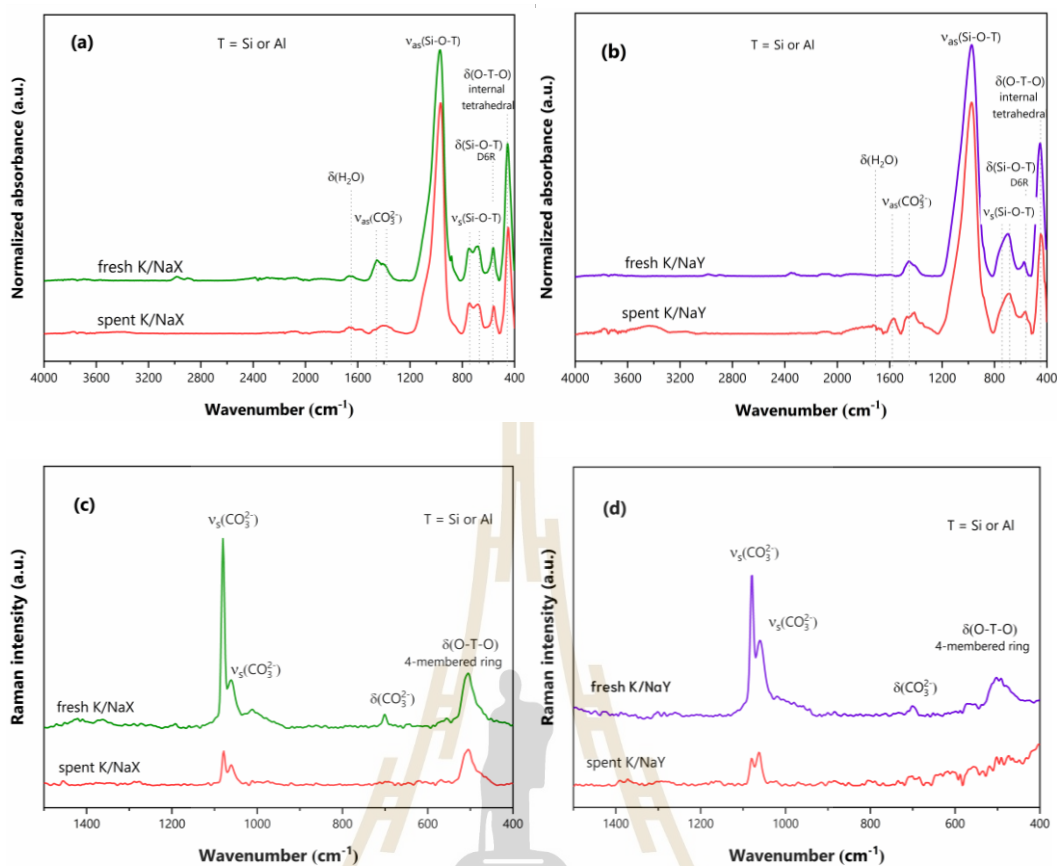


Figure 3.11 Comparison between fresh and spent catalysts by FTIR (ATR mode) spectra of (a) K/NaX and (b) K/NaY and Raman spectra of (c) K/NaX and (d) K/NaY.

From this study, both K/NaX and K/NaY deactivate after being tested in transesterification. The causes are the leaching of potassium species, the collapse of the zeolite structure and the changes of carbonate species. However, the contribution of each cause is not clear. Therefore, further investigation is recommended to provide insightful information to improve the catalyst design and development.

3.5 Conclusions

Potassium catalysts supported on FAU zeolites (K/NaX and K/NaY) were prepared using potassium acetate buffer through ultrasound-assisted impregnation. Calcination converts potassium precursor to potassium carbonate and causes the

collapse of zeolite structures. The collapse in K/NaY is more than that in K/NaX. In addition, the basicity of K/NaX is higher than that of K/NaY.

In transesterification of palm oil and methanol, both catalysts provided high biodiesel yields in the first run. The yield decreased 1.6 times for K/NaX in the second run, but K/NaY was almost inactive. Possible causes of the lower performance of the catalysts could be the leaching of potassium species, the collapse of the zeolite structure and the changes of the carbonate species. The effects are less pronounced on K/NaX; therefore, it is the better catalyst for this reaction. Further study to understand the interaction of potassium carbonate on the zeolite is recommended to design catalysts with high stability.

3.6 References

- Bashir, M. A., Wu, S., Zhu, J., Krosuri, A., Khan, M. U., and Ndeddy Aka, R. J. (2022). Recent development of advanced processing technologies for biodiesel production: A critical review. *Fuel Processing Technology*. 227, 107120.
- Binet, C., Daturi, M., and Lavalley, J.-C. (1999). IR study of polycrystalline ceria properties in oxidised and reduced states. *Catalysis Today*. 50(2), 207-225.
- Čapek, L., Hájek, M., Kutálek, P., and Smoláková, L. (2014). Aspects of potassium leaching in the heterogeneously catalyzed transesterification of rapeseed oil. *Fuel*. 115, 443-451.
- Edwards, H. G. M., Villar, S. E. J., Jehlicka, J., and Munshi, T. (2005). FT-Raman spectroscopic study of calcium-rich and magnesium-rich carbonate minerals. *Spectrochimica Acta Part A: Molecular and Biomolecular Spectroscopy*. 61(10), 2273-2280.
- Frantz, J. D. (1998). Raman spectra of potassium carbonate and bicarbonate aqueous fluids at elevated temperatures and pressures: comparison with theoretical simulations. *Chemical Geology*. 152(3), 211-225.
- Ganesan, R., Manigandan, S., Shanmugam, S., Chandramohan, V. P., Sindhu, R., Kim, S.-H., Brindhadevi, K., and Pugazhendhi, A. (2021). A detailed scrutinize on

- panorama of catalysts in biodiesel synthesis. *Science of the Total Environment*. 777.
- Ginter, D. (2016). Linde Type Y. In S. Mintova (Ed.), *Verified syntheses of zeolitic materials* (third ed., pp. 221-223): The Synthesis Commission of the International Zeolite Association.
- Hindryawati, N., Maniam, G. P., Karim, M. R., and Chong, K. F. (2014). Transesterification of used cooking oil over alkali metal (Li, Na, K) supported rice husk silica as potential solid base catalyst. *Engineering Science and Technology, an International Journal*. 17(2), 95-103.
- Intarapong, P., Luengnaruemitchai, A., and Jai-In, S. (2011). Transesterification of palm oil over KOH-NaY zeolite in a packed-bed reactor. *International Journal Of Renewable Energy Research*. 1, 271-280.
- Ishimaru, Y., Oshima, Y., Imai, Y., Iimura, T., Takanezawa, S., Hino, K., and Miura, H. (2018). Raman spectroscopic analysis to detect reduced bone quality after sciatic neurectomy in mice. *Molecules*. 23(12), 3081.
- Ketzer, F., Celante, D., and de Castilhos, F. (2020). Catalytic performance and ultrasonic-assisted impregnation effects on WO₃/USY zeolites in esterification of oleic acid with methyl acetate. *Microporous and Mesoporous Materials*. 291, 109704.
- Lauron-Pernot, H., Luck, F., and Popa, J. M. (1991). Methylbutynol: a new and simple diagnostic tool for acidic and basic sites of solids. *Applied Catalysis*. 78(2), 213-225.
- Lavalley, J. C. (1996). Infrared spectrometric studies of the surface basicity of metal oxides and zeolites using adsorbed probe molecules. *Catalysis Today*. 27(3), 377-401.
- Lechert, H., and Staelin, P. (2016). Linde Type X. In S. Mintova (Ed.), *Verified syntheses of zeolitic materials* (third ed., pp. 215-217): The Synthesis Commission of the International Zeolite Association.
- Manadee, S., Sophiphun, O., Osakoo, N., Supamathanon, N., Kidkhunthod, P., Chanlek, N., Wittayakun, J., and Prayoonpokarach, S. (2017). Identification of potassium phase in catalysts supported on zeolite NaX and performance in transesterification of Jatropha seed oil. *Fuel Processing Technology*. 156, 62-67.

- Mathew, G. M., Raina, D., Narisetty, V., Kumar, V., Saran, S., Pugazhendi, A., Sindhu, R., Pandey, A., and Binod, P. (2021). Recent advances in biodiesel production: Challenges and solutions. *Science of the Total Environment*. 794, 148751.
- Mohiddin, M. N. B., Tan, Y. H., Seow, Y. X., Kansedo, J., Mubarak, N. M., Abdullah, M. O., Chan, Y. S., and Khalid, M. (2021). Evaluation on feedstock, technologies, catalyst and reactor for sustainable biodiesel production: A review. *Journal of Industrial and Engineering Chemistry*. 98, 60-81.
- Montalbo, K. D., Leon, R. L. d., Sophiphun, O., Manadee, S., Prayoonpokarach, S., and Wittayakun, J. (2013). Characterization and catalytic performance of potassium loaded on rice husk silica and zeolite nay for transesterification of jatropha seed oil. *Química Nova*. 36, 1116-1120.
- Muciño, G. E. G., Romero, R., García-Orozco, I., Serrano, A. R., Jiménez, R. B., and Natividad, R. (2016). Deactivation study of K_2O/NaX and Na_2O/NaX catalysts for biodiesel production. *Catalysis Today*. 271, 220-226.
- Mukhtar, A., Saqib, S., Lin, H., Hassan Shah, M. U., Ullah, S., Younas, M., Rezakazemi, M., Ibrahim, M., Mahmood, A., Asif, S., and Bokhari, A. (2022). Current status and challenges in the heterogeneous catalysis for biodiesel production. *Renewable and Sustainable Energy Reviews*. 157, 112012.
- Noiroj, K., Intarapong, P., Luengnaruemitchai, A., and Jai-In, S. (2009). A comparative study of KOH/Al_2O_3 and KOH/NaY catalysts for biodiesel production via transesterification from palm oil. *Renewable Energy*. 34(4), 1145-1150.
- Novikova, L., Roessner, F., Belchinskaya, L., AlSawalha, M., and Krupskaya, V. (2014). Study of surface acid-base properties of natural clays and zeolites by the conversion of 2-methylbut-3-yn-2-ol. *Applied Clay Science*. 101, 229-236.
- Okolie, J. A., Ivan Escobar, J., Umenweke, G., Khanday, W., and Okoye, P. U. (2022). Continuous biodiesel production: A review of advances in catalysis, microfluidic and cavitation reactors. *Fuel*. 307, 121821.
- Okwundu, O. S., El-Shazly, A. H., and Elkady, M. (2019). Comparative effect of reaction time on biodiesel production from low free fatty acid beef tallow: a definition of product yield. *SN Applied Sciences*. 1(2), 140.

- Peña, R., Romero, R., Martínez, S. L., Natividad, R., and Ramírez, A. (2013). Characterization of KNO_3/NaX catalyst for sunflower oil transesterification. *Fuel*. *110*, 63-69.
- Perego, C., Bosetti, A., Ricci, M., and Millini, R. (2017). Zeolite materials for biomass conversion to biofuel. *Energy and Fuels*. *31*(8), 7721-7733.
- Polisi, M., Grand, J., Arletti, R., Barrier, N., Komaty, S., Zaarour, M., Mintova, S., and Vezzalini, G. (2019). CO_2 adsorption/absorption in FAU zeolite nanocrystals: in situ synchrotron X-ray powder diffraction and in situ Fourier transform infrared spectroscopic study. *The Journal of Physical Chemistry C*. *123*(4), 2361-2369.
- Rakmae, S., Keawkumay, C., Osakoo, N., Montalbo, K. D., de Leon, R. L., Kidkhunthod, P., Chanlek, N., Roessner, F., Prayoonpokarach, S., and Wittayakun, J. (2016). Realization of active species in potassium catalysts on zeolite NaY prepared by ultrasound-assisted impregnation with acetate buffer and improved performance in transesterification of palm oil. *Fuel*. *184*, 512-517.
- Refaat, A. A. (2011). Biodiesel production using solid metal oxide catalysts. *International Journal of Environmental Science & Technology*. *8*(1), 203-221.
- Romero, M. D., Ovejero, G., Rodríguez, A., and Gómez, J. M. (2005). Enhancement of the basic properties in FAU zeolites by impregnation with cesium hydroxide. *Microporous and Mesoporous Materials*. *81*(1-3), 313-320.
- Roschat, W., Siritanon, T., Yoosuk, B., and Promarak, V. (2016). Biodiesel production from palm oil using hydrated lime-derived CaO as a low-cost basic heterogeneous catalyst. *Energy Conversion and Management*. *108*, 459-467.
- Sheldon, R. A., Wallau, M., Arends, I. W. C. E., and Schuchardt, U. (1998). Heterogeneous catalysts for liquid-phase oxidations: Philosophers' stones or Trojan horses? *Accounts of Chemical Research*. *31*, 485-493.
- Sosa, N., Chanlek, N., and Wittayakun, J. (2020). Facile ultrasound-assisted grafting of silica gel by aminopropyltriethoxysilane for aldol condensation of furfural and acetone. *Ultrasonics Sonochemistry*. *62*, 104857.
- Sun, P., Yu, D., Tang, Z., Li, H., and Huang, H. (2010). NaY zeolites catalyze dehydration of lactic acid to acrylic acid: studies on the effects of anions in potassium salts. *Industrial & Engineering Chemistry Research*. *49*(19), 9082-9087.

- Supamathanon, N., Wittayakun, J., and Prayoonpokarach, S. (2011). Properties of Jatropha seed oil from Northeastern Thailand and its transesterification catalyzed by potassium supported on NaY zeolite. *Journal of Industrial and Engineering Chemistry*. 17(2), 182-185.
- Supamathanon, N., Wittayakun, J., Prayoonpokarach, S., Supronowicz, W., and Roessner, F. (2012). Basic properties of potassium oxide supported on zeolite Y studied by Pyrrole-TPD and catalytic conversion of methylbutynol. *Química Nova*. 35(9), 1719-1723.
- Swathy, J. R., Pugazhenthiran, N., Sudhakar, C., Anil Kumar, A., and Pradeep, T. (2016). Sparingly soluble constant carbonate releasing inert monolith for enhancement of antimicrobial silver action and sustainable utilization. *ACS Sustainable Chemistry & Engineering*. 4(7), 4043-4049.
- Thommes, M., Kaneko, K., Neimark Alexander, V., Olivier James, P., Rodriguez-Reinoso, F., Rouquerol, J., and Sing Kenneth, S. W. (2015). Physisorption of gases, with special reference to the evaluation of surface area and pore size distribution (IUPAC Technical Report). *Pure and Applied Chemistry*. 87(9-10), 1051-1069.
- Verboekend, D., Nuttens, N., Locus, R., Van Aelst, J., Verolme, P., Groen, J. C., Perez-Ramirez, J., and Sels, B. F. (2016). Synthesis, characterisation, and catalytic evaluation of hierarchical faujasite zeolites: milestones, challenges, and future directions. *Chemical Society Reviews*. 45(12), 3331-3352.
- Xie, W., Huang, X., and Li, H. (2007). Soybean oil methyl esters preparation using NaX zeolites loaded with KOH as a heterogeneous catalyst. *Bioresource Technology*. 98(4), 936-939.
- Zito, P. F., Caravella, A., Brunetti, A., Drioli, E., and Barbieri, G. (2015). Estimation of Langmuir and Sips models adsorption parameters for NaX and NaY FAU zeolites. *Journal of Chemical & Engineering Data*. 60(10), 2858-2868.

CHAPTER IV

MORPHOLOGICAL EFFECT OF BPH ZEOLITE NANOSHEETS ON CONVERSION OF GLYCEROL TOWARDS GLYCEROL CARBONATE

4.1 Abstract

The utilization of glycerol to high-valued chemicals is the key success of economic and sustainable biodiesel production. For glycerol conversion by transesterification, BPH-type zeolite nanosheets (Linde Q) with different morphologies are among promising catalysts to overcome the diffusion transport limitation inside the pore topology and inhibit the formation of glycidol as a by-product. As-prepared forms of both nanosheet as called nano CsBPH_AP (192 nm size) and micron-sized zeolite as called micro KBPH_AP (600 nm size) were prepared by hydrothermal treatment with different Si/Al ratios. With a morphological-dependent reaction, nano CsBPH_AP gives a better transesterification activity of glycerol (Gly) to glycerol carbonate (GC) than micro KBPH_AP. After the ion-exchange step, nano CsBPH_AP, ion-exchanged by potassium precursor, as nano K-CsBPH_IE and micro KBPH_AP, ion-exchanged by cesium precursor, as micro Cs-KBPH_IE exhibit slightly different thermal property against their parents. However, they provide a lower reaction activity than their parents. The nano CsBPH_AP with the loading of 6 wt.% shows good catalytic performance up to the fourth run under an optimal condition at 120 °C for 3 h and the Gly-to-DMC molar ratio of 1:5. Hence, this study reveals a crucial effect of catalyst morphology on the conversion of glycerol towards glycerol carbonate.

4.2 Introduction

With the dramatic decrease of fossil resources, biodiesel has become alternative energy. Although transesterification has been used to make biodiesel, a significant amount of glycerol (Gly) was produced as a byproduct. As a result, the industrial challenge is to find ways to convert glycerol into high-value-added compounds such as acrolein through dehydration (Qureshi et al., 2019), glycerol carbonate (GC) through transesterification (She et al., 2021), and 1,3-propanediol through dihydroxylation (Tan et al., 2013). Glycerol carbonate via transesterification with dimethyl carbonate has been suggested as a promising approach for glycerol upgrading in heterogeneous catalysis by zeolites (Khanday et al., 2017), micro-mesoporous silicas (Qureshi et al., 2019; She et al., 2021), silicates (Wang et al., 2017), titanosilicate (Xiang, and Wu, 2018), and hydrotalcite (Liu et al., 2014). Although these catalysts provide high performance in reaction testing, they suffer from molecular hindrance due to reactant and product diffusion limitations and basic site accessibility (She et al., 2021). As a result, one of the possible solutions to such problems is the enhancement of catalyst morphology (e.g., pore diameters, particle sizes, and shapes).

From previous studies in the Gly upgrading, zeolite-based and mesoporous catalysts with different pore sizes are reported. Micron-sized chabazite (Si/Al = 2.4) with the aggregate of quadratic prism-like crystals from coal fly ash was hydrothermally prepared at 160 °C in the upgrading of glycerol via transesterification (Algoufi, and Hameed, 2014). Although the ash-derived chabazite gave a high GC yield (96%) without the leaching of metallic species (K, Ca, Ti, and Fe), glycidol as a by-product was formed because of its highly strong basicity. In addition, the small pore window of chabazite (0.38 nm) could hinder molecular diffusion and slightly reduce accessible internal surfaces after a few test cycles. With different pore topologies, as-prepared zeolites including 3A (0.31×0.35 nm), 4A (0.41×0.41 nm), NaZSM-5 (0.51×0.55 and 0.53×0.56 nm), NaBEA (0.66×0.67 and 0.56×0.56 nm), and NaY (0.74×0.74 nm) were compared by GC production from Gly and dimethyl carbonate (DMC) (Pan et al., 2012). Both NaBEA and NaY only gave the conversion of Gly to GC with complete selectivity. In addition, NaY was the best one among them. Hence, zeolite-based catalysts with a pore size more than 0.56 nm are preferable for the transesterification due to the geometric

dimension of Gly (0.47×0.52 nm), DMC (0.37×0.45 nm) as reactants, and GC (0.33×0.65 nm) as a product (Pan et al., 2012).

For the conversion of the Gly towards GC, not only the proper pore size of porous catalysts is preferable, but also their shapes and particle sizes are also necessary. With tunable *b*-axis crystal length (60-70 nm), microporous H-ZSM-5 (Si/Al = 25-125) was utilized for Gly dehydration to acrolein (Qureshi et al., 2019). Because of the short *b*-axis, it exhibited a higher Gly conversion than a commercial ZSM-5 with a *b*-axis of 1.5-1.7 μm. This also suggested that short diffusional lengths facilitated high Gly diffusion inside pore channels (0.51-0.56 nm). With three different shapes (rice shape, short and long rods), mesoporous silicas containing layered double hydroxides (LDH) were proposed as nanosized composites for transesterification between Gly and DMC (She et al., 2021). The rice-shaped catalyst with shorter meso-channels improved the internal diffusion pathlengths of both reactants and reaction products. Moreover, the nanosized composite with the largest surface area exhibited a high density of surface basic sites resulting in a promising catalytic activity. Hence, the transesterification could be a morphology-dependent reaction.

To enhance the Gly conversion to the desired GC product under environment-friendly catalysis, it is necessary to use intrinsic basic nanosized zeolites with a specific morphology. BPH-type zeolite (Linde Q) has a pore window of 0.63×0.63 nm, which is larger than the appropriate pore according to the literature (Moliner et al., 2015). Clatworthy et al. (2021) recently synthesized BPH zeolite nanosheets with varying morphologies (shapes, thickness, and particle sizes). The nanosheets containing three alkali cations (Na⁺, K⁺, and Cs⁺) were synthesized at a hydrothermal temperature of 60 °C without the use of an organic structure-directing agent (OSDA). Herein, BPH zeolite nanosheets with different morphologies were studied in terms of the correlation of their morphologies and catalytic activities for transesterification between glycerol and dimethyl carbonate. The reaction factors affecting the catalytic abilities including BPH morphologies, reactant mole ratios, catalyst dosage, reaction temperature and time, and reusability were discussed.

4.3 Experimental

4.3.1 Synthesis of BPH zeolite nanosheet

BPH zeolite nanosheet was synthesized according to Clatworthy et al. (2021) with the molar composition 0.3 Cs₂O: 1.25 K₂O: 8.07 Na₂O: 10 SiO₂: 0.8 Al₂O₃: 120 H₂O. The alkali aluminate mixture was prepared by dissolving 0.518 g of sodium aluminate (NaAlO₂, 50-56% Al₂O₃, 40-45% Na₂O, Sigma-Aldrich) and 3.78 g of double distilled water followed by mixing 1.78 g of sodium hydroxide (NaOH, 99%, VWR Chemicals), 0.495 g of potassium hydroxide (KOH, 90%, Sigma Aldrich), and 0.506 g of cesium hydroxide solution (50 wt.% CsOH solution, CsOH·xH₂O (15-20% H₂O), 99.9%, Alfa Aesar) in double-distilled water. All water used was double distilled using an Aquatron water still A4000D in a 60-mL polypropylene bottle. The aluminate solution was rapidly stirred for 2 h at room temperature until the clear solution was obtained. After that, 4.77 g of LUDOX[®] AS-40 colloidal silica (SiO₂, 40 wt.% suspension, Aldrich) was added dropwise to the clear aluminate solution resulting in the presence of a turbid mixture. The mixture was vigorously stirred for 24 h following by hydrothermal at 60 °C for 16 h. The zeolite product was centrifuged at 20,000 rpm for 20 min, washed with double distilled water until the pH of the supernatant was ~7-8, and dried in an oven at 60 °C overnight. The as-prepared BPH zeolite nanosheet was abbreviated as nano CsBPH_AP.

4.3.2 Synthesis of micron-sized BPH (Linde Q)

The chemical composition of micron-sized BPH was: 16 K₂O: 4 SiO₂: 1 Al₂O₃: 192 H₂O (Clatworthy et al., 2021). The potassium silicate solution was prepared by adding 6.47 g of potassium silicate (K₂SiO₃, anhydrous ~48 Mesh, SiO₂:K₂O 2.5:1 wt.%, Alfa Aesar), to 23.92 g of double-distilled water. Then, the mixture was stirred overnight followed by heating at 60 °C for 30 min. The potassium aluminate solution was prepared by dissolving 3.0 g of aluminium hydroxide (Al(OH)₃, extra pure, Acros Organics) and 35.92 g of potassium hydroxide (KOH, 90%, Sigma Aldrich) in 42.6 g of double distilled water followed by heating at 90 °C for 30 min. After that, the potassium aluminate solution was slowly added to the potassium silicate solution with rapid stirring to form a cloudy gel. The gel was treated hydrothermally at 50 °C for 162 h. The product was collected and washed by centrifugation (20,000 rpm, 20 min) with

double distilled water until the pH of the supernatant was ~7-8. The product was dried in an oven at 60 °C overnight. The as-prepared micron-sized BPH zeolite was abbreviated as micro KBPH_AP.

4.3.3 Preparation of ion-exchange

The suspension of nano CsBPH_AP (5 wt.% solid) was ion-exchanged with 25.00 g of potassium solution (pH 9.8) containing 5 mM mixed solution of potassium nitrate (KNO₃, 99%, Sigma Aldrich) and potassium hydroxide (KOH, 90%, Sigma Aldrich) (10:1 w/w). For micro BPH_AP suspension (5 wt.% solid), cesium solution containing 5mM mixed solution of cesium nitrate (CsNO₃, 99%, Sigma Aldrich) and cesium hydroxide hydrate (CsOH·xH₂O (15-20% H₂O), 99.9%, Alfa Aesar) (10:1 w/w). Each mixture was stirred at room temperature for 1 h, washed with double distilled water and centrifuged (20,000 rpm, 20 min) until the pH of the supernatant was ~7-8. This procedure was repeated twice. The ion-exchanged of nano CsBPH_AP and micro BPH_AP zeolite were denoted as nano K-CsBPH_IE and micro Cs-KBPH_IE, respectively.

4.3.4 Catalyst characterization

Morphology of zeolite samples was recorded by field emission scanning electron microscopy (FE-SEM) using a Zeiss AURIGA FE-SEM/FIB/EDX with an upper electron detector operating at an accelerated voltage of 3 kV with a working distance of 7.1 mm. Each sample was placed on a carbon tape adhered to a copper stub and then coated by gold, using an operating current at 10 mA under an argon atmosphere for 5 min. A particle size distribution was processed by an ImageJ software version 1.49.

Phase characteristics of samples were determined by powder X-ray diffraction (XRD) with a PANalytical X'Pert PRO-MPD diffractometer with Cu K_α radiation ($\lambda = 1.5418 \text{ \AA}$). All patterns were collected by 2θ range of 4-50° with a step size of 0.0167° and time per step of 950 s. Functional groups of samples were confirmed by Fourier transform infrared spectroscopy (FTIR) equipped with a microscope on a Bruker, Tensor27-Hyperion using ATR technique. The spectrum was recorded from 4000-400 cm⁻¹ with a resolution of 4 cm⁻¹ and 64 scans.

Thermal analysis was performed by a Setsys SETARAM analyzer. The sample around 5-10 mg was placed in an alumina cup and then heated from 30-800 °C with a heating rate of 5 °C·min⁻¹ under dry air flow with a rate of 40 mL·min⁻¹. The

chemical composition of the zeolites was determined by Inductively coupled plasma mass spectrometry (ICP-MS) using a 7900 ICP-MS from Agilent Technologies. N_2 adsorption-desorption Isotherms of all samples were measured using a Micrometrics ASAP 2020 volumetric adsorption analyzer. The samples were degassed at 350 °C under vacuum overnight for nano K-CsBPH_IE, degassed at 300 °C for fresh and reused nano CsBPH_AP, and degassed at 120 °C for micro KBPH_AP and micro Cs-KBPH_IE. Surface areas were calculated by Brunauer-Emmett-Teller (BET) method and micropore volumes were estimated by the *t*-plot method.

The basicity of the catalysts was investigated by temperature-programmed desorption of carbon dioxide (CO_2 -TPD) using a BELCAT-B chemisorption analyzer. Initially, catalyst of 50 mg was packed in a tubular glass reactor and pretreated at 150 °C under helium (He) gas flow with a rate of 30 mL·min⁻¹ for 180 min. Then, it was cooled down to 50 °C and a gas mixture of 10% CO_2 /He was adsorbed on the catalyst for 90 min with flow rate of 30 mL·min⁻¹. Afterwards, it was purged with He gas and held for 30 min to remove non-adsorbed CO_2 . The desorbed CO_2 was quantified by TPD process in a temperature range of 50 to 150 °C with a temperature ramp of 5 °C·min⁻¹ and held at 150 °C for 120 min with helium gas flow rate of 30 mL·min⁻¹. The basicity was obtained by integration of peak area.

²⁷Al MAS NMR spectra were recorded on a Bruker Advance III-HD 500 (11.7 T) spectrometer using 4 mm-OD zirconia rotors. ²⁷Al MAS NMR was done with a $\pi/12$ pulse (selective pulse), a spinning speed of 14 kHz and a recycle delay of 1 s. Prior to measurement, the samples were fully hydrated in a water vapor-saturated chamber at ambient temperature. $Al(NO_3)_3$ (1 M) was used as a chemical shift reference for ²⁷Al nuclei.

4.3.5 Transesterification between glycerol and dimethyl carbonate

The catalytic properties of samples in the transesterification of glycerol and dimethyl carbonate (DMC) to yield glycerol carbonate (GC) were carried out in a heavy wall pressure vessel at atmospheric pressure. In a typical experiment, 1.5 g (16.29 mmol) of glycerol ($C_3H_8O_3$, 99.5%, Alfa Aesar), 4.40 g (48.84 mmol) of dimethyl carbonate ($C_3H_6O_3$, 99%, Alfa Aesar), and 120 mg of catalyst (8 wt.% compared with an amount of glycerol used) were added and the reaction was carried out at the desired

temperature and time under magnetic stirring speed of 800 rpm in a silicone oil bath. After the reaction, the product mixture was separated from the catalysts by centrifugation. The separated catalyst was washed with ethanol and deionized water to remove the adsorbed organic residue, dried in an oven at 80 °C overnight and used in the next run. The optimum reaction condition including temperature, time, catalyst loading, DMC-to-glycerol ratios, and catalyst reusability were determined.

Reaction liquid products were determined by high-performance liquid chromatography (1260 Infinity II LC System, Agilent, United States of America) equipped with a Aminex HPX-87H column and a refractive index detector. 5 mM of sulfuric acid solution (H₂SO₄, 98%, QRëC) was used as the mobile phase with a flow rate of 0.6 mL·min⁻¹ and column temperature of 55 °C. When glycerol is the limiting reactant, glycerol conversion, GC yield, and GC selectivity were calculated using the equations (1-3), respectively.

$$\% \text{Glycerol conversion} = \frac{\text{mole of glycerol added} - \text{mole of glycerol remained}}{\text{mole of glycerol added}} \times 100 \quad (1)$$

$$\% \text{GC yield} = \frac{\text{mole of glycerol carbonate produced}}{\text{mole of glycerol added}} \times 100 \quad (2)$$

$$\% \text{GC selectivity} = \frac{\text{glycerol carbonate yield}}{\text{glycerol conversion}} \times 100 \quad (3)$$

4.4 Results and discussion

4.4.1 Characterization of the catalysts

The SEM images of the as-prepared nano CsBPH_{AP} and micro KBPH_{AP} samples are shown in **Figure 4.1(a)** and **4.1(b)**, respectively. The nano CsBPH_{AP} has plate-like crystals with highly aggregation. The crystal dimension is 192±15 nm across and 20±3 nm thick. The morphology is similar to the nanosized BPH zeolite synthesized by (Clatworthy et al., 2021). In the case of micro KBPH_{AP}, it has plate-like morphology with dimension of 541±40 nm across and 57±9 nm thick. The SEM images of both samples confirm that they have different crystal sizes and dimension which may affect

the catalytic performance. In general, the smaller size provides the better diffusion of the reactants and products in and out of the zeolite cavities.

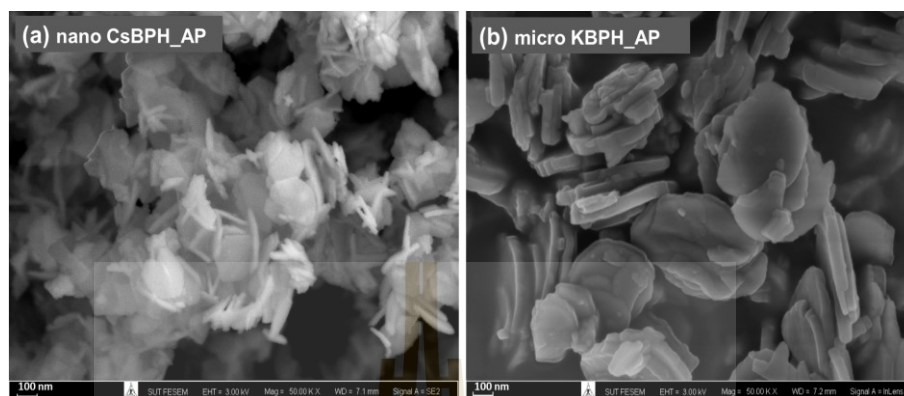


Figure 4.1 SEM images of (a) nano CsBPH_AP and (b) micro KBPH_AP.

From the ICP analysis in **Table 4.1**, cesium concentration from the nano K-CsBPH_IE slightly decreased after ion-exchange by potassium solution. Meanwhile, the cesium amount from micro Cs-KBPH_IE increased after ion-exchange by cesium solution. These results showed that although these BPH-type zeolite nanosheets were ion-exchange by different alkali solutions, original alkali metal ions (Na^+ , K^+ , Cs^+) were still preserved probably due to the strong ionic interaction between the intrinsic alkali ions and the zeolite structure (Walton et al., 2006; Yang et al., 2010). From the different gel composition of synthesis recipes, the nano CsBPH_AP sample has a higher Si/Al molar ratio than the micro KBPH_AP. After the ion-exchange process, the Si/Al ratio of the ion-exchanged zeolites was similar to their parents.

Table 4.1 Elemental composition of BPH-type zeolite nanosheets by ICP-MS and basicity by CO₂-TPD

Catalyst	Concentration (wt.%)					Si/Al ratio (mol)	Basicity (mmol CO ₂ ·g ⁻¹)
	Si	Al	Na	K	Cs		
micro KBPH_AP	12.97	12.13	-	18.56	-	1.03	0.327
micro Cs-KBPH_IE	12.56	11.68	-	16.71	3.79	1.04	0.350
nano CsBPH_AP	15.00	9.87	4.61	2.89	13.39	1.46	0.130
nano K-CsBPH_IE	15.45	10.13	3.99	4.14	14.95	1.47	0.105
reused nano CsBPH_AP	14.16	9.63	4.33	2.72	14.30	1.41	0.080

All synthesized BPH nanosized and micronsized zeolites with different morphologies give the distinctive BPH characteristic in the XRD patterns as shown in **Figure 4.2**. The XRD patterns from both parent micro KBPH_AP and nano CsBPH_AP samples agree with the space group *P321* as part of the trigonal structure (Clatworthy et al., 2021). The peak intensity of the nano CsBPH_AP is lower than that of another one possibly due to the significant difference of lattice parameter. Comparing the morphology of these BPH zeolites in terms of lattice parameters (*a* and *c* axes) defined by our previous work (Clatworthy et al., 2021), the nano CsBPH_AP has a smaller lattice parameter of the *a* axis and the lower unit cell volume than the micro KBPH_AP. The contraction of the unit cell and lattice parameter could be from the isomorphous substitution of Al³⁺ ions (0.39 Å) with the original site of Si⁴⁺ ions (0.26 Å), (Blackwell et al., 2003; Clatworthy et al., 2021) related to the Si/Al molar ratio determined by ICP-OES analysis as listed in **Table 4.1**. After the course of the ion-exchange process, the XRD patterns from both micro Cs-KBPH_IE and nano K-CsBPH_IE are similar to their parent ones. This indicates that the crystal structure and the morphology of these ion-exchanged samples are stable against the ion-exchange condition.

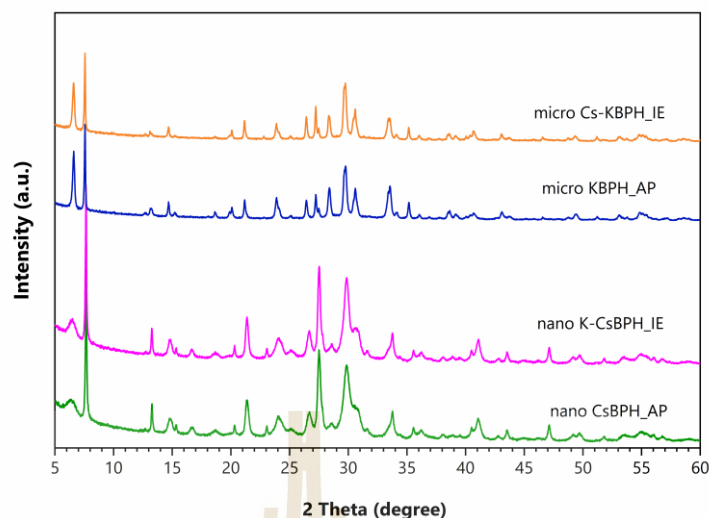


Figure 4.2 XRD pattern of as-prepared BPH zeolite and ion-exchanged BPH zeolite compared with their parent zeolites.

The FTIR spectra of as-prepared and ion-exchanged BPH zeolites are shown in **Figure 4.3**. The nano CsBPH_AP and micro KBPH_AP have similar FTIR spectrum but different peak position due to the different Si/Al ratio (Ma et al., 2021). The characteristic peaks of BPH zeolite at 1150-950 cm^{-1} and 740-660 cm^{-1} are attributed to asymmetric and symmetric stretching of the zeolite framework, respectively. The vibration band at 598, 496, and 410 cm^{-1} are assigned to bending mode of Si-O-T, where T is Si or Al atom of the zeolites (Andries et al., 1991). Moreover, the bands of OH groups or water are observed at 1649 and 3400 cm^{-1} . After ion-exchanged with alkali ion, the spectrum of nano K-CsBPH_IE and micro Cs-KBPH_IE are similar to their parent zeolites.

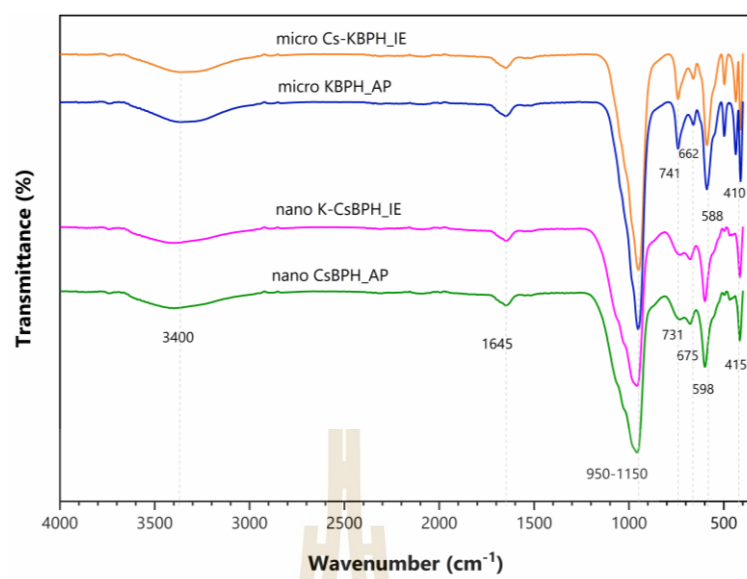


Figure 4.3 FTIR spectra of as-prepared BPH zeolite and ion-exchanged BPH zeolite compared with their parent zeolites.

Figure 4.4 compares thermal stability of BPH-type zeolite nanosheets after ion exchanging with different alkali ion, TGA curves of these zeolites under dry air condition. The nano CsBPH_AP sample gives one step of mass loss below 130 °C while the micro KBPH_AP sample exhibits two steps of mass loss at 110 °C and 220 °C. The difference of thermal dehydration behavior related to the different external surface area was been described in the literature (Clatworthy et al., 2021). After 300 °C, both sample show almost complete dehydration. The nano K-CsBPH_IE, exchanged by K precursor, shows total mass loss (16.0%), higher than its parent nano CsBPH_AP (15.5%) implying less thermal stability after the process of alkali ion-exchange. The micro Cs-KBPH_IE, exchanged by Cs precursor, prevents the dehydration step leading to the lower mass loss (14.5%) than its parent (15.1%) due to the decrease in the free volume of zeolite cavities by increasing cationic size (Ng, and Mintova, 2008). The finding indicate that the Cs ions could play more important role on thermal stability.

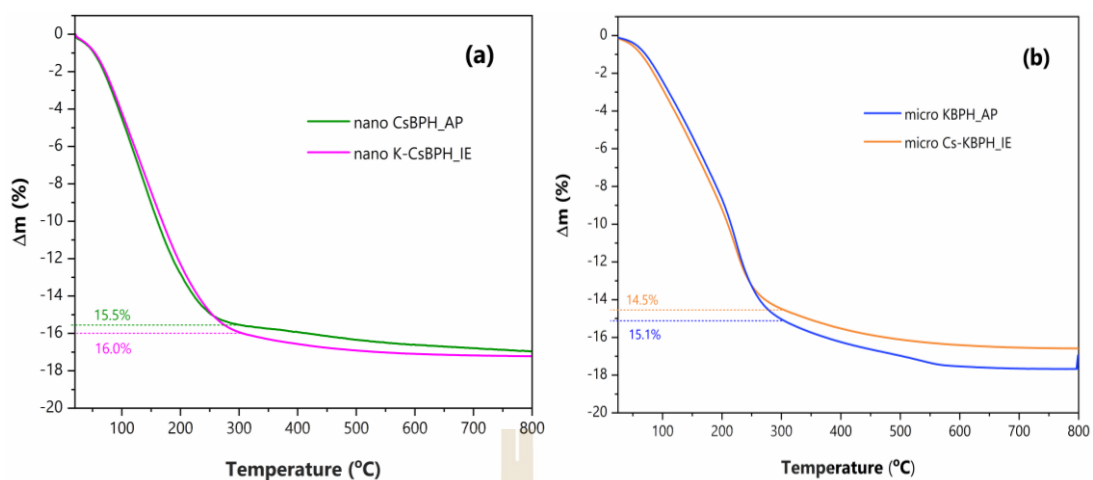


Figure 4.4 TG profiles of (a) nano CsBPH_AP and nano K-CsBPH_IE and (b) micro KBPH_AP and micro Cs-KBPH_IE.

The CO₂-TPD profiles and basicity from as-prepared and ion-exchanged BPH zeolites are shown in **Figure 4.5** and listed in **Table 4.1**, respectively. Micro KBPH_AP and nano CsBPH_AP show a desorption peak at 93 °C and 94 °C, respectively implying the same interaction with the probe molecule CO₂. However, micro KBPH_AP gives the stronger intrinsic basicity because of a lower Si/Al ratio (Al-Ani et al., 2018; Beltrao-Nunes et al., 2019; Busca, 2017). After ion-exchange, the feature of CO₂-TPD profiles from micro Cs-KBPH_IE and nano K-CsBPH_IE are similar to their parents. With a higher Cs content, micro Cs-KBPH_IE provides a stronger basicity than its parent; nano CsBPH_AP gives a higher basicity than nano K-CsBPH_IE with a lower Cs content. These results consistent with CO₂ adsorption on zeolite Y at low pressure that the basicity of oxygen atoms in the zeolite Y framework decreased from Cs⁺ to Li⁺ ion (Pirngruber et al., 2010). The simultaneous interaction of CO₂ with Cs⁺ and neighboring framework oxygen atoms stabilized CO₂ adsorption on CsY more than that on KY.

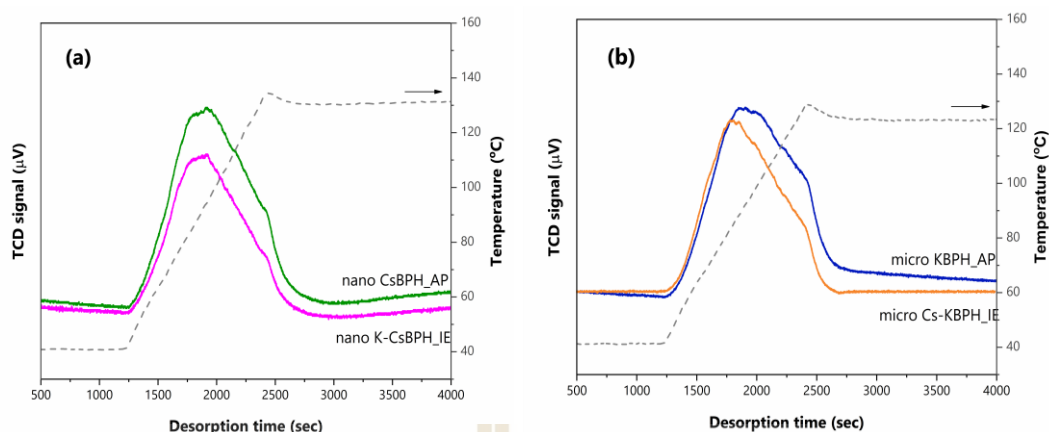


Figure 4.5 CO₂-TPD profiles of (a) nano CsBPH_AP and nano K-CsBPH_IE and (b) micro KBPH_AP and micro Cs-KBPH_IE.

4.4.2 Catalytic activity on transesterification of glycerol and DMC

4.4.2.1 Catalyst screening

The effect of BPH nanosheets from hydrothermal and ion-exchange method on transesterification of glycerol and DMC is summarized in **Table 4.2**. Before catalytic activity evaluation, the reaction was conducted without catalyst for transesterification of glycerol and DMC. It gave poor reaction activity including the conversion of glycerol and yield of GC product. It confirmed that the transesterification reaction requires catalysts. Comparing the morphology in term of particle sizes of BPH nanosheets, the smaller particle size of nano CsBPH_AP catalyst provides the better transesterification activity than that of micro KBPH_AP. These results are consistent with the work by She et al. (2021). They reported the rice-shaped LDH/SBA-15 nanocomposite gave a higher activity in the transesterification of glycerol and DMC than the other morphologies including short and long rods. This was a result from a shorter internal diffusion path length and a larger accessible basic site. Consequently, the morphology of BPH nanosheet in term of particle sizes is responsible to the glycerol conversion to GC product. According to the different cations (Na⁺, K⁺, Cs⁺) in as-prepared BPH nanosheet, this might affect the reaction performance. Hence, the role of such cations by ion-exchange method was investigated, and the result is concluded in **Table 4.1**. After ion-exchange of the nano-sized BPH by potassium

precursor, nano K-CsBPH_IE with the lower Cs amount give a lower catalytic activity than the nano CsBPH_AP. In contrast by increasing the Cs content in the micron-sized BPH, micro Cs-KBPH_IE show a higher activity than the parent. At a high Cs content, the basicity of nano CsBPH_AP and micro Cs-KBPH_IE nanosheets increases. This finding corresponds with the basicity by CO₂-TPD and the previous report by Al-Ani et al. (2018). Hence, not only the morphology of BPH nanosheets is crucial, but also the basicity is also a key in the transesterification of glycerol and DMC. In accordance with the results, the nano CsBPH_AP catalyst is suitable for further reaction study.

Table 4.2 Comparison of BPH nanosheets with various particle sizes from hydrothermal and ion-exchange method for transesterification of glycerol and DMC.

Sample	Gly conversion (mol %)	GC yield (mol %)	GC selectivity (mol %)
Blank test	5	3	60
micro KBPH_AP	48	44	92
micro Cs-KBPH_IE	54	53	98
nano CsBPH_AP	67	64	95
nano K-CsBPH_IE	57	55	98

Conditions: temperature of 120 °C; time of 3 h; Gly-to-DMC molar ratio of 1:3; catalyst loading of 8 wt.%.

4.4.2.2 Effect of different reaction parameters

The effect of reaction temperature in the range of 90-135 °C on the transesterification over nano CsBPH_AP catalyst is shown in **Figure 4.6**. The reaction activity increases with the temperature indicating that the reaction is endothermic. The finding suggests that the viscosity of reactants is reduced, and the miscibility of glycerol and DMC is enhanced (Algoufi, and Hameed, 2014). It relates to the Arrhenius equation, which states that increasing the reaction temperature can enhance the miscibility of the multiphase reaction system, reaction rate, and potentially improving product yield. Although the highest catalytic activity is achieved at the reaction temperature of 135

°C, the selectivity of GC decreases. This result indicates the reaction temperature higher than 120 °C is unsuitable due to the formation of by-products. Comparing with the literature, the as-prepared nano CsBPH_AP with an intrinsic basicity requires a higher reaction temperature than other catalysts with stronger basicity such as metal oxides (Kaur, and Ali, 2021; Ochoa-Gómez et al., 2009) and metal oxide-supported catalysts (Algoufi, and Hameed, 2014; Keogh et al., 2022; Liu et al., 2022; She et al., 2021). However, the nanosheet catalyst is economically prepared without any further modification and prevent the formation of by-product glycidol. Accordingly, the optimal temperature for the transesterification of glycerol and DMC catalyzed by nano CsBPH_AP is 120 °C.

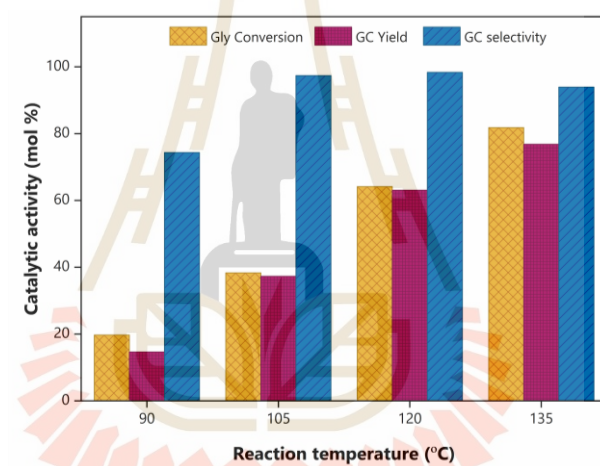


Figure 4.6 Effects of temperature on transesterification of glycerol with DMC using nano CsBPH_AP catalyst. Condition: Gly-to-DMC molar ratio of 1:3, 8 wt.% catalyst, 3 h.

Figure 4.7 shows the effect of reaction time from 1 to 6 h on the transesterification of glycerol with DMC over nano CsBPH_AP catalyst. The reaction activity including glycerol conversion and GC yield increases with the reaction duration. From the previous report, the reactivity of the first and second -OH groups in glycerol are faster than the third -OH group. It requires more reaction time to ensure complete access of these -OH groups to DMC molecules and facilitate the formation of stable cyclic carbonate (Xiang, and Wu, 2018). Moreover, the result is consistent with the previous report (Das, and Mohanty, 2019; Wang et al., 2017). Considering the significant

increase of the reaction activity with time, the duration of 3 h is suitable for further evaluation.

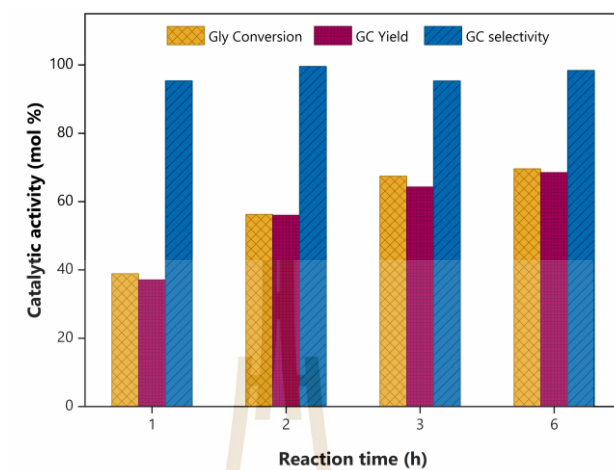


Figure 4.7 Effects of time on transesterification of glycerol with DMC using nano CsBPH_{AP} catalyst. Condition: Gly-to-DMC molar ratio of 1:3, 8 wt.% catalyst, 120 °C.

Figure 4.8 compares the catalyst dosage in the range of 4-12 wt.% on the transesterification of glycerol and DMC over the nano CsBPH_{AP} catalyst. The reaction activity consistent of glycerol conversion and GC yield increases with the catalyst loading up to 6 wt.%. This could be from the increase in the concentration of active basic sites which initiate the transesterification of glycerol by abstracting its proton from the first hydroxyl group (Algoufi, and Hameed, 2014). When the loading of the catalyst is higher than 6 wt.%, the reaction activity decreases possibly due to the increase of the reaction viscosity and the adsorption of the reactants and products on the catalyst surface. Moreover, the different catalyst dosages do not affect the selectivity of GC product. Thus, the catalyst loading of 6 wt.% is optimal for the reaction.

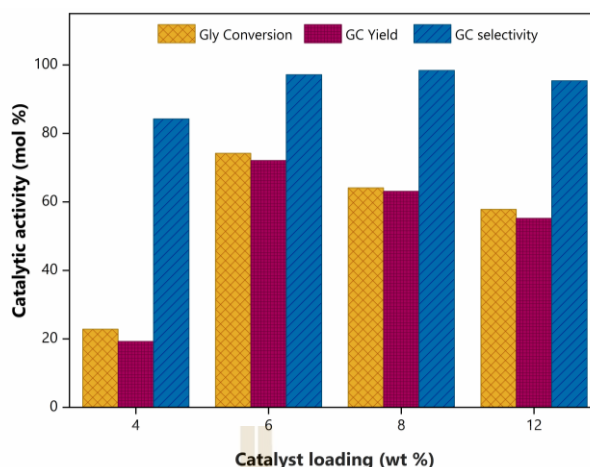


Figure 4.8 Effects of catalyst loading on transesterification of glycerol with DMC using nano CsBPH_{AP} catalyst. Condition: Gly-to-DMC molar ratio of 1:3, 120 °C, 3 h.

The comparison of the molar ratios of glycerol to DMC on the transesterification is shown in **Figure 4.9**. In the transesterification of glycerol and DMC, not only the molar ratio of DMC: glycerol (1:1) required but also consider the biphasic system generated by hydrophilic glycerol and hydrophobic DMC. Herein, an excessive amount of DMC is always used to increase the contact between glycerol and DMC, force forward the reaction equilibrium, and prevent the reaction from becoming reversible. At the equivalent molar ratio, both glycerol conversion and GC yield are below 50 mol % due to the increase of viscosity and poor mass transfer of reactants in the reaction system. At a molar ratio of glycerol to DMC above 1:3, the reaction activity increases because the molar ratio higher than this point is enough to shift the reaction equilibrium toward the GC product (Algoufi, and Hameed, 2014; Arora et al., 2020; Das, and Mohanty, 2019). Considering the reaction manipulation, the molar ratio of 1:5 can facilitate the magnetic stirring system of the reaction by decreasing the reaction viscosity. Using the molar ratio of 1:9, the excess amount of DMC is consumed without any change in the reaction activity. Therefore, the glycerol-to-DMC molar ratio of 1:5 is appropriated for transesterification.

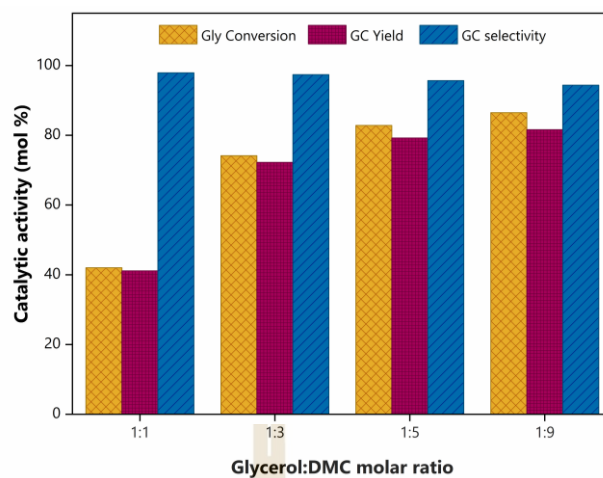


Figure 4.9 Effects of Gly-to-DMC molar ratio on transesterification of glycerol with DMC using nano CsBPH_{AP} catalyst. Condition: 6 wt.% catalyst, 120 °C, 3 h.

4.4.2.3 Reusability of the catalyst

In the reusability study of the nano CsBPH_{AP} catalyst, the catalyst was separated from the liquid product and washed with ethanol and water through centrifugation. Then, the washed catalyst was dried at 80 °C overnight and further used in each cycle. **Figure 4.10** shows the reusability and leaching results of nano CsBPH_{AP} catalyst in the transesterification of glycerol and DMC. The reduction of glycerol conversion (14%) and GC product (13%) are observed in the fourth run while the selectivity of the GC product is constant. The loss in the catalyst activity of nano CsBPH_{AP} becomes a problem in transesterification. Thus, a leaching test is performed to confirm the catalyst stability.

In the leaching test, the catalyst was removed at the reaction time of 1 h by hot filtration and then the filtrate was kept in the same condition for another 2 h. In the comparison to glycerol conversion with no filtration and hot filtration, the conversion increases with the presence of the catalyst, while there is no further glycerol conversion after the catalyst removal. In addition, the elemental results by ICP-MS (see **Table 4.1**) of both fresh and reused catalysts show the weight percentage of Na and K ions slightly decreases. The disappearance of the ionic species could be from the leaching effect during transesterification, corresponding to the previous report by Wang et al. (2018).

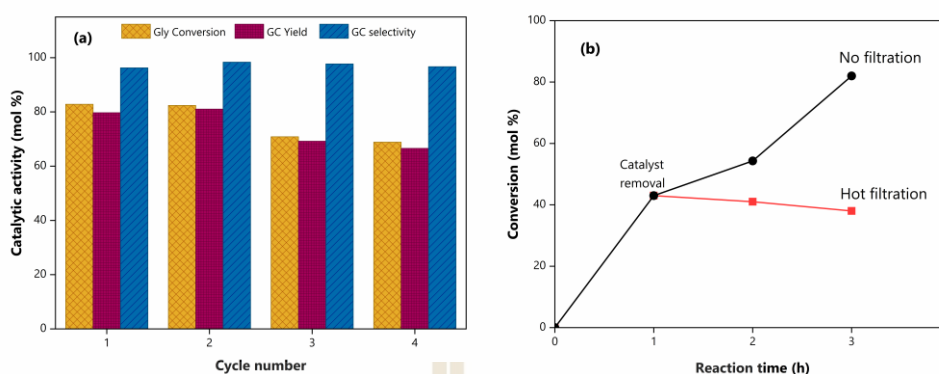


Figure 4.10 (a) Reusability test and (b) leaching test of nano CsBPH_AP under reaction conditions: temperature of 120 °C; time of 3h; molar ratio of Gly-to-DMC of 1:5; catalyst loading of 6 wt.%.

In general, catalyst deactivation is caused by active site covering, sintering of the active phase, fouling of active site, and loss of active component. The fourth reused catalyst was further characterized by XRD, ^{27}Al MAS NMR, TGA, and CO_2 -TPD techniques. The XRD and ^{27}Al MAS NMR are used to identify the structural stability of reused and fresh catalysts. **Figure 4.11** show no significant change, indicating the change of both structural property and Al framework species are not observed.

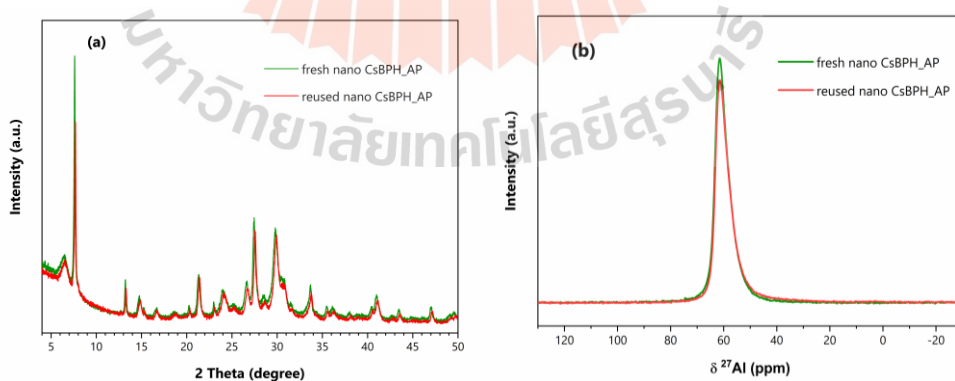


Figure 4.11 Comparison of structural stability between reused and fresh catalysts by (a) XRD patterns and (b) ^{27}Al MAS NMR spectra.

To find the catalyst deactivation in terms of fouling effect and to get the suitable solvent for the washing step, The reused catalyst is washed with different solvents such as ethanol and water after reaction testing. Thermogravimetric analysis (TGA) is used for the measurement of volatile components by monitoring the weight change. **Figure 4.12** shows the TGA profiles of reused catalysts washed with ethanol and water as solvents. The TGA curve in the blue line shows three-step of mass losses at 90 °C , 200 °C , and 300 °C which is attributed to the loss of deposited organic residue. It's confirmed that ethanol is not a suitable solvent for the washing step. Therefore, water as a more polar solvent is used to remove the polar organic residue on the catalyst surface. From the results of reused catalyst washed with ethanol and water, the TGA curve in the red line shows a mass loss similar to the fresh catalyst in the black line. This indicated the washing of the catalyst with ethanol and water can remove the deposited organic compound on the catalyst surface. As a result of the TGA study, ethanol and water were used to wash the catalyst after reaction testing.

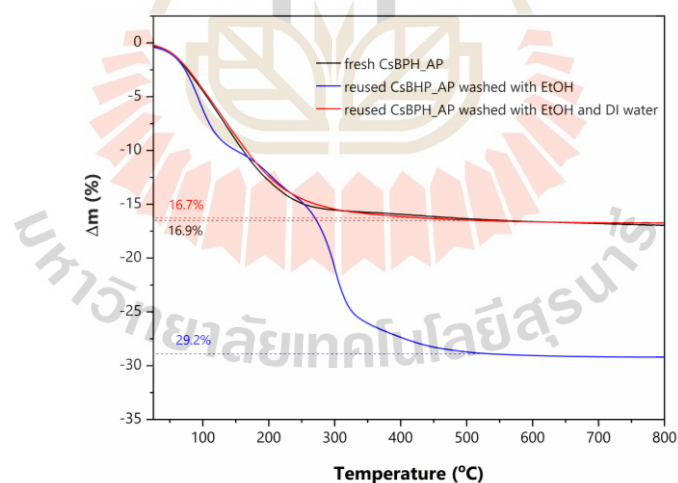


Figure 4.12 TG profiles of reused catalysts washed with different solvents compared with fresh catalysts.

The basicity of reused catalyst was determined by CO₂-TPD (see Table 4.1, Figure 4.7). After the catalytic testing, the basicity of the reused catalyst decreased as a result of the leaching effect confirmed by the ICP-MS mentioned above. Therefore, although there is less reduction of the catalyst activity after the fourth run, the nano CsBPH_AP provides promising catalyst stability and reusability in the glycerol conversion to glycerol carbonate product.

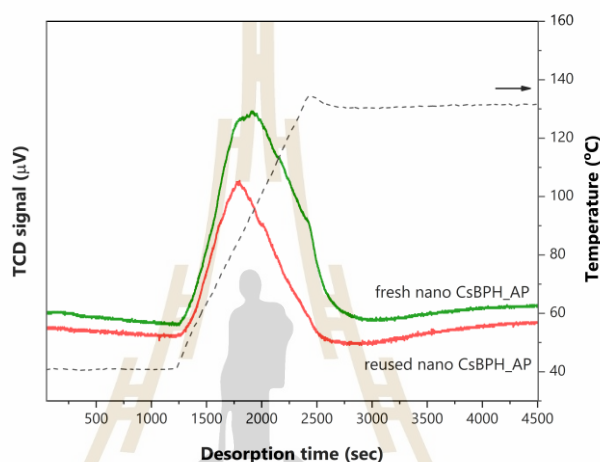


Figure 4.13 CO₂-TPD profiles of the reused catalyst compared with fresh catalyst.

4.5 Conclusions

BPH-type zeolite nanosheets with different morphologies and Si/Al ratios were successfully synthesized by hydrothermal treatment. As-prepared BPH zeolite nanosheet (nano CsBPH_AP) with the particle size of 192 ± 15 nm had a higher Si/Al ratio than as-prepared micron-sized BPH zeolite (micro KBPH_AP) with the particle size of 541 ± 40 nm. Due to the difference of K⁺/Cs⁺ cation in the zeolite framework, both as-prepared ones were ion-exchanged by either K or Cs precursors. The structural and morphological characteristics and functional groups of ion-exchanged nano CsBPH_AP (nano K-CsBPH_IE) and ion-exchanged micro BPH_AP (micro Cs-KBPH_IE) are stable. In addition, they behave with slightly different thermal properties against their parents. Moreover, BPH zeolite nanosheet with a higher Cs content has stronger basicity than others, confirmed by CO₂-TPD. Comparing catalytic performance by the

transesterification of glycerol towards glycerol carbonate, nano CsBPH_{AP} with a small particle size provides the best reaction activity because of the smallest particle size and shortest diffusional path. These catalysts give the product selectivity towards only glycerol carbonate. Consequently, the optimal reaction condition is at 120 °C for 3 h with the catalyst loading of 6 wt.% and the glycerol-to-dimethyl carbonate molar ratio of 1:5. The nano CsBPH_{AP} shows good catalytic performance up to the fourth run. Hence, the catalyst morphology could play important to control the conversion of glycerol towards glycerol carbonate.

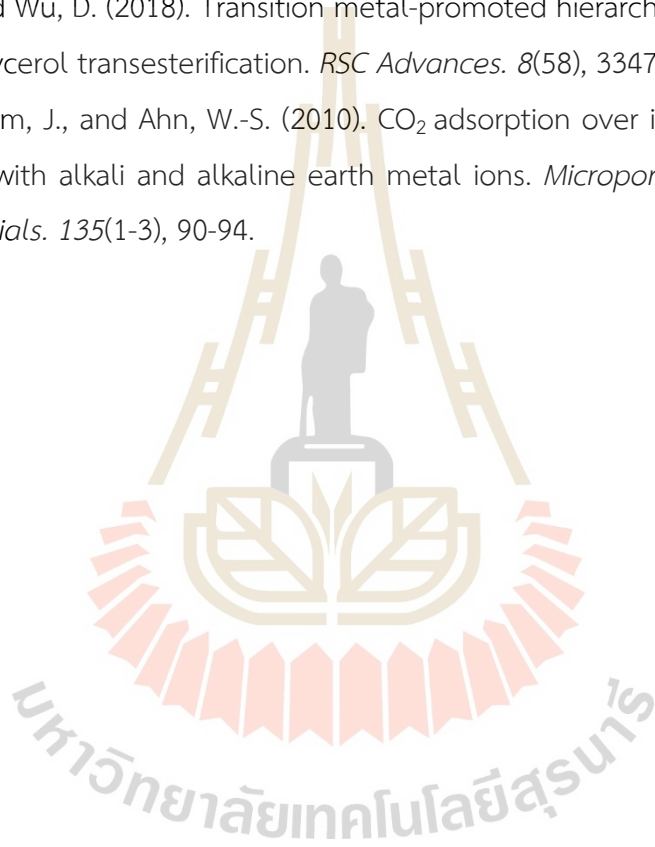
4.6 References

- Al-Ani, A., Darton, R. J., Sneddon, S., and Zholobenko, V. (2018). Nanostructured zeolites: the introduction of intracrystalline mesoporosity in basic faujasite-type catalysts. *ACS Applied Nano Materials*. 1(1), 310-318.
- Algoufi, Y. T., and Hameed, B. H. (2014). Synthesis of glycerol carbonate by transesterification of glycerol with dimethyl carbonate over K-zeolite derived from coal fly ash. *Fuel Processing Technology*. 126, 5-11.
- Andries, K. J., Wit, B. D., Grobet, P. J., and Bosmans, H. J. (1991). The synthesis and properties of synthetic zeolite Linde Q. *Zeolites*. 11(2), 116-123.
- Arora, S., Gosu, V., and Subbaramaiah, V. (2020). One-pot synthesis of glycerol carbonate from glycerol using three-dimensional mesoporous silicates of K/TUD-1 under environmentally benign conditions. *Molecular Catalysis*. 496, 111188.
- Beltrao-Nunes, A.-P., Sennour, R., Arus, V.-A., Anoma, S., Pires, M., Bouazizi, N., Roy, R., and Azzouz, A. (2019). CO₂ capture by coal ash-derived zeolites- roles of the intrinsic basicity and hydrophilic character. *Journal of Alloys and Compounds*. 778, 866-877.
- Blackwell, C. S., Broach, R. W., Gatter, M. G., Holmgren, J. S., Jan, D.-Y., Lewis, G. J., Mezza, B. J., Mezza, T. M., Miller, M. A., Moscoso, J. G., Patton, R. L., Rohde, L. M., Schoonover, M. W., Sinkler, W., Wilson, B. A., and Wilson, S. T. (2003). Open-Framework Materials Synthesized in the TMA⁺/TEA⁺ Mixed-Template System:

- The New Low Si/Al Ratio Zeolites UZM-4 and UZM-5. *Angewandte Chemie International Edition*. 42(15), 1737-1740.
- Busca, G. (2017). Acidity and basicity of zeolites: A fundamental approach. *Microporous and Mesoporous Materials*. 254, 3-16.
- Clatworthy, E. B., Debost, M., Barrier, N., Gascoin, S., Boullay, P., Vicente, A., Gilson, J.-P., Dath, J.-P., Nesterenko, N., and Mintova, S. (2021). Room-Temperature Synthesis of BPH Zeolite Nanosheets Free of Organic Template with Enhanced Stability for Gas Separations. *ACS Applied Nano Materials*. 4(1), 24-28.
- Das, B., and Mohanty, K. (2019). A green and facile production of catalysts from waste red mud for the one-pot synthesis of glycerol carbonate from glycerol. *Journal of Environmental Chemical Engineering*. 7(1), 102888.
- Kaur, A., and Ali, A. (2021). Surface-modified CaO catalyst for the production of glycerol carbonate. *ChemistrySelect*. 6(24), 6102-6114.
- Keogh, J., Deshmukh, G., and Manyar, H. (2022). Green synthesis of glycerol carbonate via transesterification of glycerol using mechanochemically prepared sodium aluminate catalysts. *Fuel*. 310, 122484.
- Khanday, W. A., Okoye, P. U., and Hameed, B. H. (2017). Biodiesel byproduct glycerol upgrading to glycerol carbonate over lithium–oil palm ash zeolite. *Energy Conversion and Management*. 151, 472-480.
- Liu, P., Derchi, M., and Hensen, E. J. M. (2014). Promotional effect of transition metal doping on the basicity and activity of calcined hydrotalcite catalysts for glycerol carbonate synthesis. *Applied Catalysis B: Environmental*. 144, 135-143.
- Liu, Z., Li, B., Qiao, F., Zhang, Y., Wang, X., Niu, Z., Wang, J., Lu, H., Su, S., Pan, R., Wang, Y., and Xue, Y. (2022). Catalytic performance of Li/Mg composites for the synthesis of glycerol carbonate from glycerol and dimethyl carbonate. *ACS Omega*. 7(6), 5032-5038.
- Ma, Y.-K., Rigolet, S., Michelin, L., Paillaud, J.-L., Mintova, S., Khoerunnisa, F., Daou, T. J., and Ng, E.-P. (2021). Facile and fast determination of Si/Al ratio of zeolites using FTIR spectroscopy technique. *Microporous and Mesoporous Materials*. 311, 110683.

- Moliner, M., Martinez, C., and Corma, A. (2015). Multipore zeolites: synthesis and catalytic applications. *Angewandte Chemie International Edition*. 54(12), 3560-3579.
- Ng, E.-P., and Mintova, S. (2008). Nanoporous materials with enhanced hydrophilicity and high water sorption capacity. *Microporous and Mesoporous Materials*. 114(1-3), 1-26.
- Ochoa-Gómez, J. R., Gómez-Jiménez-Aberasturi, O., Maestro-Madurga, B., Pesquera-Rodríguez, A., Ramírez-López, C., Lorenzo-Ibarreta, L., Torrecilla-Soria, J., and Villarán-Velasco, M. C. (2009). Synthesis of glycerol carbonate from glycerol and dimethyl carbonate by transesterification: Catalyst screening and reaction optimization. *Applied Catalysis A: General*. 366(2), 315-324.
- Pan, S., Zheng, L., Nie, R., Xia, S., Chen, P., and Hou, Z. (2012). Transesterification of glycerol with dimethyl carbonate to glycerol carbonate over Na-based zeolites. *Chinese Journal of Catalysis*. 33(11), 1772-1777.
- Pirngruber, G. D., Raybaud, P., Belmabkhout, Y., Čejka, J., and Zúkal, A. (2010). The role of the extra-framework cations in the adsorption of CO₂ on faujasite Y. *Physical Chemistry Chemical Physics*. 12(41), 13534-13546.
- Qureshi, B. A., Lan, X., Arslan, M. T., and Wang, T. (2019). Highly active and selective nano H-ZSM-5 catalyst with short channels along b-axis for glycerol dehydration to acrolein. *Industrial & Engineering Chemistry Research*. 58(28), 12611-12622.
- She, Q. M., Huang, W. J., Talebian-Kiakalaieh, A., Yang, H., and Zhou, C. H. (2021). Layered double hydroxide uniformly coated on mesoporous silica with tunable morphologies for catalytic transesterification of glycerol with dimethyl carbonate. *Applied Clay Science*. 210, 106135.
- Tan, H. W., Abdul Aziz, A. R., and Aroua, M. K. (2013). Glycerol production and its applications as a raw material: A review. *Renewable and Sustainable Energy Reviews*. 27, 118-127.
- Walton, K. S., Abney, M. B., and Douglas LeVan, M. (2006). CO₂ adsorption in Y and X zeolites modified by alkali metal cation exchange. *Microporous and Mesoporous Materials*. 91(1-3), 78-84.

- Wang, S., Hao, P., Li, S., Zhang, A., Guan, Y., and Zhang, L. (2017). Synthesis of glycerol carbonate from glycerol and dimethyl carbonate catalyzed by calcined silicates. *Applied Catalysis A: General*. 542, 174-181.
- Wang, S., Xu, L., Okoye, P. U., Li, S., and Tian, C. (2018). Microwave-assisted transesterification of glycerol with dimethyl carbonate over sodium silicate catalyst in the sealed reaction system. *Energy Conversion and Management*. 164, 543-551.
- Xiang, M., and Wu, D. (2018). Transition metal-promoted hierarchical ETS-10 solid base for glycerol transesterification. *RSC Advances*. 8(58), 33473-33486.
- Yang, S.-T., Kim, J., and Ahn, W.-S. (2010). CO₂ adsorption over ion-exchanged zeolite beta with alkali and alkaline earth metal ions. *Microporous and Mesoporous Materials*. 135(1-3), 90-94.



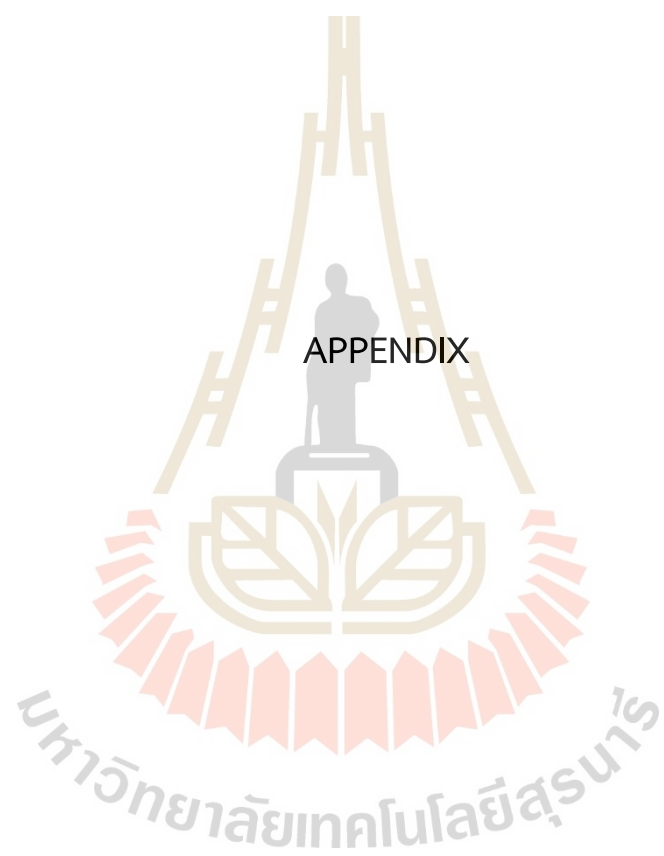
CHAPTER V

CONCLUSIONS

Potassium from potassium acetate buffer was successfully impregnated on FAU zeolites (K/NaX and K/NaY) under an ultrasound condition. After calcination, potassium precursor converted to potassium carbonate while the zeolite structures were destroyed. The NaX structure was more stable than that NaY. Besides, the basicity of K/NaX was higher than that of K/NaY. In the first run of transesterification of palm oil and methanol, high biodiesel yield was obtained from both K/NaX and K/NaY catalysts. In the second run, K/NaX gave a higher yield than K/NaY. Therefore, K/NaX catalyst is suitable for this reaction. In addition, the catalyst deactivation from the reaction has three possible causes including i) the leaching of potassium species, ii) the collapse of the zeolite structure, and iii) the change of the carbonate species.

As-prepared BPH-type zeolites with micro and nano sizes were achieved by hydrothermal method. As-prepared nano-sized one (nano CsBPH_AP) had a higher Si/Al ratio than another as-prepared micro-sized one (micro KBPH_AP). These as-prepared zeolites were ion-exchanged by either K or Cs precursors. Ion-exchanged nano CsBPH_AP (nano K-CsBPH_IE) and ion-exchanged micro BPH_AP (micro Cs-KBPH_IE) had structures, morphologies, and functional groups similar to their parents. For glycerol conversion to glycerol carbonate, nano CsBPH_AP gave an optimal reaction activity due to a small particle size and a short diffusional path. The optimal condition was at the temperature of 120 °C for 3 h with the catalyst loading of 6 wt.% and the glycerol-to-dimethyl carbonate molar ratio of 1:5. The catalysts showed an acceptable activity up to the fourth run.

Overall, these research findings demonstrated an economical and sustainable process for the conversion of palm oil into high quality biodiesel as a main product and glycerol as co-product to high-valued chemicals.



APPENDIX

มหาวิทยาลัยเทคโนโลยีสุรนารี

APPENDIX

SUPPORTING INFORMATION FOR THE BASICITY CALCULATION OF

MBOH AND FUNCTIONAL GROUP OF K/NAX AND K/NAY

CATALYSTS

A.1 Basicity calculation of Decomposition of 2-methylbut-3-yn-2-ol

The calculation method is based on the relative response factor defined by the effective carbon number concept (ECN). A response factor is calculated by an equation below. Each effective carbon number for a GC with flame ionization detector (FID) is shown in **Table A.1**.

$$rRF_i = \frac{Mw_i \times ECN_{\text{toluene}}}{Mw_{\text{toluene}} \times ECN_i}$$

where, Mw_i = Molecular weight of all components
 Mw_{toluene} = Molecular weight of toluene
 ECN_i = Effective carbon number of all components
 ECN_{toluene} = Effective carbon number of toluene

Table A.1 An effective carbon number of each chemical.

Compound	ECN _i	Mw _i	rRF _i
acetylene	1.95	26.04	1.01
MBYNE	5.50	66.10	0.91
acetone	2.00	58.08	2.21
MBOH	5.35	84.12	1.19
toluene	7.00	92.14	1.00

A.2 Vibration and peak assignments of functional groups of as-prepared and calcined catalyst

Table A.2 Vibration and peak assignments of functional groups of samples before and after calcination.

Assignment	Wavenumber (cm ⁻¹)						Reference
	NaX	as-prepared K/NaX	calcined K/NaX	NaY	as-prepared K/NaY	calcined K/NaY	
Functional groups of zeolites							
O-T-O bending vibration of S4R (T = Si or Al)	458	453	459	463	449	460	(Abu-Zied, 2011; Ma et al., 2021; Mozgawa, 2001; Phung et al., 2014)
T-O-T bending vibrations of double rings (D6R)	561	563	563	573	569	567	
Symmetric stretching of O-T-O	673-748	671-752	679-746	698-779	690-775	685-762	
Asymmetric stretching of Si-O-T	984-1069	962	989	1013-1089	978	999	
Asymmetric stretching of Si-O-Si (shoulder)	1082	1067	1089	1128	1066	1090	

Table A.2 Vibration and peak assignments of functional groups of samples before and after calcination (Continued).

Assignment	Wavenumber (cm ⁻¹)						Reference
	NaX	as-prepared K/NaX	calcined K/NaX	NaY	as-prepared K/NaY	calcined K/NaY	
Functional groups of CH₃COOK							
Symmetric stretching of COO ⁻		1414			1414		
Asymmetric stretching of COO ⁻		1574			1574		(Zhong et al., 2018)
C-H stretching of -CH ₃		2977			2980		
Functional groups of K₂CO₃							
Symmetric stretching of CO ₃ ²⁻ (n ₁)			1060, 1080			1060, 1080	(Binet et al., 1999; Frantz, 1998;
Out of plane bending of CO ₃ ²⁻ (n ₂)			883			881	Lavalley, 1996;
Asymmetric stretching of CO ₃ ²⁻ (n ₃)			1448			1456	Manadee et al.,
In-plane bending of CO ₃ ²⁻ (n ₄)			700			700	2017)
Hydroxyl regions of zeolites							
Symmetric stretching of T-OH	3458	3393	3454	3458	3416	3462	
In-plane bending of -OH (H ₂ O)	1641		1659	1641		1653	(Fan et al., 2011)

A.3 References

- Abu-Zied, B. M. (2011). Cu²⁺-acetate exchanged X zeolites: Preparation, characterization and N₂O decomposition activity. *Microporous and Mesoporous Materials*. 139(1-3), 59-66.
- Binet, C., Daturi, M., and Lavalley, J.-C. (1999). IR study of polycrystalline ceria properties in oxidised and reduced states. *Catalysis Today*. 50(2), 207-225.
- Fan, M., Zhang, P., and Zhang, Y. (2011). NaY zeolite-supported potassium salt catalysts for dipropyl carbonate synthesis from transesterification route *Chemical Engineering Communications*. 198(8), 1033-1040.
- Frantz, J. D. (1998). Raman spectra of potassium carbonate and bicarbonate aqueous fluids at elevated temperatures and pressures: comparison with theoretical simulations. *Chemical Geology*. 152(3), 211-225.
- Lavalley, J. C. (1996). Infrared spectrometric studies of the surface basicity of metal oxides and zeolites using adsorbed probe molecules. *Catalysis Today*. 27(3), 377-401.
- Ma, Y.-K., Rigolet, S., Michelin, L., Paillaud, J.-L., Mintova, S., Khoerunnisa, F., Daou, T. J., and Ng, E.-P. (2021). Facile and fast determination of Si/Al ratio of zeolites using FTIR spectroscopy technique. *Microporous and Mesoporous Materials*. 311, 110683.
- Manadee, S., Sophiphun, O., Osakoo, N., Supamathanon, N., Kidkhunthod, P., Chanlek, N., Wittayakun, J., and Prayoonpokarach, S. (2017). Identification of potassium phase in catalysts supported on zeolite NaX and performance in transesterification of Jatropha seed oil. *Fuel Processing Technology*. 156, 62-67.
- Mozgawa, W. (2001). The relation between structure and vibrational spectra of natural zeolites. *Journal of Molecular Structure*. 596(1), 129-137.
- Phung, T. K., Carnasciali, M. M., Finocchio, E., and Busca, G. (2014). Catalytic conversion of ethyl acetate over faujasite zeolites. *Applied Catalysis A: General*. 470, 72-80.
- Zhong, X.-H., Liu, Y., Xu, T., and Liu, W.-Y. (2018). Influencing factors of intercalation of potassium acetate into dickite using immersion method. *Journal of Alloys and Compounds*. 742, 996-1001.

CURRICULUM VITAE

SIRIPORN KOSAWATTHANAKUN

Education

- 2014 B.Sc. in Chemistry (1st Class Honors), Maejo University, Thailand
- 2015 – 2022 Ph.D. candidate in Chemistry, Suranaree University of Technology, Institute of Science, Thailand

Scholarship & Fellowship

- 2015 – 2022 The Royal Golden Jubilee (RGJ) Ph.D. Programme (PhD – BSc program) by The Thailand Research Fund (TRF)
- 2019-2021 The French Embassy in Thailand with contribution to the RGJ-Ph.D. program
- October 2018 Thai-German S&T Cooperation 3rd Researcher Mobility Scheme by International Bureau of the German Federal Ministry of Education and Research, Germany and the National Science and Technology Development Agency, Thailand

Publications

1. Kosawatthanakun, S., Clatworthy, EB., Ghojavand, S., Sosa, N., Wittayakun, J., Mintova, S. (2023). *Inorg. Chem. Front.* <https://doi.org/10.1039/D2QI02023H>.
2. Kosawatthanakun, S., Pansakdanon, C., Sosa, N., Chanlek, N., Roessner, F., Prayoonpokarach, S., and Wittayakun, J. (2022). *ACS Omega*. 7, 9130-9141.
3. Bunthiam, N., Kosawatthanakun, S., and Wittayakun, J. (2021) *KKU Sci. J.* 49(1), 094-101.
4. Rattanawangsa, W., Osakoo, N., Kosawatthanakun, S., Roessner, F., and Wittayakun, J. (2022). *Suranaree J. Sci. Technol.* 29(5), 030080(1-7).